

MAJORANA SPHERE REPRESENTATION FOR THE
TIME EVOLUTION OF ONE QUBIT – SPIN
COHERENT STATE MODEL

BY

MUHAMMAD NADZIM BIN ZAMRI

A dissertation submitted in fulfilment of the requirement
for the degree of Master of Science

Kulliyyah of Science

International Islamic University Malaysia

JANUARY 2024

ABSTRACT

The interaction between qubit – field has attracted many researchers' curiosity as it sparked the development of quantum technologies such as quantum computing, quantum cryptography, and quantum metrology. There is a need to study the behavior of the qubit – field interaction system especially with a consideration of realistic errors to simulate the practical system for experimental purposes. This dissertation investigated the interaction system between a single qubit with a collection of N qubits or known as the spin coherent state, where the event of collapse and revival in the time evolution of the qubit state was focused. In this study, the time evolution of the qubit state in the one qubit – spin coherent state model was reproduced, and the dynamics of the qubit state probabilities was transformed into the little known Majorana Sphere representation. The dynamics in the Majorana Sphere was then analysed by considering three different initial state of the qubit. The results demonstrated that for the case of the qubit initially in the excited state and ground state, the dynamics started at a point on the surface of the Majorana Sphere at the north pole and south pole respectively, and we observed the oscillations of the dynamics in the sphere as time evolves. On the other hand, for the case of an equal probability between the excited state and ground state, we cannot see the same type of oscillations like in the previous case, and the dynamics just moved around in circle at the center of the sphere. The research was extended by considering the effect of having an off-resonant frequencies attributes to the system, then the frequency differences with distributions of varying width were averaged over to address the decoherence effects. It was found that for the case of qubit initially in excited state, the dynamics is more squished towards the north pole of the Majorana Sphere with increasing value of detuning. However, with an increasing width of 'error' distribution, the amplitude of the oscillations in the Majorana Sphere decreased and the dynamics remain averaged at the center of the sphere, which shows the suppression of the collapse and revival activity in the interaction system.

ملخص البحث

تفاعل الكيوبت - الميدان قد أثار فضول العديد من الباحثين، حيث شجّع على تطوير التكنولوجيا الكمومية مثل الحوسبة الكمومية والتشفير الكمومي وقياسات الكم. هناك حاجة لدراسة سلوك نظام تفاعل الكيوبت - الميدان خاصةً مع مراعاة الأخطاء الواقعية لمحاكاة النظام العملي لأغراض تجريبية. استقصت هذه الأطروحة نظام التفاعل بين كيوبت أو ما يعرف بحالة الدورة التكافؤ، حيث N الكيوبت الفردي مع مجموعة من تم التركيز على حدوث الانهيار والإحياء في تطور الزمن لحالة الكيوبت. في هذه الدراسة، تمت إعادة إنتاج تطور الزمن لحالة الكيوبت في نموذج حالة الكيوبت - حالة التكافؤ الدورية، وتحولت ديناميات احتمالات حالة الكيوبت إلى التمثيل القليل المعروف لكرة ماجورانا. تم تحليل ديناميات كرة ماجورانا من خلال النظر في ثلاث حالات بداية مختلفة للكيوبت. أظهرت النتائج أنه في حالة الكيوبت بدايةً في الحالة المثارة والحالة الأساسية، بدأت الديناميات من نقطة على سطح كرة ماجورانا عند القطب الشمالي والقطب الجنوبي على التوالي، وشاهدنا تذبذب الديناميات في الكرة مع تطور الزمن. من ناحية أخرى، في حالة الاحتمال المتساوي بين الحالة المثارة والحالة الأساسية، لا يمكننا رؤية نفس نوع التذبذب كما في الحالة السابقة، وكانت الديناميات تتحرك حول الدائرة في مركز الكرة فقط. تم توسيع البحث عن طريق النظر في تأثير وجود ترددات خارجة عن الموازنة تتعلق بالنظام، ثم تم متوسطة فروق التردد مع توزيعات عرض متغير لمعالجة تأثيرات فقدان التماثل. وتبين أنه في حالة الكيوبت بدايةً في الحالة المثارة، تنقص الديناميات أكثر نحو القطب الشمالي لكرة ماجورانا مع زيادة قيمة التشويش. ومع زيادة عرض توزيع "الخطأ"، قلت شدة التذبذبات في كرة ماجورانا وظلت الديناميات متوسطة في مركز الكرة، مما يظهر تقليل نشاط الانهيار والإحياء في نظام التفاعل.

APPROVAL PAGE

I certify that I have supervised and read this study and that in my opinion, it conforms to acceptable standards of scholarly presentation and is fully adequate, in scope and quality, as a dissertation for degree of Master of Science.

.....
Iskandar bin Bahari
Supervisor

I certify that I have read this study and that in my opinion it conforms to acceptable standards of scholarly presentation and is fully adequate, in scope and quality, as a dissertation for the degree of Master of Science.

.....
Mohd Zamani bin Zulkifli
Examiner

.....
Razif bin Razali
External Examiner

This dissertation was submitted to the Department of Physics and is accepted as a fulfilment of the requirements for the degree of Master of Science.

.....
Mohd Zamani bin Zulkifli
Head, Department of Physics

This dissertation was submitted to the Kulliyah of Science and is accepted as a fulfilment of the requirement for the degree of Master of Science.

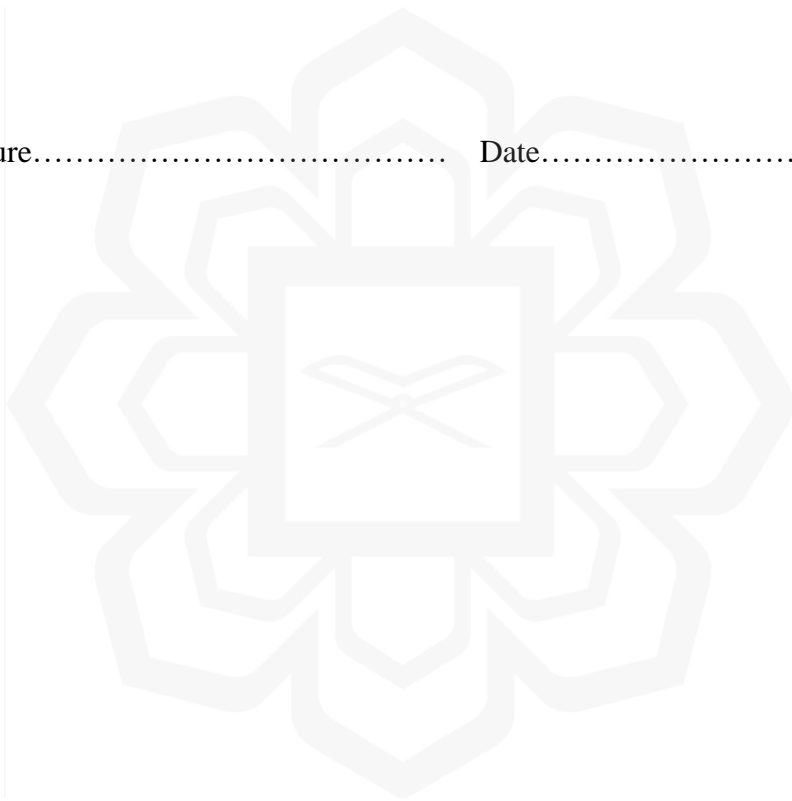
.....
Zarina bt Zainuddin
Dean, Kulliyah of Science

DECLARATION PAGE

I hereby declare that this dissertation is the result of my own investigations except where otherwise stated. I also declare that it has not been previously or concurrently submitted as a whole for any other degrees at IIUM or other institution.

Muhammad Nadzim bin Zamri

Signature..... Date.....



INTERNATIONAL ISLAMIC UNIVERSITY MALAYSIA

**DECLARATION OF COPYRIGHT AND AFFIRMATION OF
FAIR USE OF UNPUBLISHED RESEARCH**

**MAJORANA SPHERE REPRESENTATION FOR THE TIME
EVOLUTION OF ONE QUBIT – SPIN COHERENT STATE
MODEL**

I declare that the copyright holder of this dissertation is jointly owned by the student and IIUM.

Copyright © 2024 Muhammad Nadzim bin Zamri and International Islamic University Malaysia. All rights reserved.

No part of this unpublished research may be reproduced, stored in a retrieval system, or transmitted, in any form or by any means, electronic, mechanical, photocopying, recording or otherwise without prior written permission of the copyright holder except as provided below

1. Any material contained in or derived from this unpublished research may only be used by others in their writing with due acknowledgement.
2. IIUM or its library will have the right to make and transmit copies (print or electronic) for institutional and academic purposes.
3. The IIUM library will have the right to make, store in a retrieval system and supply copies of this unpublished research if requested by other universities and research libraries.

By signing this form, I acknowledged that I have read and understand the IIUM Intellectual Property Right and Commercialization policy.

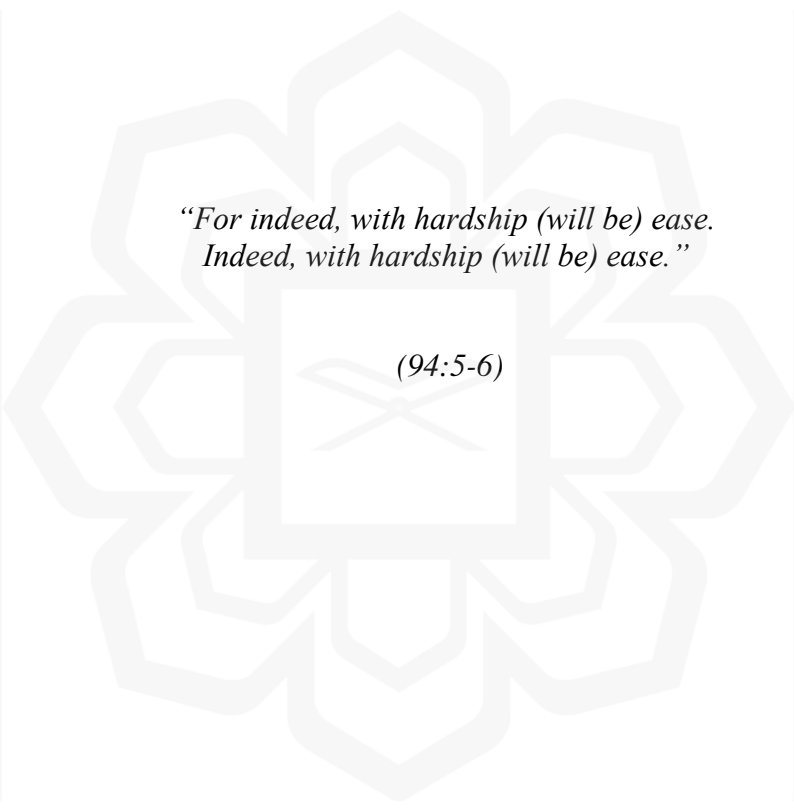
Affirmed by Muhammad Nadzim bin Zamri.

.....

Signature

.....

Date



*“For indeed, with hardship (will be) ease.
Indeed, with hardship (will be) ease.”*

(94:5-6)

ACKNOWLEDGEMENT

In the name of Allah, The Most Gracious and The Most Merciful.

All praises to the Almighty that in His will and given strength, I managed to complete this dissertation in partial fulfillment of the requirement for the Master of Science in International Islamic University Malaysia.

Special and heartfelt thanks to my supervisor Asst. Prof. Dr. Iskandar bin Bahari from the Department of Physics, for always being supportive, friendly, giving valuable guidance, motivations and advice during this memorable journey. Although he was busy with his commitments as the Deputy Dean of Student Development & Community Engagement in Kulliyyah of Science, he always spared his time to oversee me and his professionalism had brought this work towards completion. His mentorship is not only limited to academic lessons, but also contributes to my personal and professional growth. I chose this moment to acknowledge his contribution gratefully.

I want to take this opportunity to express my sincere gratitude to Dr. Z, who loves to share his wise opinions and insights that really helped me in being firm to make some big decisions in my life. The friendship and teamwork values that he shows made me feel comfortable and belong there. Thank you very much Dr. Z. You know who you are.

My special appreciation also goes to my postgraduate colleagues: Lukman, Amirul, Syafie, Ridzwan, Najwa, Aida, Fatinah, Fathinah, Fatihah, Samad, Farid, Khudhori, Nadzimuddin, Den, Faris, Nazren, and Idham. I thank them for the ups and downs memories throughout this journey, also for being wonderful friends who understand the struggles of doing postgraduate studies. Not to forget Dr. Razik who always being generous and willing to befriended me, although we rarely see each other. A token of gratitude to the genius and independent guy Ainul Zaim, whom I felt honored to work with under the same supervisor.

Million thanks to my parents, Zamri bin Jaafar and Nora binti Musa; and my family for the financial and emotional support. To my lovely wife Nur Athirah Syamimi, who is so far yet so close, thank you for always being there. I am forever indebted to them. Without their support, I would certainly fail to face the obstacles in this two-year period.

Lastly, thanks to all who were involved directly and indirectly to help me in doing this research as well as helping me in the process of writing this dissertation. May Allah accept all of our good deeds and guide us to His paradise. Allahumma amiin.

TABLE OF CONTENTS

Abstract	ii
Abstract in Arabic	Error! Bookmark not defined.
Approval Page.....	v
Declaration Page	vi
Permission Page	vii
Dedication	viii
Acknowledgement	x
Table of Contents	x
List of Tables	xii
List of Figures	xiii
List of Abbreviations	xvi
List of Symbols	xvii
CHAPTER 1: INTRODUCTION.....	1
1.1 General Background.....	1
1.2 Problem Statement	3
1.3 Research Questions	3
1.4 Research Objectives	3
1.5 Research Hypothesis	4
1.6 Research Scopes and Limitations.....	4
CHAPTER 2: LITERATURE REVIEW.....	5
2.1 Dirac Notation	5
2.2 Operator.....	6
2.3 Purity of States and Density Matrix	7
2.4 Coherent States.....	8
2.5 Spin Coherent States	9
2.6 Jaynes-Cummings Model.....	12
2.6.1 Collapse and Revival of Qubit State Probabilities.....	13
2.6.2 Single Qubit Attractor State	14
2.6.3 Linear Entropy	15
2.7 Spin Coherent State Model	16
2.7.1 Exact Solution of the One Qubit – Spin Coherent State Model.....	19
2.7.2 Collapse and Revival of Qubit State Probabilities.....	23
2.7.3 Single Qubit Attractor State.....	25
2.7.4 Linear Entropy	26
2.8 Bloch Sphere	27
2.9 Majorana Sphere	28
CHAPTER 3: METHODOLOGY.....	29
3.1 Workflow of Research	29
3.2 Methodology	30
3.2.1 Bloch Sphere Transformation	31
3.2.2 Majorana Sphere Transformation	32

3.2.3	Bloch Sphere and Majorana Sphere Equivalency	34
3.2.4	Decoherence Effects	37
CHAPTER 4: RESULTS AND DISCUSSIONS		40
4.1	Collapse and Revival of the Qubit State Probabilities in One Qubit – Spin Coherent State Model at Zero Detuning	40
4.2	Majorana Sphere Representation of the Qubit State Probabilities at Zero Detuning.....	43
4.2.1	Initial State $C_e = 1, C_g = 0$	43
4.2.2	Initial State $C_e = 0, C_g = 1$	47
4.2.3	Initial State $C_e = \frac{1}{\sqrt{2}}, C_g = \frac{1}{\sqrt{2}}$	51
4.3	Majorana Sphere Representation of the Qubit State Probabilities with Decoherence Effects	53
4.3.1	Finite Detuning	53
4.3.2	Distribution of Errors	60
CHAPTER 5: CONCLUSION.....		65
REFERENCES.....		68
APPENDIX I: CODING SCRIPT		74

LIST OF TABLES

Table 4.1	The revival time t_r of the qubit state probabilities for respective value of detuning δ .	54
-----------	---	----



LIST OF FIGURES

Figure 2.1	Time evolution for one qubit Jaynes-Cummings model at zero detuning with the qubit being initially in excited state, $\lambda = 1$, $n = 100$ and $ \alpha ^2 = 16$. The probability of being in the state $ e\rangle$ is shown as the blue line, the probability of being in attractor state is shown as the yellow line, and the linear entropy is shown as the red line.	16
Figure 2.2	Time evolution for one qubit – spin coherent state model at zero detuning with the qubit being initially in excited state, $\lambda = 1$, $N = 120$ and $ \zeta ^2 = 16$. The probability of being in the state $ e\rangle$ is shown as the blue line, the probability of being in attractor state is shown as the yellow line, and the linear entropy is shown as the red line.	26
Figure 3.1	Workflow of the research.	29
Figure 3.2	A single pure state on Majorana Sphere.	36
Figure 3.3	A single mixed state on Majorana Sphere.	36
Figure 3.4	Plots of Gaussian distribution where the distribution given by Equation (3.33) is centered at an expectation value zero $\delta = 0$ and standard deviation $\Delta = 0.3$.	38
Figure 4.1	The dynamics of the qubit state probabilities in the one qubit – spin coherent state model at zero detuning from $t = 0$ to $t = 50$ seconds, $\lambda = 1$, $N = 120$ and $ \zeta ^2 = 16$ with three different initial states. a) $C_e = 1$ and $C_g = 0$ b) $C_e = 0$ and $C_g = 1$ c) $C_e = \frac{1}{\sqrt{2}}$ and $C_g = \frac{1}{\sqrt{2}}$	41-42
Figure 4.2	Majorana Sphere representation for initial qubit state $C_e = 1$, $C_g = 0$ with $\lambda = 1$, $N = 120$ and $ \zeta ^2 = 16$ from $t = 0$ to $t = 50$ seconds.	43
Figure 4.2 a)	Period $0 \leq t \leq 5$ seconds.	45
Figure 4.2 b)	Period $5 \leq t \leq 15$ seconds.	45
Figure 4.2 c)	Period $15 \leq t \leq 33$ seconds.	46
Figure 4.2 d)	Period $33 \leq t \leq 50$ seconds.	46

Figure 4.3	Majorana Sphere representation for initial qubit state $C_e = 0, C_g = 1$ with $\lambda = 1, N = 120$ and $ \zeta ^2 = 16$ from $t = 0$ to $t = 50$ seconds.	47
Figure 4.3 a)	Period $0 \leq t \leq 5$ seconds.	49
Figure 4.3 b)	Period $5 \leq t \leq 15$ seconds.	49
Figure 4.3 c)	Period $15 \leq t \leq 31$ seconds.	50
Figure 4.3 d)	Period $31 \leq t \leq 50$ seconds.	50
Figure 4.4	Majorana Sphere representation for initial qubit state $C_e = C_g = \frac{1}{\sqrt{2}}$ with $\lambda = 1, N = 120$ and $ \zeta ^2 = 16$ for two different periods.	52
	a) Period $0 \leq t \leq 50$ seconds.	
	b) Period $0 \leq t \leq 200$ seconds.	
Figure 4.5	The time evolution of one qubit – spin coherent state model being initially in excited state, $\lambda = 1, N = 120, \zeta ^2 = 16$ with different values of detuning δ . The blue line shows $\delta = 0$, red $\delta = 5$, green $\delta = 10$, black $\delta = 25$ and orange $\delta = 50$.	54
Figure 4.6	Majorana Sphere representation for qubit initially in excited state with $\lambda = 1, N = 120$ and $ \zeta ^2 = 16$ from time $t = 0$ to $t = 50$ seconds for $\delta = 0$.	55
Figure 4.6 a)	Rotated horizontally.	55
Figure 4.6 b)	Rotated vertically.	55
Figure 4.7	Majorana Sphere representation for qubit initially in excited state with $\lambda = 1, N = 120$ and $ \zeta ^2 = 16$ from time $t = 0$ to $t = 60$ seconds for $\delta = 5$.	57
Figure 4.7 a)	Rotated horizontally.	57
Figure 4.7 b)	Rotated vertically.	57
Figure 4.8	Majorana Sphere representation for qubit initially in excited state with $\lambda = 1, N = 120$ and $ \zeta ^2 = 16$ from time $t = 0$ to $t = 130$ seconds for $\delta = 25$.	59
Figure 4.8 a)	Rotated horizontally.	59
Figure 4.8 b)	Rotated vertically.	59
Figure 4.9	Majorana Sphere representations of the one qubit – spin coherent state model for an ideal case of zero detuning with decoherence effects from time $t = 0$ to $t = 50$ seconds. The qubit is initially in the excited state with $\lambda = 1, N = 120, \zeta ^2 = 16$ and the	60-61

subfigures show the differences in the system with respective values of $\Delta = 0.3, 0.5$ and 0.7 .

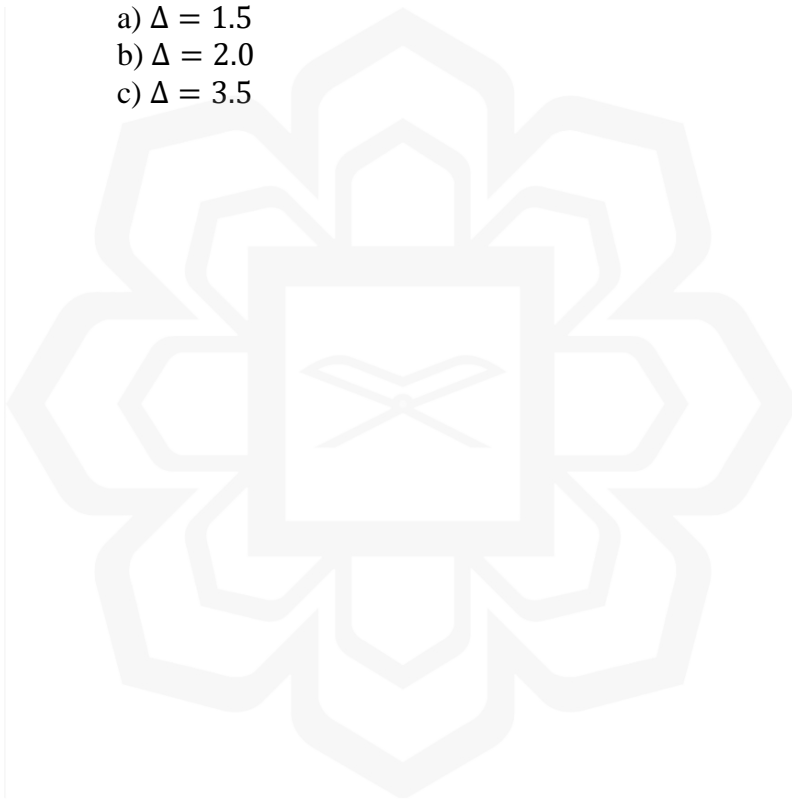
- a) $\Delta = 0.3$
- b) $\Delta = 0.5$
- c) $\Delta = 0.7$

Figure 4.10

Majorana Sphere representations of the one qubit – spin coherent state model for an ideal case of zero detuning with decoherence effects from time $t = 0$ to $t = 50$ seconds. The qubit is initially in the excited state with $\lambda = 1$, $N = 120$, $|\zeta|^2 = 16$ and the subfigures show the differences in the system with respective values of $\Delta = 1.5, 2.0$ and 3.5 .

63-64

- a) $\Delta = 1.5$
- b) $\Delta = 2.0$
- c) $\Delta = 3.5$



LIST OF ABBREVIATIONS

JCM	Jaynes-Cummings Model
QED	Quantum Electrodynamics
SCSM	Spin Coherent State Model



LIST OF SYMBOLS

\hbar	Planck's Constant
Ω	Frequency of the qubit
ω_N	Frequency of the spin coherent state
λ	Dipole interaction strength between qubit – spin coherent state
$ e\rangle$	Excited state
$ g\rangle$	Ground state
$\hat{\rho}_q(t)$	Reduced density matrix of the qubit system
t_r	Revival time
C_e	Coefficient of qubit being in the excited state
C_g	Coefficient of qubit being in the ground state
C_n	Coefficient for the spin coherent state model
δ	Value of detuning
Δ	Value of error distribution
β	Majorana points

CHAPTER 1

INTRODUCTION

1.1 GENERAL BACKGROUND

Quantum computing has been the talk of the town in recent years as it is evident that there is an increase in the number of companies and start-ups who invest in quantum computing research (Gibney, 2019). Since a quantum algorithm was developed in 1994 (Shor, 1994), there has been continuous experimental progress to implement the quantum computers; a machine that is designed to solve certain types of classically burdensome problems that the classical computers cannot. Using two pivotal concepts of quantum mechanics which are the superposition and entanglement in its operation (Horowitz & Grumbling, 2019), the future of quantum computer looks bright as its application starts to emerge in daily life such as navigation (Feng, 2019; Yarkoni et al., 2020), seismology (Albino, Pires, Nogueira, de Souza & Nascimento, 2022; Bhatta & Dang, 2023) and pharmaceuticals (Zinner et al., 2022; Izsák et al., 2023).

Quantum information and quantum computation are the studies of information processing activities that can be accomplished by using quantum mechanical systems. It is built upon the quantum binary digit, or qubit as the unit of quantum processing. While the classical binary digit has either state 0 or 1, qubit on the other hand has the states $|0\rangle$ and $|1\rangle$ that are analogous to the classical bit (Nielsen & Chuang, 2010). The contrast is that qubit can be in another state other than $|0\rangle$ or $|1\rangle$, and it is possible to form a superposition of states (Elani, 2021). Quantum technology applies the important principles of quantum physics like entanglement, tunnelling, superposition and many more (Dowling & Milburn, 2003). These applied principles lead to several applications such as quantum computing, quantum cryptography, and quantum metrology which uses the entanglement theory in the interaction between atom and field to detect weak forces (Munro, Nemoto, Milburn & Braunstein, 2002), and to increase measurement precision (Joo, Munro & Spiller, 2011). This in turn leads to the study of the atom-field interaction system until nowadays, there are many quantum systems that describe the interaction between a qubit with a field, and their corresponding physical applications. Some examples of the applications are the Circuit Quantum Electrodynamics (Schuster

et al., 2007), Cooper Pair Boxes (Wallraff et al., 2004), Cavity QED (Berman, 1994), and trapped ions (Cirac & Zoller, 1995).

Over 80 years ago, Isidor Isaac Rabi introduced a model (thus called Rabi model) that describes the interaction of a two-level atom with a semi-classical field, in which he uses an electromagnetic field (Rabi, 1937; Eckle & Johannesson, 2017). This model showed an interesting physical phenomenon known as Rabi oscillatory (Rabi, 1937; Gerry & Knight, 2005), and later become the research topic for other physicists to extend his work. The Jaynes-Cummings model, developed by Edwin T. Jaynes and Fred W. Cummings, is one of the continuation works from Rabi model which describes the qubit-field system in a fully quantized way (Jaynes & Cummings, 1963). Through this model, many interesting events can be observed as compared to the Rabi model and it provides more understanding about the spontaneous emission event in quantum theory of radiation (Jaynes & Cummings, 1963).

There have been so many extensions that have been made from the Jaynes-Cummings model such as the two qubits JCM (Jarvis, 2009) or the Tavis-Cummings model (Tavis & Cummings, 1968), and the spin star model (Hutton & Bose, 2004). Dooley, McCrossan, Harland, Everitt and Spiller (2013) later introduce an extension of the Jaynes-Cummings model where the coherent state is replaced by a collection of N qubits, which in this dissertation will be referred to as the spin coherent state. This fully quantum mechanical system also exhibits a similar phenomenon with the Jaynes-Cummings model, due to the correspondence of the spin coherent state of a large value of N with the coherent state. Thus, similar interesting events can be observed in both models like collapse and revival activity of Rabi oscillation, qubit-field entanglement, the attractor state, and the occurrence of the Schrödinger cat state. Following their work is the study on two qubits – spin coherent state interaction system (Bahari, Spiller, Dooley, Hayes & McCrossan, 2018), where they considered the effect of adding decoherence to the interaction system.

In this dissertation, we study the particular works done by Dooley et al. (2013) and Bahari et al. (2018). We focused more on the collapse and revival activity of Rabi oscillation in the one qubit – spin coherent state model with decoherence, and then illustrate the dynamics of the qubit state probabilities in the Majorana Sphere representation.

1.2 PROBLEM STATEMENT

From the spin coherent state model, where a qubit interacts with a spin coherent state, many interesting events that is analogous to the Jaynes-Cummings model can be observed. One of the events that will be mainly focused in this work is the collapse and revival activity of the qubit state probabilities. Prior work by Jarvis (2009) displays the dynamics of the qubit state probabilities for the Jaynes-Cummings model in the Majorana Sphere representation. There is still no Majorana Sphere representation made for the spin coherent state model yet. It is a vital part in understanding the time evolution of the qubit state for the interaction system. Furthermore, we wanted to address the problem that exists in experimental works, where there is always the possibility for an error to occur which will cause the system to deviate from its ideal behaviour. Therefore in this research, the Majorana Sphere representation for the time evolution of the qubit state in the one qubit – spin coherent state model will be studied, and the effect of decoherence in the interaction system will be taken into consideration.

1.3 RESEARCH QUESTIONS

This dissertation will answer the following questions:

- 1) How does the time evolution of the qubit state in a one qubit – spin coherent state model behave in a Majorana Sphere representation?
- 2) What will happen to the dynamics of the qubit state probabilities in the Majorana Sphere when we change the qubit's initial state?
- 3) How does the decoherence and error distribution affect the dynamics of the qubit state probabilities in the Majorana Sphere?

1.4 RESEARCH OBJECTIVES

- 1) To illustrate the time evolution of a qubit state in a one qubit – spin coherent state model and represent it in the Majorana Sphere.
- 2) To study the dynamics of the qubit state probabilities in the Majorana Sphere representation with different initial states.

- 3) To investigate the effect of decoherence and error distribution to the dynamics of the qubit state probabilities in the Majorana Sphere representation.

1.5 RESEARCH HYPOTHESIS

This research has a few possible outcomes, which are hypotheses as below:

- 1) The Majorana Sphere representation for the time evolution of the qubit state in the one qubit – spin coherent state model is consistent with the Jaynes-Cummings model.
- 2) For each initial state of the qubit, there will be some effects to the movement of the qubit state probabilities, giving a different time evolution of the qubit state in the Majorana Sphere representation.
- 3) The presence of decoherence effects will cause the behaviour of the interaction system to deviate from its ideal case of resonance frequencies.

1.6 RESEARCH SCOPES AND LIMITATIONS

The main focus of this research is to study the dynamics of the qubit state probabilities in the one qubit – spin coherent state model and transform it into the Majorana Sphere representation. This research is limited on the interaction system between one qubit and spin coherent state. Only the collapse and revival activity of the qubit state probabilities will be mainly focused. To address the decoherence effects, there are some probabilistic distributions that can be applied which depends on the systems that being monitored. In this work, the Gaussian distribution was chosen to simulate errors that might actually occur in an actual system. MAPLE programming software was utilized to ease the process of complex calculations and do the simulation works. However, in the case of finite detuning, it was difficult to analyse the dynamics of the qubit state probabilities for each specific detuning. The coding had to be adjusted at specific detuning and reran multiple times, which is time consuming. Moreover, transforming the qubit state probabilities from the spin coherent state model into the Majorana Sphere causes rounding off error in MAPLE especially in the case of finite detuning, hence the points inside the sphere appeared to be a bit scattered.

CHAPTER 2

LITERATURE REVIEW

2.1 DIRAC NOTATION

Paul Dirac had invented the Dirac notation (Dirac, 1981), a very convenient tool for representing state vectors in the theory of quantum mechanics. The notation allows us to represent a vector state by kets $|\psi\rangle$ and its Hermitian conjugate by bras $\langle\psi|$ (Zettili, 2009). In Dirac notation, a qubit state can be written in the form of $|\psi\rangle = \alpha|e\rangle + \beta|g\rangle$ where $|e\rangle$ and $|g\rangle$ are the basis state that represents the excited state and ground state of the system respectively, while α and β are the probability amplitude written as complex numbers. This ket state of the qubit can be written in a matrix form as a column vector

$$|\psi\rangle = \begin{pmatrix} \alpha \\ \beta \end{pmatrix} \quad (2.1)$$

while the bra of this ket in the form of $\langle\psi| = \alpha^*\langle e| + \beta^*\langle g|$ is the conjugate transpose of the ket, which is written as a row vector

$$\langle\psi| = (\alpha^* \quad \beta^*) . \quad (2.2)$$

The combination of a bra and a ket, also called bra-ket is represented by $\langle\psi|\psi\rangle$ and the product of it will give an inner product that is helpful to calculate the orthogonality of the states, where the states are orthogonal if the inner product is zero:

$$\langle e|e\rangle = \langle g|g\rangle = 1 \quad (2.3)$$

$$\langle e|g\rangle = \langle g|e\rangle = 0. \quad (2.4)$$

Thus, we can say the qubit states $|e\rangle$ and $|g\rangle$ are orthogonal to each other. We can also use the inner product to identify the normalisation of a vector by calculating if $\langle\psi|\psi\rangle = 1$. Two states are said to be orthonormal to each other when both are orthogonal and normalised. For example,

$$\begin{aligned} \langle\psi|\psi\rangle &= (\alpha^*\langle e| + \beta^*\langle g|)(\alpha|e\rangle + \beta|g\rangle) \\ &= |\alpha|^2\langle e|e\rangle + \alpha\beta^*\langle g|e\rangle + \alpha^*\beta\langle e|g\rangle + |\beta|^2\langle g|g\rangle \\ &= |\alpha|^2 + |\beta|^2 = 1 . \end{aligned} \quad (2.5)$$

2.2 OPERATOR

To form an operator with Dirac notation, we consider the outer products of $|\psi\rangle$ and $|\phi\rangle$ with $|\phi\rangle = \delta|e\rangle + \epsilon|g\rangle$,

$$\begin{aligned} |\psi\rangle\langle\phi| &= (\alpha|e\rangle + \beta|g\rangle)(\delta^*\langle e| + \epsilon^*\langle g|) \\ &= \alpha\delta^*|e\rangle\langle e| + \beta\delta^*|g\rangle\langle e| + \alpha\epsilon^*|g\rangle\langle e| + \beta\epsilon^*|g\rangle\langle g| \end{aligned} \quad (2.6)$$

which can be represented in matrix form as

$$|\psi\rangle\langle\phi| = \begin{pmatrix} \alpha \\ \beta \end{pmatrix} (\delta^* \quad \epsilon^*) \quad (2.7)$$

$$= \begin{pmatrix} \alpha\delta^* & \alpha\epsilon^* \\ \beta\delta^* & \beta\epsilon^* \end{pmatrix}. \quad (2.8)$$

Operators have a hat above their symbols to differentiate them from numbers. $|e\rangle\langle e|$, $|e\rangle\langle g|$, $|g\rangle\langle e|$ and $|g\rangle\langle g|$ are the possible operators for a system of a single qubit. Examples of these are the Pauli operators, where in the matrix form is written as

$$\hat{\sigma}_x = \begin{pmatrix} 0 & 1 \\ 1 & 0 \end{pmatrix}, \quad \hat{\sigma}_y = \begin{pmatrix} 0 & -i \\ i & 0 \end{pmatrix}, \quad \hat{\sigma}_z = \begin{pmatrix} 1 & 0 \\ 0 & -1 \end{pmatrix} \quad (2.9)$$

with raising and lowering operators given by

$$\hat{\sigma}_+ = 2 \begin{pmatrix} 0 & 1 \\ 0 & 0 \end{pmatrix}, \quad \hat{\sigma}_- = 2 \begin{pmatrix} 0 & 0 \\ 1 & 0 \end{pmatrix}, \quad (2.10)$$

where

$$\hat{\sigma}_\pm = \hat{\sigma}_x \pm i\hat{\sigma}_y. \quad (2.11)$$

Hence, the Pauli operators in Dirac form can be written as

$$\hat{\sigma}_x = \frac{1}{2}(\hat{\sigma}_+ + \hat{\sigma}_-) = \frac{1}{2}(|e\rangle\langle g| + |g\rangle\langle e|) \quad (2.12)$$

$$\hat{\sigma}_y = \frac{i}{2}(\hat{\sigma}_- - \hat{\sigma}_+) = \frac{i}{2}(|g\rangle\langle e| - |e\rangle\langle g|) \quad (2.13)$$

$$\hat{\sigma}_z = \frac{1}{2}(\hat{\sigma}_+\hat{\sigma}_- - \hat{\sigma}_-\hat{\sigma}_+) = \frac{1}{2}(|e\rangle\langle e| - |g\rangle\langle g|). \quad (2.14)$$

These operators abide the Pauli spin algebra commutation relations as follows:

$$[\hat{\sigma}_+, \hat{\sigma}_-] = \hat{\sigma}_z \quad (2.15)$$

$$[\hat{\sigma}_z, \hat{\sigma}_\pm] = \pm 2\hat{\sigma}_\pm \quad (2.16)$$

where the commutator of two operators \hat{A} and \hat{B} is defined as

$$[\hat{A}, \hat{B}] = \hat{A}\hat{B} - \hat{B}\hat{A}. \quad (2.17)$$

Hermitian operator, also known as the self-adjoint operator, is another example of an operator. It is represented by a square matrix that satisfies $\hat{A} = \hat{A}^\dagger$. This matrix can be diagonalised by a unitary matrix if all the diagonal elements are real. This Hermitian matrix represent the Unitary operators \hat{U} , given by $\hat{U}\hat{U}^\dagger = \hat{U}^\dagger\hat{U} = \hat{I}_n$ where \hat{U}^\dagger is the conjugate transpose of \hat{U} , and \hat{I}_n is the $n \times n$ identity matrix. The Hermitian matrix has the property of having real eigenvalues, and an eigenvector associated with a particular eigenvalue is orthogonal to another eigenvectors (Lowdin, 1964; Lax, 2007).

The photon creation \hat{a}^\dagger and annihilation \hat{a} operators satisfy $[\hat{a}^\dagger, \hat{a}] = 1$. The creation operator \hat{a}^\dagger increase the number of quanta by one while the annihilation operator \hat{a} decrease it by one. Both operators act on photon number states or Fock states $|n\rangle$ as they are usually constituted with a field state, which is then they become the eigenstates of the photon number operator $\hat{a}^\dagger\hat{a}$:

$$\hat{a}^\dagger\hat{a}|n\rangle = n|n\rangle \quad (2.18)$$

$$\hat{a}^\dagger|n\rangle = \sqrt{n+1}|n+1\rangle \quad (2.19)$$

$$\hat{a}|n\rangle = \sqrt{n}|n-1\rangle. \quad (2.20)$$

2.3 PURITY OF STATES AND DENSITY MATRIX

In quantum systems, a pure state is a well-defined state in which the information about it in a system is completely known. Subsequently, there is also a state that is known as mixed state. Different than the earlier one, the information of this state in a system is not completely known. Mixed state can be written as the probabilistic sum P_i of several pure states $|\psi_i\rangle$ (Jarvis, 2009) such that

$$\hat{\rho} = \sum_i P_i |\psi_i\rangle\langle\psi_i| \quad (2.21)$$

This formulation is known as density matrix and it has the following properties:

$$\hat{\rho} = \hat{\rho}^\dagger \quad (2.22)$$

$$\text{Tr}(\hat{\rho}) = 1 \quad (2.23)$$

$$\langle \hat{O} \rangle = \text{Tr}(\hat{\rho} \hat{O}) . \quad (2.24)$$

Assuming a square m -by- m matrix with elements $a_{ij} \langle i | \hat{\rho} | j \rangle$ where $i = 1, 2, \dots, m$ and $j = 1, 2, \dots, m$, the trace of this matrix is the sum of its eigenvalues or diagonal entries where

$$\text{Tr}(\hat{\rho}) = \sum_i \langle i | \hat{\rho} | i \rangle = \sum_{i=1}^m a_{ii} . \quad (2.25)$$

A pure state is obtained when $P_i = 1$, with only one state $|\psi_i\rangle$ in Equation (2.21). This pure state takes a trace value of $\text{Tr}(\hat{\rho}) = 1$, while mixed state takes $\text{Tr}(\hat{\rho}) < 1$.

Density matrix is an important tool in this work as it allows the calculation of pure state and mixed state for our quantum system. The corresponding trace values will then lead us to our measurable quantities.

2.4 COHERENT STATES

Coherent states are a type of quantum harmonic oscillator whose dynamics are the most similar to the classical harmonic oscillator system (Glauber, 1963). They are denoted as $|\alpha\rangle$ and they are the eigenstates of the annihilation operator \hat{a} . They satisfy the relation

$$\hat{a}|\alpha\rangle = \alpha|\alpha\rangle \quad (2.26)$$

$$\langle \alpha | \hat{a}^\dagger = \alpha^* \langle \alpha | \quad (2.27)$$

for operator \hat{a} and \hat{a}^\dagger respectively. α is a complex number. A complete basis formed by the number states $|n\rangle$ helps us to expand $|\alpha\rangle$ and the states become

$$|\alpha\rangle = e^{|\alpha|^2/2} \sum_{n=0}^{\infty} \frac{\alpha^n}{\sqrt{n!}} |n\rangle \quad (2.28)$$

where

$$\alpha = |\alpha|e^{-i\theta} . \quad (2.29)$$

The state $|n\rangle$ is the eigenstate of the photon number operator $\hat{n} = \hat{a}^\dagger \hat{a}$ with eigenvalue n and initial phase of the radiation field is θ , and the size is $|\alpha|$ with

$$\bar{n} = \langle \alpha | \hat{n} | \alpha \rangle = |\alpha|^2. \quad (2.30)$$

The initial state of an ideal interaction system of zero detuning between a qubit and a coherent state $|a\rangle$ is given by

$$|\psi\rangle = |a\rangle(C_e|e\rangle + C_g|g\rangle) \quad (2.31)$$

$$= \sum_{n=0}^{\infty} C_n |n\rangle (C_e|e\rangle + C_g|g\rangle) \quad (2.32)$$

where

$$C_n = e^{-|\alpha|^2/2} \frac{\alpha^n}{\sqrt{n!}} \quad (2.33)$$

with $|n\rangle$ is the energy eigenstates of the field, and the average photon number in the coherent state is $\bar{n} = |\alpha|^2$.

2.5 SPIN COHERENT STATES

Spin states that correspond to the coherent state of harmonic oscillator are called the spin coherent state. The state in this quantum state is a single spin-1/2 particle since it is in a two-dimensional space where $\mathcal{H} = \mathcal{C}^2$. The Bloch Sphere can be used to represent this state as a three-dimensional vector \vec{r} , where $\vec{r} = (r_x, r_y, r_z)$ and $|\vec{r}| \leq 1$. A pure state is located on the surface of the sphere such that $|\vec{r}| = 1$, and a mixed state is located inside the sphere where $|\vec{r}| < 1$ (Nielsen & Chuang, 2010). The single spin-1/2 state can also be represented into the Majorana Sphere. A single spin-1/2 particle is written in the form of spin up $|\uparrow\rangle$ and spin down $|\downarrow\rangle$ as

$$|\rightarrow\rangle = \frac{1}{\sqrt{2}}(|\uparrow\rangle + |\downarrow\rangle) \quad (2.34)$$

$$|\leftarrow\rangle = \frac{1}{\sqrt{2}}(|\uparrow\rangle - |\downarrow\rangle) \quad (2.35)$$

$$|\oplus\rangle = \frac{1}{\sqrt{2}}(|\uparrow\rangle + i|\downarrow\rangle) \quad (2.36)$$

$$|\odot\rangle = \frac{1}{\sqrt{2}}(|\uparrow\rangle - i|\downarrow\rangle) \quad (2.37)$$

where $|\uparrow\rangle = \begin{pmatrix} 1 \\ 0 \end{pmatrix}$, $|\downarrow\rangle = \begin{pmatrix} 0 \\ 1 \end{pmatrix}$, \oplus represents an arrow pointing into the page and \odot represents an arrow pointing out of the page. These states are related to the Pauli operators given by Equation (2.9) to Equation (2.11) and obey the commutation relations given by Equation (2.12) to Equation (2.16), and when those operators acted on these states, they become:

$$\begin{aligned} \hat{\sigma}_x|\rightarrow\rangle &= |\rightarrow\rangle & \hat{\sigma}_y|\oplus\rangle &= |\oplus\rangle & \hat{\sigma}_z|\uparrow\rangle &= |\uparrow\rangle \\ \hat{\sigma}_x|\leftarrow\rangle &= -|\leftarrow\rangle & \hat{\sigma}_y|\odot\rangle &= -|\odot\rangle & \hat{\sigma}_z|\downarrow\rangle &= -|\downarrow\rangle \end{aligned} \quad (2.38)$$

A system of an N spin-1/2 particles lie in a Hilbert space with a dimension of $\mathcal{H} = \mathcal{C}^2 \otimes \mathcal{C}^2 \dots \otimes \mathcal{C}^2 = (\mathcal{C}^2)^{\otimes N}$ with collective spins operators

$$\hat{j}^x = \frac{1}{2} \sum_{i=1}^N \hat{\sigma}_{(i)}^x ; \quad \hat{j}^y = \frac{1}{2} \sum_{i=1}^N \hat{\sigma}_{(i)}^y ; \quad \hat{j}^z = \frac{1}{2} \sum_{i=1}^N \hat{\sigma}_{(i)}^z \quad (2.39)$$

and the total spin operator is

$$\hat{j}^2 = (\hat{j}^x)^2 + (\hat{j}^y)^2 + (\hat{j}^z)^2 . \quad (2.40)$$

The eigenstates of operators \hat{j}^z and \hat{j}^2 are associated with the Dicke states of N spin system $|j, m\rangle_N$ (hence the subscript N) in the form of

$$\hat{j}^z |j, m\rangle_N = m |j, m\rangle_N \quad (2.41)$$

$$\hat{j}^2 |j, m\rangle_N = j(j+1) |j, m\rangle_N \quad (2.42)$$

where the raising and lowering operators are given as

$$\hat{j}^{\pm} = \hat{j}^x \pm i\hat{j}^y \quad (2.43)$$

that obeys the commutation relations

$$[\hat{j}^+, \hat{j}^-] = -2\hat{j}^z \quad (2.44)$$

$$[\hat{j}^z, \hat{j}^{\pm}] = \pm\hat{j}^{\pm} \quad (2.45)$$

$$[\hat{j}^2, \hat{j}^\pm] = 0 \quad (2.46)$$

and they act on the Dicke states as

$$\hat{j}^\pm |j, m\rangle_N = \sqrt{j(j+1) - m(m \pm 1)} |j, m \pm 1\rangle_N. \quad (2.47)$$

A spin coherent state is defined as a state in which each individual N spins is in the same pure state (Radcliffe, 1971; Areechi, Courtens, Gilmore & Thomas, 1972). One of the properties of this state is that it is separable and can be written in the state space of $j = \frac{N}{2}$ as

$$\left| \frac{N}{2}, \zeta \right\rangle_N = \bigotimes_{i=1}^N \left(\frac{1}{\sqrt{1+|\zeta|^2}} |\downarrow^{(i)}\rangle + \frac{\zeta}{\sqrt{1+|\zeta|^2}} |\uparrow^{(i)}\rangle \right) \quad (2.48)$$

where the complex parameter ζ is the parametrization to transform the spin coherent state into spherical coordinates (θ, ϕ) defined as

$$\zeta = e^{-i\phi} \tan \frac{\theta}{2}. \quad (2.49)$$

The identical portrayal of the spin coherent state in terms of Dicke states can be written as

$$|N, \zeta\rangle_N = \sum_{n=0}^N C_n \left| \frac{N}{2}, n - \frac{N}{2} \right\rangle_N \quad (2.50)$$

where

$$C_n = \frac{1}{(1 + |\zeta|^2)^{N/2}} \sqrt{\frac{N!}{(N-n)! n!}} \zeta^n. \quad (2.51)$$

Considering the limit $N \rightarrow \infty$, the field mode system of the coherent state is similar to the N -spin system of the spin coherent state. By linear mapping, the operators that belong to the spin coherent state system can be transformed from a Dicke state $\left| \frac{N}{2}, n - \frac{N}{2} \right\rangle_N$ into a Fock or number state $|n\rangle_N$ (Brattke, Varcoe & Walther, 2001).

2.6 JAYNES-CUMMINGS MODEL

The Jaynes-Cummings model is one of the simplest of quantum-electrodynamical systems. The Jaynes-Cummings model consists of a single two-level atom (qubit) interacting with a single near-resonant quantized cavity mode of the electromagnetic field, represented by a harmonic oscillator (Shore & Knight, 1993). Later discovery from this model results in the collapse and revival of Rabi oscillation in the qubit system (Cummings, 1965; Eberly, Narozhny & Sanchez-Mondragon, 1980; Gea-Banacloche, 1990; Gerry & Knight, 2005), and many interesting events can be observed such as the sudden death of entanglement (Yu & Eberly, 2004; Qing, Ming & Zhuo-Liang, 2008; Yu & Eberly, 2009), collapse and revival of qubits entanglement (Jarvis et al., 2009), and cat swapping (Jarvis et al., 2010).

The approximation of the total Hamiltonian for the case of one qubit Jaynes-Cummings model (Bahari, 2018) is in the form of

$$\hat{H} = \frac{1}{2} \hbar \Omega \hat{\sigma}_z + \hbar \omega \hat{a}^\dagger \hat{a} + \hbar \lambda (\hat{\sigma}_+ \hat{a} + \hat{\sigma}_- \hat{a}^\dagger). \quad (2.52)$$

Ω and ω are the frequency of the qubit and the field respectively. The Pauli z operator in Dirac form is given as $\hat{\sigma}_z = |e\rangle\langle e| - |g\rangle\langle g|$. \hbar is the Planck's constant and λ is the dipole-interaction strength between the qubit and the field. \hat{a}^\dagger and \hat{a} are the photon creation and annihilation operators, while $\hat{\sigma}_+$ and $\hat{\sigma}_-$ are the raising and lowering operators respectively.

The eigenvalues, eigenvectors and the time evolutions of the Hamiltonian are found by solving the eigenvalue equation

$$\hat{H}|\psi(t)\rangle = E|\psi(t)\rangle. \quad (2.53)$$

The wavefunction for the system at time t is written as

$$|\psi(t)\rangle = \sum_{n=0}^{\infty} a_{e,n}(t)|e, n\rangle + a_{g,n}(t)|g, n\rangle \quad (2.54)$$

where $t = 0$ is for initial state. We can use the initial state to find the eigenvalues and from there, we can find eigenstates that will give us the general time dependence. The exact solution is then calculated by solving the time-dependent Schrödinger equation.

2.6.1 Collapse and Revival of Qubit State Probabilities

One of the interesting events that can be observed in the single qubit and coherent state interaction model is the phenomenon of ‘collapse and revival’ of Rabi oscillation in the system. This event occurs when the oscillation of the dynamics of the qubit state probabilities seems to be dampening before completely vanish after some time (Bahari, 2018). As later time, the oscillation of the qubit state revives at the same frequency but at different amplitude. These activities of collapse, complete disappearance and revival in the oscillation of the qubit state probability occurs periodically, which at longer times we can notice a sequence of collapse and revival events. The collapse and revival activity can be seen from the blue-coloured line in Figure 2.1.

The probability of the qubit is either in ground state $|g\rangle$ or excited state $|e\rangle$ are

$$P_g(t) = \langle g | \hat{\rho}_q(t) | g \rangle = e^{-\bar{n}} \sum_{n=1}^{\infty} \frac{\bar{n}^n}{n!} \cos^2(\lambda t \sqrt{n}) \quad (2.55)$$

$$P_e(t) = \langle e | \hat{\rho}_q(t) | e \rangle = e^{-\bar{n}} \sum_{n=1}^{\infty} \frac{\bar{n}^n}{n!} \sin^2(\lambda t \sqrt{n}) \quad (2.56)$$

where $\hat{\rho}_q(t)$ is defined as the reduced density matrix of the system in the form of

$$\hat{\rho}_q(t) = \text{Tr}_f(|\psi(t)\rangle\langle\psi(t)|) . \quad (2.57)$$

These collapse and revival events can be described by the destructive and constructive interference (Bahari, 2018). The collapse and total disappearance happened because of the destructive interference; where there are two different phases of two oscillating terms added together which leads to the cancellation of phase. As the time evolves, the phase difference will become smaller and at later time, the phase of oscillating terms will start to give a constructive interference. The revival phase has a climax at revival time t_r , where for a given positive integer j , the j th revival time can be calculated as

$$2\pi j = t_r(\omega_{n+1} - \omega_n) \quad (2.58)$$

$$= t_r(2\lambda\sqrt{n+1} - 2\lambda\sqrt{n}) \quad (2.59)$$

$$= t_r(2\lambda\sqrt{\bar{n}} + \frac{\lambda}{\sqrt{\bar{n}}} - 2\lambda\sqrt{\bar{n}}) \quad (2.60)$$

$$t_r = \frac{2\pi j\sqrt{\bar{n}}}{\lambda} \quad (2.61)$$

and since $\bar{n} = |\alpha|^2$, then the revival time for case $j = 1$ is

$$t_r = \frac{2\pi\sqrt{\bar{n}}}{\lambda} = \frac{2\pi|\alpha|}{\lambda}. \quad (2.62)$$

2.6.2 Single Qubit Attractor State

Another interesting event that can occur in the one qubit Jaynes-Cummings model is the occurrence of ‘attractor state’ (Gea-Banacloche, 1990; Gea-Banacloche, 1991). He had revealed that at halfway to the revival time t_r , the qubit disentangles itself from the field unconditionally, and the qubit state evolves to the ‘attractor state’.

In Figure 2.1, the attractor state is given by yellow-coloured line. At $t = 0$, the graph starts at value 0, which indicates that there is no presence of attractor state at the beginning of interaction. As time evolves, we can see the line slowly moves towards the maximum value 1 at half revival time, at about $t = 13$. At this moment, the qubit disentangles itself from the field and become attractor state, which has the form of

$$|\psi_{1,att}^+\rangle = \frac{1}{\sqrt{2}}(e^{-i\theta}|e\rangle + i|g\rangle) \quad (2.63)$$

and the probability of the qubit being in this state is calculated as

$$P_{1,att}^+(t) = \langle \psi_{1,att}^+ | \hat{\rho}_q(t) | \psi_{1,att}^+ \rangle \quad (2.64)$$

where $\hat{\rho}_q(t)$ is the reduced density matrix given in Equation (2.57). The attractor state does not depend on the initial qubit state since the initial coefficients C_e and C_g has no contributions at the beginning of interaction, but it depends on the phase of starting coherent field state θ (Bahari, 2018). Hence the qubit and field are a product state at time $\frac{t_r}{2}$ because the qubit state can be factorised out of the wavefunction.

Simultaneously, all information about the initial qubit state is exchanged into the field, where the field is currently in a Schrödinger cat state because of the coherent superposition of two coherent state with opposite phase $|\alpha\rangle$ and $|-\alpha\rangle$ (Bužek, Moya-Cessa, Knight & Phoenix, 1992; Knight & Shore, 1993). At revival time t_r , all the information in the field will be transferred back to the qubit. As the interaction is happening through time, the system evolves from a product state to an entangled state and back again repeatedly.

2.6.3 Linear Entropy

One more phenomenon that occurs in the one qubit Jaynes-Cummings model is the entanglement between the qubit and the field. Entropy can be used to measure the entanglement between two subsystems (Vedral, Plenio, Jacobs & Knight, 1997; Munro, James, White & Kwiat, 2001). Linear entropy (Bose & Vedral, 2000) is used to measure the entanglement due to its simplicity. In Jaynes-Cummings model, the system always begins in a pure state, and the time evolution of the system depends on the time-dependent Schrödinger dynamics. We can observe the dynamics of either the qubit or the field, and hence the entanglement in the system.

The linear entropy is defined as

$$S_q^L(t) = 1 - \text{Tr}(\hat{\rho}_q(t)^2) \quad (2.65)$$

where $\hat{\rho}_q(t)$ is the reduced density matrix given in Equation (2.57). This number ranges from zero to unity, where they correspond to the completely pure state and maximally mixed state respectively. Qubit-field entanglement is present when the value of entropy is greater than zero.

Linear entropy is represented by the red line in Figure 2.1. It is shown that at half-way to the revival time, at $\frac{t_r}{2}$ the line is approaching value 0, which indicates that the qubit and field completely disentangles, the qubit gains all information about itself, and thus becomes an attractor state which is a pure state. Then, as the time is approaching the revival time t_r at about $t = 25$, the line gradually approaches value 1, which means that there is a presence of entanglement between the qubit and field. At this moment, all information from the qubit is swapped to the field, and the qubit

becomes a mixed state. We can see a dip on the line, because the width of this dip is on a time much smaller than entropy at $\frac{t_r}{2}$ (Jarvis et al., 2009). To prevent this, we can put higher value of \bar{n} in the numerical calculation so that the value of entropy at this time can get closer to zero.

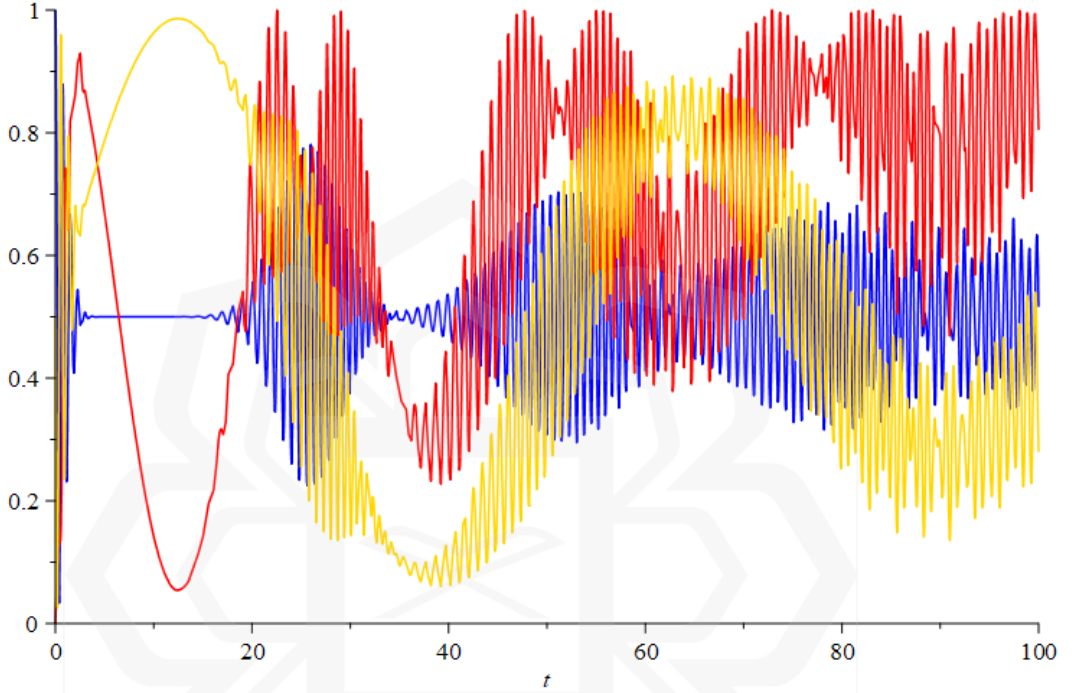


Figure 2.1: Time evolution for one qubit Jaynes-Cummings model at zero detuning with the qubit being initially in excited state, $\lambda = 1$, $n = 100$ and $|\alpha|^2 = 16$. The probability of being in the state $|e\rangle$ is shown as the blue line, the probability of being in attractor state is shown as the yellow line, and the linear entropy is shown as the red line.

2.7 SPIN COHERENT STATE MODEL

Previously, we have discussed about a quantum system in which a single qubit interacts with a quantum field. The interaction system displays quantum properties such as the event of collapse and revival of qubit state probabilities, the presence of attractor and Schrödinger cat states, as well as the entanglement between the qubit and field. Inspired by the Jaynes-Cummings model, there is a further continuation on this single qubit interacting system. This time around, the system of a single qubit is coupled to a spin coherent state, which is a collection of N qubits or spin/12 particles (Dooley et al., 2013;

Dooley & Spiller, 2014; Dooley, 2014). In this work, this model is called as spin coherent state model and its quantum properties closely resembles the Jaynes-Cummings model. This model is also sometimes called as the spin star model or the big spin model (Hutton & Bose, 2004).

The Hamiltonian to the one qubit – spin coherent state model consists of the Hamiltonians for the spin coherent state \hat{H}_S , the single qubit \hat{H}_A , and the coupling interaction \hat{H}_I , between them such that

$$\hat{H}_N = \hat{H}_S + \hat{H}_A + \hat{H}_I \quad (2.66)$$

$$= \hbar\omega_N \left(\hat{J}^z + \frac{N}{2} \right) + \frac{\hbar\Omega}{2} \hat{\sigma}^z + \frac{\hbar\lambda}{\sqrt{N}} (\hat{J}^+ \hat{\sigma}^- + \hat{J}^- \hat{\sigma}^+). \quad (2.67)$$

ω_N and Ω is the frequency of the spin coherent state and frequency of the qubit respectively. \hbar is the Planck's constant and λ is the dipole-interaction strength between the qubit and the spin coherent state. $\hat{J}^z = \sum_{i=1}^N \hat{\sigma}^z_{(i)}$ and $\hat{J}^\pm = \sum_{i=1}^N \hat{\sigma}^\pm_{(i)}$ are operators that act on the spin coherent state and $\hat{\sigma}^z_{(i)} = |e_{(i)}\rangle\langle e_{(i)}| - |g_{(i)}\rangle\langle g_{(i)}|$ acts on the independent spins that compose the spin coherent state. The constant term $\frac{\omega_N N}{2}$ is introduced so that the ground state eigenvalue of the spin coherent state Hamiltonian \hat{J}^z is zero. In our case where we are restricted to the $\frac{N}{2}$ subspace, operators \hat{J}^z and \hat{J}^\pm can be written as

$$\hat{J}^z + \frac{N}{2} = \sum_{n=0}^N n \left| \frac{N}{2}, n - \frac{N}{2} \right\rangle \left\langle \frac{N}{2}, n - \frac{N}{2} \right| \quad (2.68)$$

$$\frac{\hat{J}^+}{\sqrt{N}} = \sum_{n=0}^N \sqrt{(n+1) \left(1 - \frac{n}{N}\right)} \left| \frac{N}{2}, n + 1 - \frac{N}{2} \right\rangle \left\langle \frac{N}{2}, n - \frac{N}{2} \right| \quad (2.69)$$

$$\frac{\hat{J}^-}{\sqrt{N}} = \sum_{n=0}^N \sqrt{n \left(1 - \frac{n-1}{N}\right)} \left| \frac{N}{2}, n - 1 - \frac{N}{2} \right\rangle \left\langle \frac{N}{2}, n - \frac{N}{2} \right|. \quad (2.70)$$

The “ n ” used in this model represents the number of excitations in the system as compared to the Jaynes-Cummings model where it denotes the number of photons. Same goes to the expectation value in this model where it is given as $\bar{n} = |\zeta|^2$ for the spin coherent state.

The eigenvalues and eigenvectors of the spin coherent state Hamiltonian can be found by solving the eigenvalue equation

$$\hat{H}_N |\psi(t)\rangle_N = E |\psi(t)\rangle_N. \quad (2.71)$$

The wavefunction for the system at time t is written as

$$|\psi(t)\rangle_N = \sum_{n=0}^N a_{e,n}(t) |e, n\rangle_N + a_{g,n}(t) |g, n\rangle_N \quad (2.72)$$

and the initial state of prepared wavefunction at time $t = 0$ has the form of

$$|\Psi(0)\rangle_N = |\phi(0)\rangle_N |\psi(0)\rangle_N. \quad (2.73)$$

The initial state is used to find the eigenvalues and from there, we can find eigenstates that will give us the general time dependence. By operating the Hamiltonian in Equation (2.67) on the wavefunction in Equation (2.72), we can solve Equation (2.71). After converting the basis to be in terms of $|e, n\rangle_N$ and $|g, n+1\rangle_N$, then rearrange the equation, we get

$$\begin{aligned} \hat{H}_N |\psi\rangle_N = & \sum_{n=0}^{N-1} \left[\left(\hbar\omega_N n a_{e,n} + \frac{\hbar\Omega}{2} a_{e,n} + \hbar\lambda a_{g,n+1} \sqrt{(n+1) \left(1 - \frac{n}{N}\right)} \right) |e, n\rangle_N \right. \\ & + \left. \left(\hbar\omega_N (n+1) a_{g,n+1} - \frac{\hbar\Omega}{2} a_{g,n+1} + \hbar\lambda a_{e,n} \sqrt{(n+1) \left(1 - \frac{n}{N}\right)} \right) |g, n+1\rangle_N \right] \\ & + \hbar \left(\omega_N N + \frac{\Omega}{2} \right) a_{e,N} |e, N\rangle_N + \hbar \frac{\Omega}{2} a_{g,0} |g, 0\rangle_N. \end{aligned} \quad (2.74)$$

We can rewrite the equation above in the matrix form such that

$$\hat{H}_N |\psi\rangle_N = \sum_{n=0}^N \begin{pmatrix} \hbar\omega_N n + \frac{\hbar\Omega}{2} & \hbar\lambda \sqrt{(n+1) \left(1 - \frac{n}{N}\right)} \\ \hbar\lambda \sqrt{(n+1) \left(1 - \frac{n}{N}\right)} & \hbar\omega_N (n+1) - \frac{\hbar\Omega}{2} \end{pmatrix} |\psi\rangle_N. \quad (2.75)$$

The diagonalisation of this matrix will give us the eigenvalues as follow

$$E_{\pm, n} = \hbar\omega_N n \pm \frac{\hbar}{2} \mu_n(\delta) \quad (2.76)$$

where

$$\mu_n(\delta) = \sqrt{\delta^2 + 4\lambda^2(n+1)\left(1 - \frac{n}{N}\right)} \quad (2.77)$$

and $\delta = \Omega - \omega_N$ is the detuning between the frequency of the qubit and the frequency of the spin coherent state. The corresponding eigenvectors can be written in the form of

$$|+, n\rangle_N = \cos \phi_n |e, n\rangle_N + \sin \phi_n |g, n+1\rangle_N \quad (2.78)$$

$$|-, n\rangle_N = -\sin \phi_n |e, n\rangle_N + \cos \phi_n |g, n+1\rangle_N \quad (2.79)$$

where

$$\cos \phi_n = \frac{\mu_n(\delta) + \delta}{\sqrt{2}\sqrt{\mu_n(\delta)^2 + \delta\mu_n(\delta)}} = \frac{1}{\sqrt{2}} \left[\frac{\mu_n(\delta) + \delta}{\mu_n(\delta)} \right]^{1/2} \quad (2.80)$$

$$\sin \phi_n = \frac{\mu_n(\delta) - \delta}{\sqrt{2}\sqrt{\mu_n(\delta)^2 - \delta\mu_n(\delta)}} = \frac{1}{\sqrt{2}} \left[\frac{\mu_n(\delta) - \delta}{\mu_n(\delta)} \right]^{1/2}. \quad (2.81)$$

The resulting eigenstates will then be used to find the exact solution for the one qubit – spin coherent state model by using the time-dependent Schrödinger equation.

2.7.1 Exact Solution of the One Qubit – Spin Coherent State Model

The exact solution of the one qubit – spin coherent state model can be found by considering the time dependence of the eigenstate and solving the time-dependent Schrödinger equation given as

$$|\Psi(t)\rangle = e^{-i\hat{H}_N t/\hbar} |\Psi(0)\rangle_N. \quad (2.82)$$

The basis vectors $|e, n\rangle$ and $|g, n+1\rangle$ are transformed into the eigenvector terms in the trigonometric form

$$|e, n\rangle_N = \cos \theta_n |+, n\rangle_N - \sin \theta_n |-, n\rangle_N \quad (2.83)$$

$$|g, n+1\rangle_N = \sin \theta_n |+, n\rangle_N + \cos \theta_n |-, n\rangle_N. \quad (2.84)$$

We rewrite the wavefunction at time $t = 0$ in terms of eigenvectors as

$$|\Psi(0)\rangle_N = |\phi(0)\rangle_N |\psi(0)\rangle_N \quad (2.85)$$

$$= \sum_{n=0}^N C_n |n\rangle_N (C_e |e\rangle + C_g |g\rangle) \quad (2.86)$$

$$= \sum_{n=0}^{N-1} [C_e C_n (\cos \phi_n |+, n\rangle_N - \sin \phi_n |-, n\rangle_N) + C_g C_{n+1} (\sin \phi_n |+, n\rangle_N + \cos \phi_n |-, n\rangle_N)] + C_e C_N |e, N\rangle_N + C_g C_0 |g, 0\rangle_N \quad (2.87)$$

$$= \sum_{n=0}^{N-1} [(C_e C_n \cos \phi_n + C_g C_{n+1} \sin \phi_n) |+, n\rangle_N + (C_g C_{n+1} \cos \phi_n - C_e C_n \sin \phi_n) |-, n\rangle_N] + C_e C_N |e, N\rangle_N + C_g C_0 |g, 0\rangle_N \quad (2.88)$$

where for normalised initial states,

$$\sum_{n=0}^{N-1} |C_n|^2 = 1 \text{ and } |C_e|^2 + |C_g|^2 = 1. \quad (2.89)$$

We use this initial wavefunction to calculate $|\Psi(t)\rangle$ from Equation (2.82):

$$\begin{aligned} |\Psi(t)\rangle_N &= e^{-i\hat{H}_N t/\hbar} |\Psi(0)\rangle_N \quad (2.90) \\ &= \sum_{n=0}^N \left[e^{-i\omega_N(n+\frac{1}{2})t} \left(e^{-it\mu_n \frac{(\delta)}{2}} (C_e C_n \cos \phi_n + C_g C_{n+1} \sin \phi_n) |+, n\rangle_N \right. \right. \\ &\quad \left. \left. + e^{it\mu_n \frac{(\delta)}{2}} (C_g C_{n+1} \cos \phi_n - C_e C_n \sin \phi_n) |-, n\rangle_N \right) \right] \\ &\quad + C_e C_N e^{-it(\omega_N N + \frac{\Omega}{2})} |e, N\rangle_N + C_g C_0 e^{it\frac{\Omega}{2}} |g, 0\rangle_N. \quad (2.91) \end{aligned}$$

Then, the transformation of basis is done in the terms of $|e, n\rangle_N$ and $|g, n+1\rangle_N$ in which

$$\begin{aligned} |\Psi(t)\rangle_N &= \sum_{n=0}^{N-1} \left[e^{-i\omega_N(n+\frac{1}{2})t} \left(\left(\cos \phi_n e^{-it\mu_n \frac{(\delta)}{2}} (C_e C_n \cos \phi_n + C_g C_{n+1} \sin \phi_n) \right. \right. \right. \\ &\quad \left. \left. - \sin \phi_n e^{it\mu_n \frac{(\delta)}{2}} (C_g C_{n+1} \cos \phi_n - C_e C_n \sin \phi_n) \right) |e, n\rangle_N \right. \end{aligned}$$

$$\begin{aligned}
& + \left(\sin \phi_n e^{-it\mu_n \frac{(\delta)}{2}} (C_e C_n \cos \phi_n - C_g C_{n+1} \sin \phi_n) \right. \\
& \left. + \cos \phi_n e^{it\mu_n \frac{(\delta)}{2}} (C_g C_{n+1} C_e C_n \cos \phi_n \sin \phi_n) \right) |g, n+1\rangle_N \Big] \\
& + C_e C_N e^{-it(\omega_N N + \frac{\Omega}{2})} |e, N\rangle_N + C_g C_0 e^{it\frac{\Omega}{2}} |g, 0\rangle_N . \tag{2.92}
\end{aligned}$$

By simplifying the above equation with Euler's formula $e^{ix} = \cos x + i \sin x$, we get the following expression for the time evolution of the one qubit – spin coherent state model

$$\begin{aligned}
|\Psi(t)\rangle_N & = \sum_{n=0}^{N-1} \left[e^{-i\omega_N(n+\frac{1}{2})t} \left(\left(C_e C_n \cos \left(\frac{t}{2} \mu_n(\delta) \right) + i \sin \left(\frac{t}{2} \mu_n(\delta) \right) \right. \right. \right. \\
& \left. \left. \left(C_e C_n (\sin^2 \phi_n - \cos^2 \phi_n) - 2C_g C_{n+1} \cos \phi_n \sin \phi_n \right) \right) |e, n\rangle_N \right. \\
& \left. + \left(\left(C_g C_{n+1} \cos \left(\frac{t}{2} \mu_n(\delta) \right) + i \sin \left(\frac{t}{2} \mu_n(\delta) \right) \right) \right. \right. \\
& \left. \left. \left(C_g C_{n+1} (\cos^2 \phi_n - \sin^2 \phi_n) - 2C_e C_n \cos \phi_n \sin \phi_n \right) \right) |g, n+1\rangle_N \right] \\
& + C_e C_N e^{-it(\omega_N N + \frac{\Omega}{2})} |e, N\rangle_N + C_g C_0 e^{it\frac{\Omega}{2}} |g, 0\rangle_N . \tag{2.93}
\end{aligned}$$

Equation (2.93) will be used for the off-resonant case between the frequencies of the qubit and the spin coherent state, where the time evolution of the one qubit – spin coherent state have a non-zero value of detuning can be calculated. The case of decoherence effects will be explained in Chapter 3.

We further proceed to find the exact solution of the system by considering the case of the qubit and the spin coherent state are on resonance, where both frequencies are equal, $\Omega = \omega_N$ which means that there are no detunings in the system. The value of qubit – spin coherent state detuning is zero, $\delta = 0$ and thus from Equation (2.77) we have

$$\mu_n(0) = 2\lambda \sqrt{(n+1) \left(1 - \frac{n}{N} \right)} \tag{2.94}$$

and $\cos \phi_n = \sin \phi_n = \frac{1}{\sqrt{2}}$. The wavefunction in Equation (2.93) is then simplified into

$$\begin{aligned}
|\Psi(t)\rangle_N &= \sum_{n=0}^{N-1} \left[e^{-i\omega_N n t} \right. \\
&\left. \left(C_e C_n \cos \left(\lambda t \sqrt{(n+1) \left(1 - \frac{n}{N} \right)} \right) - i C_g C_{n+1} \sin \left(\lambda t \sqrt{(n+1) \left(1 - \frac{n}{N} \right)} \right) \right) |e, n\rangle_N \right. \\
&\left. + \left(C_g C_{n+1} \cos \left(\lambda t \sqrt{(n+1) \left(1 - \frac{n}{N} \right)} \right) - i C_e C_n \sin \left(\lambda t \sqrt{(n+1) \left(1 - \frac{n}{N} \right)} \right) \right) |g, n+1\rangle_N \right] \\
&+ C_e C_N e^{-it(\omega_N N + \frac{\Omega}{2})} |e, N\rangle_N + C_g C_0 e^{-it(\omega_N - \frac{\Omega}{2})} |g, 0\rangle_N .
\end{aligned} \tag{2.95}$$

Equation (2.95) only applies for the case of only operators are time dependent. For the case where the state vectors are also time dependent in addition with the operators, the latter has time dependence that is coming from the interaction part of the Hamiltonian, $\hat{H}_I = \frac{\hbar\lambda}{\sqrt{N}} (\hat{f}^+ \hat{\sigma}^- + \hat{f}^- \hat{\sigma}^+)$, and the vector in that interaction picture can be calculated as

$$|\Psi_I(t)\rangle_N = e^{-i\hat{H}_O t/\hbar} |\Psi(t)\rangle_N . \tag{2.96}$$

Meanwhile, the former has the time dependence that consists of the spin coherent state and the qubit parts of the Hamiltonian, which is given by $\hat{H}_O = \hat{H}_S + \hat{H}_A = \hbar\omega_N \left(\hat{J}^z + \frac{N}{2} \right) + \frac{\hbar\Omega}{2} \hat{\sigma}^z$. Hence, the time dependent terms for state vectors $|e, n\rangle$ and $|g, n+1\rangle$ are defined as

$$e^{-i\hat{H}_O t/\hbar} |e, n\rangle_N = e^{-i\omega_N \left(n + \frac{1}{2} \right) t} |e, n\rangle_N \tag{2.97}$$

$$e^{-i\hat{H}_O t/\hbar} |g, n+1\rangle_N = e^{-i\omega_N \left(n + \frac{1}{2} \right) t} |g, n+1\rangle_N \tag{2.98}$$

and then, we can do these transformations below

$$e^{-i\frac{\omega_N}{2} t} |e\rangle \rightarrow |e\rangle, \quad e^{i\frac{\omega_N}{2} t} |g\rangle \rightarrow |g\rangle, \quad e^{-i\omega_N n t} |n\rangle \rightarrow |n\rangle, \tag{2.99}$$

to obtain the exact solution for the case of zero detuning that is now given by

$$\begin{aligned}
|\Psi(t)\rangle_N &= \sum_{n=0}^{N-1} \\
&\left[\left(\left(C_e C_n \cos \left(\lambda t \sqrt{(n+1) \left(1 - \frac{n}{N} \right)} \right) - i C_g C_{n+1} \sin \left(\lambda t \sqrt{(n+1) \left(1 - \frac{n}{N} \right)} \right) \right) |e, n\rangle_N \right. \right.
\end{aligned}$$

$$\begin{aligned}
& + \left(C_g C_{n+1} \cos \left(\lambda t \sqrt{(n+1) \left(1 - \frac{n}{N}\right)} \right) - i C_e C_n \sin \left(\lambda t \sqrt{(n+1) \left(1 - \frac{n}{N}\right)} \right) \right) |g, n+1\rangle_N \Big] \\
& + C_e C_N |e, N\rangle_N + C_g C_0 |g, 0\rangle_N .
\end{aligned} \tag{2.100}$$

2.7.2 Collapse and Revival of Qubit State Probabilities

In one qubit – spin coherent state model where the spin coherent state was scaled with $\left| \frac{\zeta}{\sqrt{N}} \right\rangle_N$ studied by Dooley et al. (2014), they discovered similar phenomenon that emerged as in the one qubit Jaynes-Cummings model which is the collapse and revival of the qubit state probabilities. Similarly, the collapse happen due to the destructive interference of the individual qubits in the spin coherent state, while the revival happen due to the constructive interference of the oscillating terms (Bahari, 2018). The initial state for such interacting system that was given in Equation (2.73) then becomes

$$|\Psi(0)\rangle_N = \sum_{n=0}^N C_n \left| \frac{\zeta}{\sqrt{N}} \right\rangle_N (C_e |e\rangle + C_g |g\rangle) \tag{2.101}$$

where C_n is the coefficient for the spin coherent state in the form of

$$C_n = \sum_{n=0}^N \frac{1}{\left(1 + \frac{|\zeta|^2}{N}\right)^{N/2}} \sqrt{\frac{N!}{(N-n)! n!}} \left(\frac{\zeta}{\sqrt{N}}\right)^n \tag{2.102}$$

with $|n\rangle$ is the energy eigenstates and $\bar{n} = |\zeta|^2$ is the average excitation number in the spin coherent state. We may factorize and rewrite the solution in terms of

$$|\Psi(t)\rangle_N = |\psi_e(t)\rangle_N |e\rangle + |\psi_g(t)\rangle_N |g\rangle \tag{2.103}$$

where $|\psi_e(t)\rangle_N$ and $|\psi_g(t)\rangle_N$ are the components of the spin coherent state given by

$$|\psi_e(t)\rangle_N = \sum_{n=0}^N C_n \cos \left(\lambda t \sqrt{(n+1) \left(1 - \frac{n}{N}\right)} \right) |n\rangle \tag{2.104}$$

$$|\psi_g(t)\rangle_N = -i \sum_{n=0}^N C_n \sin \left(\lambda t \sqrt{(n+1) \left(1 - \frac{n}{N}\right)} \right) |n+1\rangle \tag{2.105}$$

and therefore, the probability of the qubit is either in ground state $|g\rangle$ or excited state $|e\rangle$ are

$$\begin{aligned}
P_g(t) &= \langle g | \hat{\rho}_q(t) | g \rangle \\
&= \frac{N!}{\left(1 + \frac{|\zeta|^2}{N}\right)^N} \sum_{n=0}^N \frac{1}{(N-n)! n!} \left(\frac{\zeta^2}{N}\right)^n \cos^2 \left(\lambda t \sqrt{(n+1) \left(1 - \frac{n}{N}\right)} \right) \quad (2.106)
\end{aligned}$$

$$\begin{aligned}
P_e(t) &= \langle e | \hat{\rho}_q(t) | e \rangle \\
&= \frac{N!}{\left(1 + \frac{|\zeta|^2}{N}\right)^N} \sum_{n=0}^N \frac{1}{(N-n)! n!} \left(\frac{\zeta^2}{N}\right)^n \sin^2 \left(\lambda t \sqrt{(n+1) \left(1 - \frac{n}{N}\right)} \right) \quad (2.107)
\end{aligned}$$

where $\hat{\rho}_q(t)$ is the reduced density matrix of the system given in Equation (2.57).

We plot the time evolution of the one qubit – spin coherent state model with zero detuning in Figure 2.2, where the event of collapse and revival is depicted as the blue-coloured line. Similar observations can be made as in the one qubit Jaynes-Cummings model, where the dynamics of the qubit state probabilities collapse and disappear after some time, and then revives at the revival time t_r .

We estimate the revival time t_r by considering the condition of $1 \ll \bar{n} \ll N$ that implies very small values of $\frac{\bar{n}}{N}$ to sustain the correlation of this model with the Jaynes-Cummings model. Given that $\bar{n} = |\zeta|^2$ and $j = 1, 2, \dots$ is a positive integer that denote the j th revival time, hence for the case of $j = 1$, the revival time of the system is approximated as

$$2\pi j = t_r (\omega_{n+1} - \omega_n) \quad (2.108)$$

$$= t_r \left(\sqrt{\delta^2 + 4\lambda^2(\bar{n} + 1) \left(1 - \frac{\bar{n}}{N}\right)} - \sqrt{\delta^2 + 4\lambda^2\bar{n} \left(1 - \frac{\bar{n} - 1}{N}\right)} \right) \quad (2.109)$$

$$\Rightarrow t_r = \frac{2\pi}{\sqrt{\delta^2 + 4\lambda^2(\bar{n} + 1) \left(1 - \frac{\bar{n}}{N}\right)} - \sqrt{\delta^2 + 4\lambda^2\bar{n} \left(1 - \frac{\bar{n} - 1}{N}\right)}} \quad (2.110)$$

2.7.3 Single Qubit Attractor State

Dooley et al. (2014) have also shown the event of attractor state of the qubit in the one qubit – spin coherent state model that corresponds to the Jaynes-Cummings model. In this model, they proposed a method to create the spin cat states within the condition of $1 \ll \bar{n} \ll N$. They also made similar observation which is at halfway to the revival time t_r , the qubit disentangles itself from the spin coherent state and evolves into an ‘attractor state’.

The attractor state is given by the yellow-coloured line in Figure 2.2. The graph starts at value 0 at $t = 0$, which indicates that there is no presence of attractor state at the beginning of interaction. At later times, we can see the line slowly moves very close towards unity at half revival time, at about $t = 18$ seconds. At this moment, the qubit disentangles itself from the spin coherent state and become the attractor state, which has the form of

$$|\psi_{1,att}^+\rangle_N = \frac{1}{\sqrt{2}}(e^{-i\phi}|e\rangle + i|g\rangle) \quad (2.111)$$

and the probability of the qubit being in this state is calculated using Equation (2.64). Similar to attractor state that happens in the Jaynes-Cummings model, this attractor state here does not depend on the initial qubit state since the initial coefficients C_e and C_g has no contributions at the beginning of interaction, but it depends on the phase of initial spin coherent state ϕ (Bahari, 2018). Hence the qubit and spin coherent state are a product state at time $\frac{t_r}{2}$ because the qubit state can be factorised out of the wavefunction.

Concurrently, the spin coherent state has now received all information about the initial qubit state, where the spin coherent state is currently in a Schrödinger cat state because of the coherent superposition of two states with opposite phase $|\frac{\zeta}{\sqrt{N}}\rangle_N$ and $|\frac{-\zeta}{\sqrt{N}}\rangle_N$ (Knight & Shore, 1993). At revival time t_r , all the information in the spin coherent state will be transferred back to the qubit. As the interaction is happening throughout time, the system evolves from a product state to an entangled state and back again to product state repeatedly. This phenomenon is described as a natural route to quantum state preparation by Gea-Banacloche (1990).

2.7.4 Linear Entropy

One more similar phenomenon that occurs in the one qubit – spin coherent state model as in the Jaynes-Cummings model is the entanglement between the qubit and the spin coherent state. Linear entropy is used to measure the entanglement in the interaction system, and the formula is given in Equation (2.65). In this model, the spin coherent state is traced over to give the reduced density matrix $\hat{\rho}_q(t)$. This number ranges from zero to unity, where they correspond to the completely pure state and maximally mixed state respectively. The qubit – spin coherent state entanglement is present when the value of entropy is greater than zero.

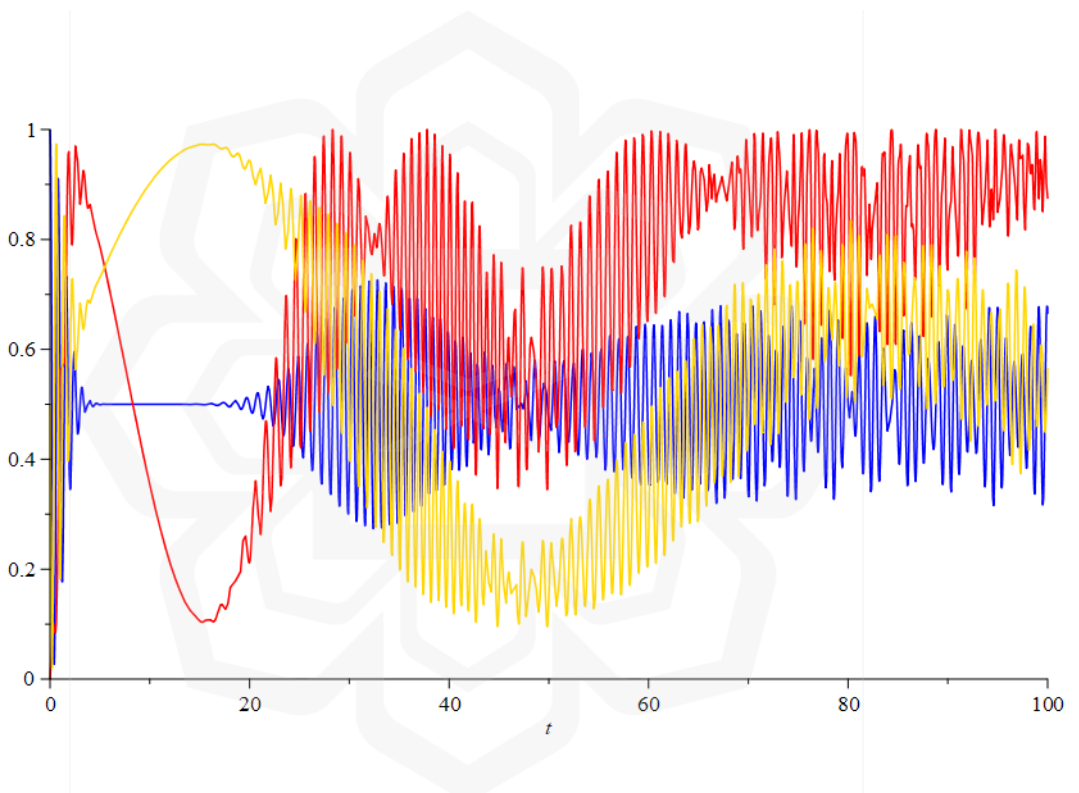


Figure 2.2: Time evolution for one qubit – spin coherent state model at zero detuning with the qubit being initially in excited state, $\lambda = 1$, $N = 120$ and $|\zeta|^2 = 16$. The probability of being in the state $|e\rangle$ is shown as the blue line, the probability of being in attractor state is shown as the yellow line, and the linear entropy is shown as the red line.

Linear entropy is represented by the red line in Figure 2.2. We can see that halfway to the revival time, at $\frac{t_r}{2}$ the line is approaching value 0, which indicates that the qubit and spin coherent state completely disentangles, the qubit gains all information about itself, and thus become an attractor state which is a pure state. Then, as the time

is approaching the revival time t_r at about $t = 33$, the line gradually approaches value 1, which means that there is a presence of entanglement between the qubit and the spin coherent state. At this moment, all information from the qubit is swapped to the spin coherent state, and the qubit becomes a mixed state. We can see a dip on the line, because the width of this dip is on a time much narrower than entropy at $\frac{t_r}{2}$. To prevent this, we can put higher value of $N \rightarrow \infty$ in the numerical calculation so that the value of entropy at this time can get closer to zero and agrees with the analytical predictions.

2.8 BLOCH SPHERE

A geometric representation of a single qubit state is called the Bloch Sphere, named after Felix Bloch (Nielsen & Chuang, 2010). In this representation, a pure state is depicted by a point on the surface of the unit sphere, while a mixed state is depicted by a point inside the unit sphere (Banacloche, 1992). This implies that the knowledge about what each system is actually doing is lost as the point advances from the sphere's surface to its interior. The origin of the sphere's coordinate represents a maximally mixed state.

Meanwhile, the sphere's north pole represents the upper energy eigenstate of the system, and the south pole represents the lower energy eigenstate (Banacloche, 1992). In the case of a qubit interaction system, the north pole and south pole corresponds to the excited state and the ground state of the system respectively. The state on the equator of the sphere corresponds to the coherent superposition of the qubit and the field with equal weights. Generally, any point at the opposite ends of any diameter on the sphere depicts a pure state. An explanation to plot the Bloch Sphere is discussed further in Chapter 3.

Although the Bloch Sphere gives a good representation for a qubit system, it is however having a limitation of no simple generalization for multiple qubit systems.

2.9 MAJORANA SPHERE

The Majorana description of a general spin state was first discovered by Ettore Majorana in 1932 (Majorana, 1932), and further studies have been made over time since then (Bacry, 1974; Leboeuf, 1991; Zimba, 2006). Majorana Sphere geometrically represents the state of an arbitrary spin as the number of spin-1/2 systems. This representation is actually a generalized case of the Riemann sphere (Griffiths & Harris, 2014). Majorana Sphere representation is not as direct as the Bloch Sphere, because it takes a product state, projects it into the symmetric subspace and all states that corresponds to the symmetric subspace are uniquely generated up to the order of β_k where $k = 1, 2 \dots$ and β_k is identical to the number of qubits. In this work, we will use the symbol β instead of β_1 as we only focus on the case of a single qubit.

The north pole corresponds to $\beta = 0$ and the south pole represents $\beta = \infty$. We can also say that the north pole indicates that the excited state $|e\rangle$ and the ground state $|g\rangle$ is located at the south pole. The right most point indicates $\beta = 1$, providing that $(|e\rangle + |g\rangle)/\sqrt{2}$ while the left most point indicates $\beta = -1$, providing that $(|e\rangle - |g\rangle)/\sqrt{2}$. The general state of a single spin-1/2 particle can be written as the linear combination

$$|\psi\rangle = a|e\rangle + b|g\rangle \quad (2.112)$$

$$= \mathcal{N}(|e\rangle + \beta|g\rangle). \quad (2.113)$$

The ratio $\beta = \frac{b}{a}$ uniquely describes the state $|\psi\rangle$ and it can take on any value in the complex plane, including ∞ . Here, \mathcal{N} is the normalization factor. The benefit of using Majorana Sphere is that it can be used to represent the time evolution of the qubit state probabilities for multiple qubits case (Jarvis, 2009; Devi, Sudha & Rajagopal, 2012), and recently it can also represent a three-level system or qutrit (Dogra, Vepsäläinen, & Paroanu, 2020). Nevertheless, this work only focuses on the case of a single qubit system. A detailed explanation on plotting the Majorana Sphere is discussed further in Chapter 3 as well.

CHAPTER 3

RESEARCH METHODOLOGY

3.1 WORKFLOW OF RESEARCH

Figure 3.1 below shows the workflow of the research methodology. Literature reviews were conducted, and necessary information was gathered, especially on prior works that discuss about the one qubit – spin coherent state model.

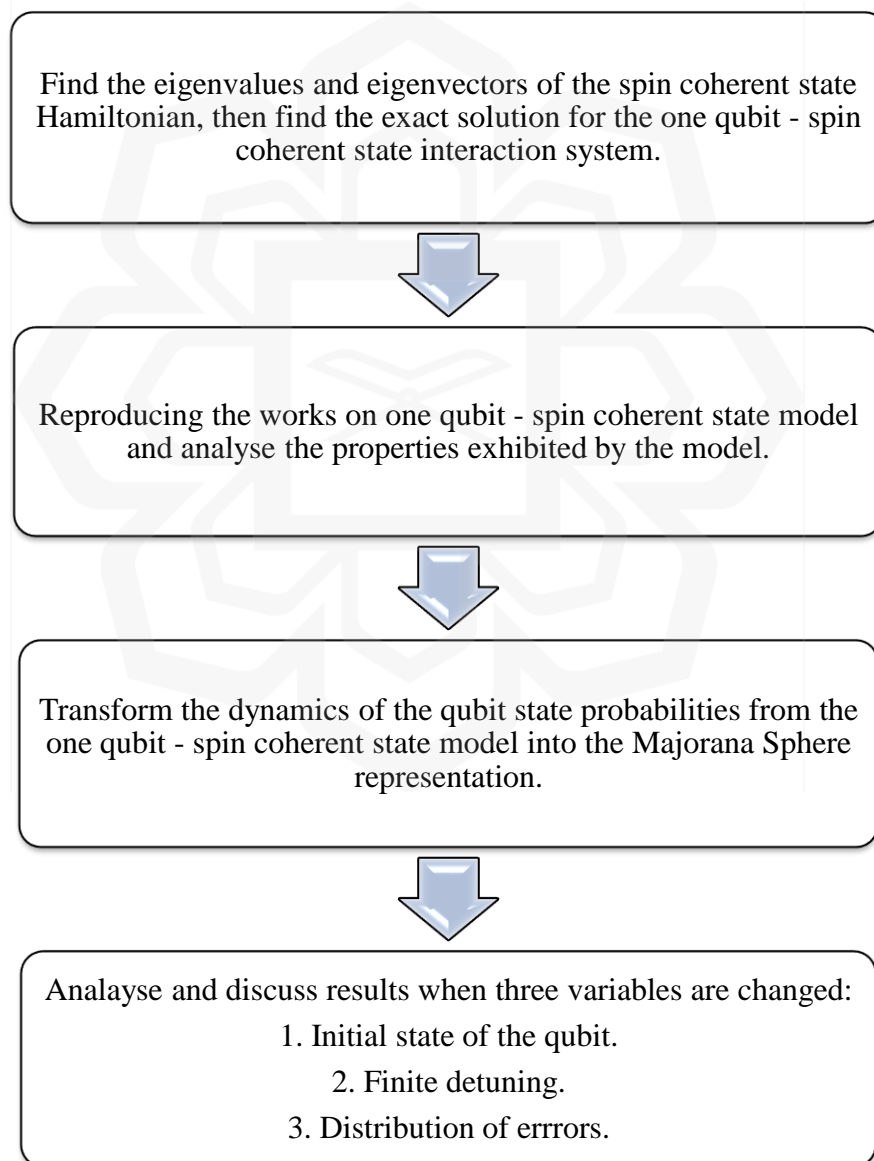


Figure 3.1: Workflow of the research.

3.2 METHODOLOGY

We started our research by doing analytical calculation to solve the eigenvalue problem that was given in Equation (2.71) by using the total approximation of the spin coherent state Hamiltonian given in Equation (2.67). After finding the eigenvalues and eigenvectors, we proceed to find the exact solution by solving the time dependence of the eigenstates using the time dependent Schrödinger equation.

Due to the problems of having large number of variables, it was not possible to just work on analytical calculation. Instead, we used MAPLE programming software to help us with the numerical calculation method, for example to calculate the probability of the qubit is either in the excited state or ground state given in Equation (2.106) and Equation (2.107). Hence, we were able to work more efficiently.

We also utilized MAPLE programming software to plot several graphs to represent the time evolutions of the qubit state probabilities. We managed to reproduce the work on one qubit – spin coherent state model (Dooley et al., 2014; Bahari, 2018) where we observed many interesting phenomena such as collapse and revival of the qubit state probabilities, the attractor state, the entanglement between the qubit and the field, and the occurrence of the Schrödinger cat state. In this work, we focused more on the event of collapse and revival of the qubit state probabilities.

After that, we proceed our research by representing the time evolution of the single qubit state in the Majorana Sphere representation by using MAPLE programming software. We used the analyzed time evolution of the qubit state in the one qubit – spin coherent state model and illustrate the dynamics of the qubit state as a Majorana Sphere representation. The formulation to plot the Majorana Sphere is further explained in the next section. We changed the initial state of the qubit and observed the differences that occur with every initial qubit state. The representations for each initial qubit state were then analyzed and interpreted. We then extend our research by considering the decoherence effects, where we divided it into two parts which are to analyze the effect of having finite value of detuning to the system, and using distribution of errors to model realistic error in practical system. Last but not least, we established a relevant conclusion related to our objectives, and provide a few recommendations for future works.

3.2.1 Bloch Sphere Transformation

Any pure state $|\psi\rangle$ can be written as a superposition of the ket vectors $|e\rangle$ and $|g\rangle$, which are the basis states that indicate the excited and ground state of the system respectively. Thus, $|\psi\rangle = a|e\rangle + b|g\rangle$ and due to normalization $|a|^2 + |b|^2 = 1$, we can rewrite $|\psi\rangle$ as follows

$$|\psi\rangle = e^{i\omega} \left(\cos\frac{\theta}{2} |e\rangle + e^{i\phi} \sin\frac{\theta}{2} |g\rangle \right), \quad (3.1)$$

with

$$0 \leq \theta \leq \pi, \quad 0 \leq \phi \leq 2\pi. \quad (3.2)$$

Since the state is normalized to one, $\langle\psi|\psi\rangle = 1$ so $|\psi\rangle$ is a unit vector. The global phase vector $e^{i\omega}$ can be ignored as it has no observable effects. Using spherical coordinates, the parameters θ and ϕ are used to define a point on the three-dimensional sphere. For pure state, the rotations of the Bloch Sphere can be described by the rotation matrices

$$\hat{R}^x(\theta) \equiv e^{-i\theta\hat{\sigma}_x/2}, \quad \hat{R}^y(\theta) \equiv e^{-i\theta\hat{\sigma}_y/2}, \quad \hat{R}^z(\theta) \equiv e^{-i\theta\hat{\sigma}_z/2} \quad (3.3)$$

which with different combinations of them will give different rotations (Jarvis, 2009). $\hat{\sigma}_x$, $\hat{\sigma}_y$, and $\hat{\sigma}_z$ are the Pauli matrices. On the other hand, mixed states cannot be written as a quantum state vector, instead it is represented as a density matrix ρ , with the relation to the Bloch Sphere coordinates as shown below.

$$\hat{\rho}_{Bloch} = \frac{1}{2} \begin{pmatrix} 1 + s_3 & s_1 - is_2 \\ s_1 + is_2 & 1 - s_3 \end{pmatrix} = \frac{1}{2} (\hat{I}_2 + \vec{s} \cdot \vec{\sigma}) \quad (3.4)$$

where \hat{I}_2 is the 2×2 identity matrix. Vector $\vec{s} = \{s_1, s_2, s_3\}$ is the Bloch vector, and $\vec{\sigma}$ is the three component vector of the Pauli matrices. s_1 , s_2 and s_3 are the coordinates for the Bloch Sphere representation, and they can be expressed in terms of θ and ϕ :

$$s_1 = \gamma \sin \theta \cos \phi \quad (3.5)$$

$$s_2 = \gamma \sin \theta \sin \phi \quad (3.6)$$

$$s_3 = \gamma \cos \theta \quad (3.7)$$

where γ is the distance of point $\{s_1, s_2, s_3\}$ from the center of sphere. We can see this formula gives a point on the surface of unit sphere for a pure state, $\gamma = 1$ and a point inside the unit sphere for a mixed state, $\gamma \leq 1$.

3.2.2 Majorana Sphere Transformation

As mentioned in Section 2.9, the value $\beta = b/a$ can take on any value in the complex plane, including infinity. This ratio is represented by performing stereographic projection from the south pole of a Riemann sphere to the Argand plane through the equator.

For the stereographic projection, the equation of a line that passes through point β is given as

$$\frac{x}{\Re(\beta)} = \frac{y}{\Im(\beta)} = z + 1 = l. \quad (3.8)$$

From the equation above, the coordinates of the point on the sphere are then as follows

$$x = l \Re(\beta) \quad (3.9)$$

$$y = l \Im(\beta) \quad (3.10)$$

$$z = l - 1 \quad (3.11)$$

where l is the length of the line. Note that a point on a sphere has the relation $|x|^2 + |y|^2 + |z|^2 = 1$. Thus, the value l can be defined as

$$l = \frac{2}{\Re(\beta)^2 + \Im(\beta)^2 + 1}. \quad (3.12)$$

Finally, a point on the Majorana Sphere has the following coordinates

$$x = \frac{2\Re(\beta)}{1 + \Re(\beta)^2 + \Im(\beta)^2} \quad (3.13)$$

$$y = \frac{2\Im(\beta)}{1 + \Re(\beta)^2 + \Im(\beta)^2} \quad (3.14)$$

$$z = \frac{1 - \Re(\beta)^2 - \Im(\beta)^2}{1 + \Re(\beta)^2 + \Im(\beta)^2}. \quad (3.15)$$

Plotting a single point might be effortless, but it is not the case if there are multiple points. For this case, a density matrix must be used. The density matrix for a pure one qubit on the Majorana Sphere is given as (Jarvis, 2009)

$$\hat{\rho}_\beta = \frac{1}{1 + |\beta|^2} \begin{pmatrix} 1 & \beta^* \\ \beta & |\beta|^2 \end{pmatrix} \quad (3.16)$$

while for a single mixed state, it can be represented as many combinations of different pure states as presented in Equation (2.21), and for this case it is given as

$$\hat{\rho}_\beta = \sum_i \frac{P_i}{1 + |\beta|^2} \begin{pmatrix} 1 & \beta^* \\ \beta & |\beta|^2 \end{pmatrix} \quad (3.17)$$

where $|\psi_i\rangle$ is a pure state and P_i is a probability. In this study, the exact solution of the one qubit – spin coherent state model is used to find the associate density matrix to the respective Majorana Sphere plotting. Then the density matrix will be used to plot the time evolution of the qubit state probabilities of the system in which after setting the basis in terms of $|e, n\rangle_N$ and $|g, n\rangle_N$, the β value is given as β_{SCSM} below:

$$\begin{aligned} \beta_{SCSM} = & \sum_{n=0}^{N-1} \left(C_g C_n \cos\left(\frac{t}{2} \mu_n(\delta)\right) \right. \\ & + i \sin\left(\frac{t}{2} \mu_n(\delta)\right) (C_g C_n (\cos^2 \phi_n - \sin^2 \phi_n) - 2C_e C_{n-1} \cos \phi_n \sin \phi_n) \\ & / C_e C_n \cos\left(\frac{t}{2} \mu_n(\delta)\right) \\ & \left. + i \sin\left(\frac{t}{2} \mu_n(\delta)\right) (C_e C_n (\sin^2 \phi_n - \cos^2 \phi_n) - 2C_g C_{n+1} \cos \phi_n \sin \phi_n) \right) \end{aligned} \quad (3.18)$$

where $\delta = \Omega - \omega_N$, $\mu_n(\delta)$ is given by Equation (2.77), and $\cos \phi_n$ as well as $\sin \phi_n$ are respectively given in Equation (2.80) and Equation (2.81). The Majorana points for the case of zero detuning can be calculated by using Equation (2.100), and hence Equation (3.18) is further simplified to

$$\beta_{SCSM} = \sum_{n=0}^{N-1} \frac{C_g C_n \cos\left(\lambda t \sqrt{(n)\left(1 - \frac{n-1}{N}\right)}\right) - i C_e C_{n-1} \sin\left(\lambda t \sqrt{(n)\left(1 - \frac{n-1}{N}\right)}\right)}{C_e C_n \cos\left(\lambda t \sqrt{(n+1)\left(1 - \frac{n}{N}\right)}\right) - i C_g C_{n+1} \sin\left(\lambda t \sqrt{(n+1)\left(1 - \frac{n}{N}\right)}\right)}. \quad (3.19)$$

The value of coefficient C_e and C_g depends on the initial condition of the qubit state, and C_n is given in Equation (2.102). Later in Chapter 4, the value of C_e and C_g will be initialized to observe the dynamics of the qubit state probabilities inside the Majorana Sphere with different initial qubit state.

3.2.3 Bloch Sphere and Majorana Sphere Equivalency

For a single qubit case, Bloch Sphere and Majorana Sphere are anonymous to one another. We can check this equivalency by evaluating the relationship between both density matrices. The relation between pure states density matrices for both Bloch Sphere and Majorana Sphere can be written as

$$\hat{\rho} = \frac{1}{2} \begin{pmatrix} 1 + s_3 & s_1 - i s_2 \\ s_1 + i s_2 & 1 - s_3 \end{pmatrix} = \frac{1}{1 + |\beta|^2} \begin{pmatrix} 1 & \beta^* \\ \beta & |\beta|^2 \end{pmatrix}. \quad (3.20)$$

By using Equation (3.13) to Equation (3.15), we arrived at

$$x = \frac{2\Re(\beta)}{1 + \Re(\beta)^2 + \Im(\beta)^2} = \frac{\beta^* + \beta}{1 + |\beta|^2} = s_1 \quad (3.21)$$

$$y = \frac{2\Im(\beta)}{1 + \Re(\beta)^2 + \Im(\beta)^2} = i \frac{(\beta^* - \beta)}{1 + |\beta|^2} = s_2 \quad (3.22)$$

$$z = \frac{2(t-1)}{1 + \Re(\beta)^2 + \Im(\beta)^2} = \frac{1 - |\beta|^2}{1 + |\beta|^2} = s_3. \quad (3.23)$$

Meanwhile for mixed state, we examine the density matrix for Majorana Sphere representation first. Recall that its density matrix can be written as multiple combinations of pure states. In this section, we will prove the equivalency between both spheres by using two pure states β_1 and β_2 . The density matrix can then be written as

$$\hat{\rho} = \lambda_1 |e_1\rangle\langle e_1| + \lambda_2 |e_2\rangle\langle e_2| \quad (3.24)$$

$$= \frac{\lambda_1}{1 + |\beta_1|^2} \begin{pmatrix} 1 & \beta_1^* \\ \beta_1 & |\beta_1|^2 \end{pmatrix} + \frac{\lambda_2}{1 + |\beta_2|^2} \begin{pmatrix} 1 & \beta_2^* \\ \beta_2 & |\beta_2|^2 \end{pmatrix}. \quad (3.25)$$

Eigenvectors of a state are orthogonal, so $\beta_2 = -\frac{1}{\beta_1^*}$ and Equation (3.25) becomes

$$\hat{\rho}_\beta = \frac{1}{1 + |\beta_1|^2} \begin{pmatrix} \lambda_1 + \lambda_2 |\beta_1|^2 & (\lambda_1 - \lambda_2) \beta_1^* \\ (\lambda_1 - \lambda_2) \beta_1 & \lambda_1 |\beta_1|^2 + \lambda_2 \end{pmatrix} \quad (3.26)$$

and then, the eigenvalues are rewritten as $\lambda_1 = \frac{1+\delta}{2}$ and $\lambda_2 = \frac{1-\delta}{2}$ and we get

$$\hat{\rho}_\beta = \frac{1}{2} \begin{pmatrix} 1 & 0 \\ 0 & 1 \end{pmatrix} + \frac{\delta}{2(1 + |\beta_1|^2)} \begin{pmatrix} 1 - |\beta_1|^2 & 2\beta_1^* \\ 2\beta_1 & -(1 - |\beta_1|^2) \end{pmatrix}. \quad (3.27)$$

The spherical coordinates (θ, ϕ) of a point are related to β by $\beta = e^{i\phi} \tan \frac{\theta}{2}$. Thus,

$$\hat{\rho}_\beta = \frac{1}{2} \begin{pmatrix} 1 & 0 \\ 0 & 1 \end{pmatrix} + \frac{\delta}{2 \left(1 + \tan^2 \frac{\theta}{2}\right)} \begin{pmatrix} 1 - \tan^2 \frac{\theta}{2} & 2e^{-i\phi} \tan \frac{\theta}{2} \\ 2e^{i\phi} \tan \frac{\theta}{2} & -\left(1 - \tan^2 \frac{\theta}{2}\right) \end{pmatrix} \quad (3.28)$$

$$= \frac{1}{2} \begin{pmatrix} 1 & 0 \\ 0 & 1 \end{pmatrix} + \frac{\delta}{2} \begin{pmatrix} \cos \theta & \cos \phi \sin \theta - i \sin \phi \sin \theta \\ \cos \phi \sin \theta + i \sin \phi \sin \theta & -\cos \theta \end{pmatrix} \quad (3.29)$$

which is basically just spherical coordinates in Bloch Sphere as in Equation (3.5) to Equation (3.7). With $\delta = \lambda_1 - \lambda_2 = \gamma$, we arrive to the equivalency between mixed states density matrices for both Bloch Sphere and Majorana Sphere as

$$\hat{\rho}_\beta = \frac{1}{2} \begin{pmatrix} 1 & 0 \\ 0 & 1 \end{pmatrix} + \frac{1}{2} \begin{pmatrix} s_3 & s_1 - is_2 \\ s_1 + is_2 & -s_3 \end{pmatrix} \quad (3.30)$$

$$= \frac{1}{2} (\hat{I}_2 + \vec{s} \cdot \vec{\sigma}) \quad (3.31)$$

where \hat{I}_2 is the 2×2 square identity matrix. Thus, it has been proven that Bloch Sphere and Majorana Sphere are equivalent for the case of a single qubit.

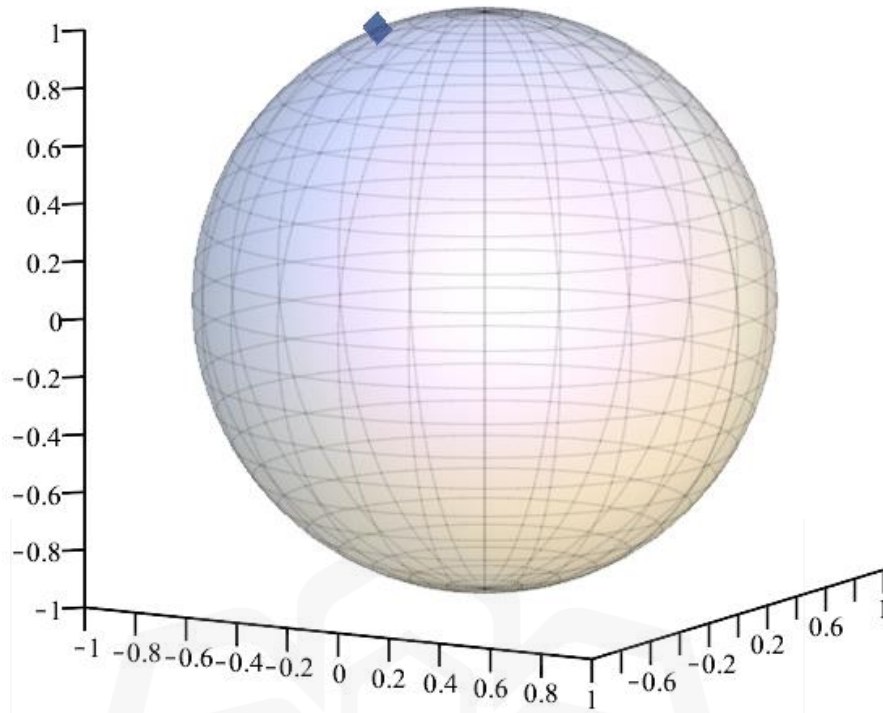


Figure 3.2: A single pure state on Majorana Sphere.

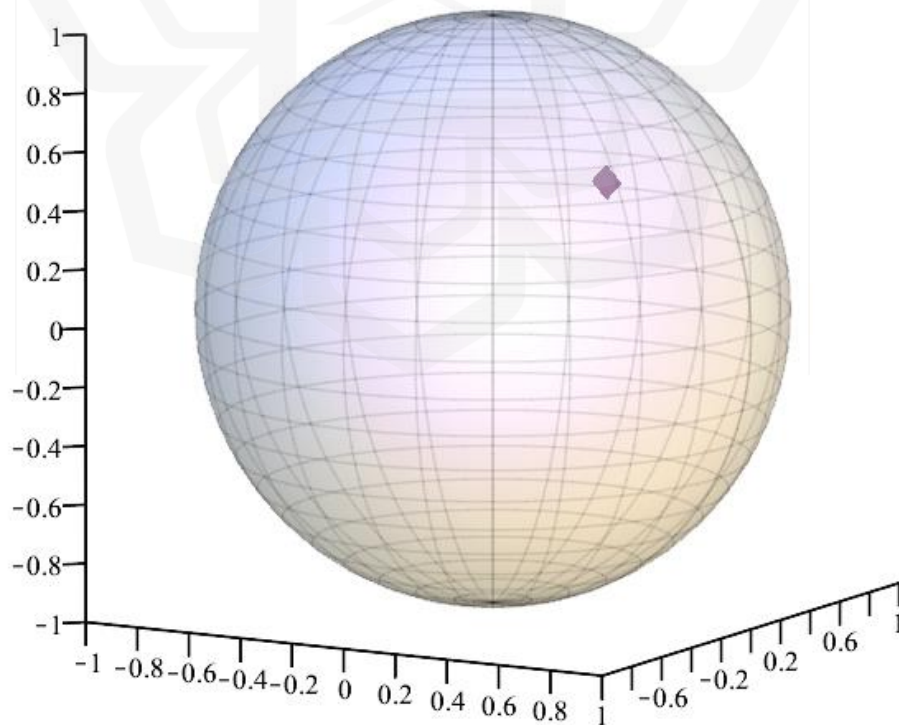


Figure 3.3: A single mixed state on Majorana Sphere.

Figure 3.2 illustrates the representation of a single qubit pure state on Majorana Sphere. It is shown that the point is located on the surface of the sphere, and this indicates that it is a pure state. On the other hand, Figure 3.3 shows a mixed state being transformed into the Majorana Sphere. This is done by combining many pure states to generate a single mixed state. It can clearly be seen that the point is now located inside the sphere, which agrees that it is indeed a mixed state. In this research, we will only be focusing on the Majorana Sphere. So throughout this work, the only discussion that will be made is only on one qubit transformation under the Majorana Sphere representation.

3.2.4 Decoherence Effects

In an actual system, there is a presence of decoherence where there will always a possibility for an error to occur due to unknown detunings that may led to some disturbance in the system. This research considers the decoherence effect for the case of an ideal system with zero detuning, but contingent to a distribution of potential errors. We used the Gaussian distribution to average over the frequency differences δ with an error distribution width Δ .

We set the Gaussian distribution to be centralized at an expectation value zero $\delta = 0$ and standard deviation Δ . The error is written as (Bahari et al., 2018)

$$f(\delta|0, \Delta) = \frac{1}{\Delta\sqrt{2\pi}} e^{-\frac{\delta^2}{2\Delta^2}} \quad (3.32)$$

where δ is the error sampled over a range of its standard deviation. Generally, to analyse the system we need to do an integral over all δ , so that the density matrix of the qubit for all of the δ values can be evaluated by averaging the density matrix over the errors such that

$$\hat{\rho}_q(\Delta) = \int_{-\infty}^{\infty} d\delta f(\delta|0, \Delta) \hat{\rho}_q(t, \delta) . \quad (3.33)$$

However, due to the problem of it cannot be done analytically, we then use an approximation to this integral which includes an adequately large number of δ . In other

words, we choose a discrete approximation approach to this ensemble of system which is in the form of

$$\hat{\rho}_q(\Delta) \approx \sum_{\delta_i} \frac{f(\delta_i|0, \Delta) \hat{\rho}_q(t, \delta_i)}{\sum_{\delta_i} f(\delta_i|0, \Delta)} \quad (3.34)$$

where i stipulates the number of discrete events. We consider a sufficient number in the spacing δ so that there is only a little error between our approximation and the analytic integral over all δ given by Equation (3.33). This brings us to Figure 3.4, where we can see in subfigure (b) that as the value is set to $i = 31$, the line curve is closely resembling the actual continuous distribution in subfigure (a) which means that $i = 31$ is sufficient to approximate the Gaussian distribution.

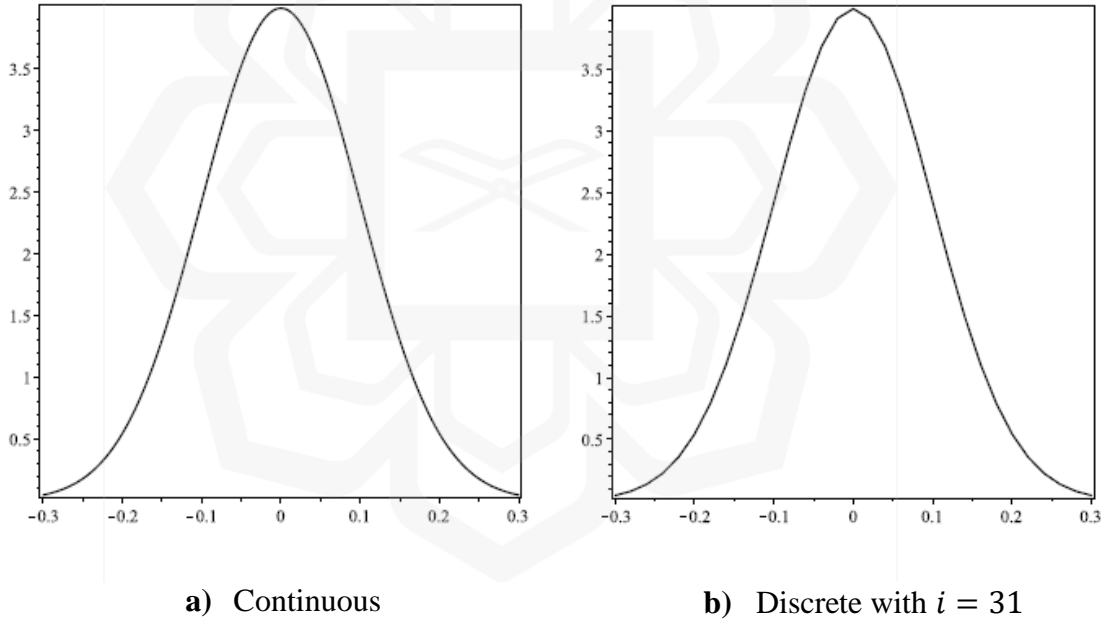


Figure 3.4: Plots of Gaussian distribution where the distribution given by Equation (3.33) is centered at an expectation value zero $\delta = 0$ and standard deviation $\Delta = 0.3$.

In Section 2.7, the eigenvalues and eigenvectors of the one qubit – spin coherent state model have been calculated. The solution for Hamiltonian was then obtained from Equation (2.67) in the form of Equation (2.93) for the case of non-zero detuning. After applying the state transformation given in Equation (2.99), we simplify the solution as

$$\begin{aligned}
|\Psi(t)\rangle_N = & \sum_{n=0}^{N-1} \left[\left(C_e C_n \cos\left(\frac{t}{2}\mu_n(\Delta)\right) + i \sin\left(\frac{t}{2}\mu_n(\Delta)\right) \right. \right. \\
& \left. \left. (C_e C_n (\sin^2 \phi_n - \cos^2 \phi_n) - 2C_g C_{n+1} \cos \phi_n \sin \phi_n) \right) |e, n\rangle_N \right. \\
& + \left(C_g C_{n+1} \cos\left(\frac{t}{2}\mu_n(\Delta)\right) + i \sin\left(\frac{t}{2}\mu_n(\Delta)\right) \right. \\
& \left. \left. (C_g C_{n+1} (\cos^2 \phi_n - \sin^2 \phi_n) - 2C_e C_n \cos \phi_n \sin \phi_n) \right) |g, n+1\rangle_N \right] \\
& + C_e C_N e^{-it(\omega_N N + \frac{\Omega}{2})} |e, N\rangle_N + C_g C_0 e^{it\frac{\Omega}{2}} |g, 0\rangle_N
\end{aligned} \tag{3.35}$$

where $\delta = \Omega - \omega_N$ and $\mu_n(\delta)$ is given by Equation (2.77). $\cos \phi_n$ and $\sin \phi_n$ were stated in Equation (2.80) and Equation (2.81) respectively. Equation (3.35) will be used to investigate and demonstrate the effect of decoherence in the interaction system, and the points will be plotted in the Majorana Sphere by using Equation (3.18).

CHAPTER 4

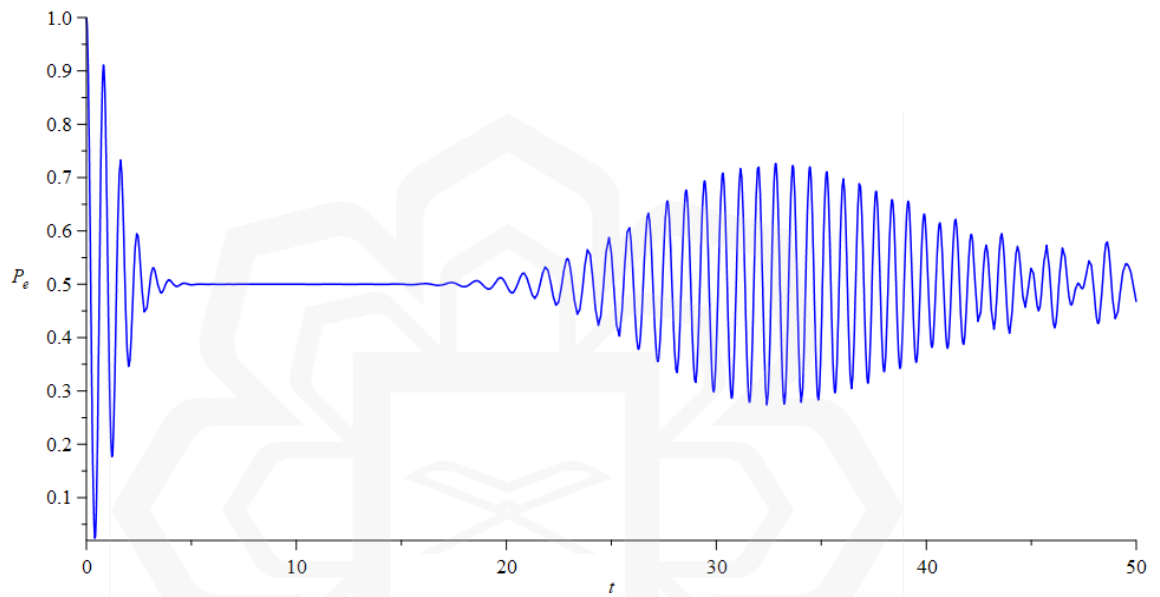
RESULTS AND DISCUSSIONS

4.1 COLLAPSE AND REVIVAL OF THE QUBIT STATE PROBABILITIES IN ONE QUBIT – SPIN COHERENT STATE MODEL AT ZERO DETUNING

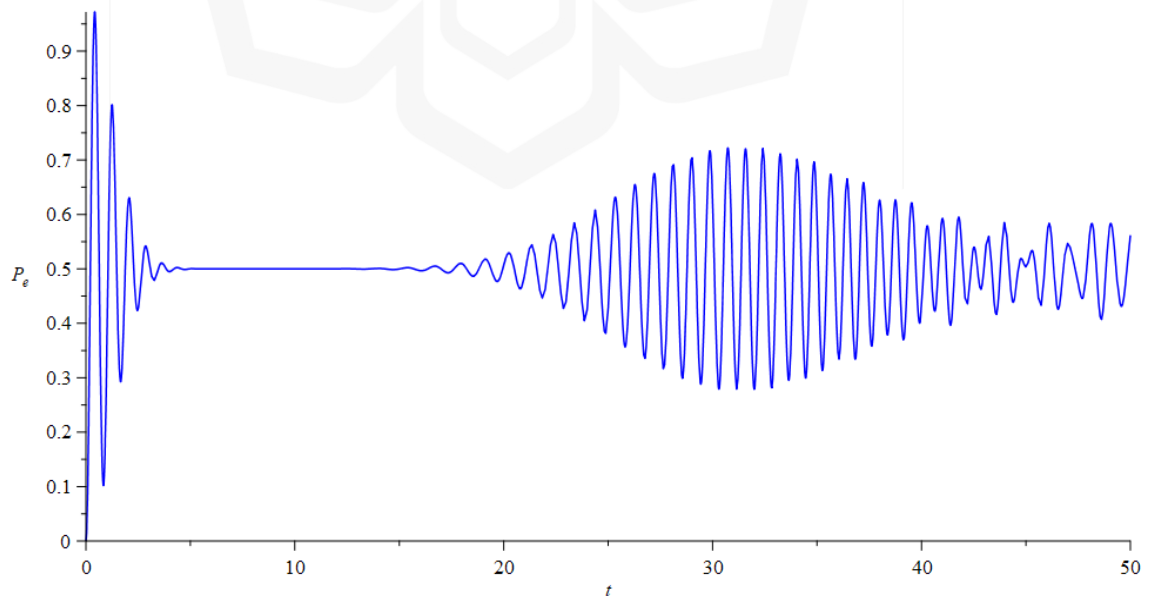
Among all the interesting events that occur in the one qubit – spin coherent state model, the collapse and revival activity of the qubit state probabilities is mainly focused. In this section, the qubit and the spin coherent state are allowed to interact at an equal frequency, thus zero detuning in the system. Figure 4.1 displays the collapse and revival activity in the spin coherent state model for one complete oscillation from time $t = 0$ to $t = 50$ seconds, for three different initial states. The y-axis depicts the probability of the qubit being in the excited state, while the x-axis represents the period of time in seconds. Only a small portion of time of the event is chosen for the purpose of comparing it with the Majorana Sphere representation in the next section.

Figure 4.1 a) shows the dynamics of the qubit state probabilities when we set the qubit being initially in the excited state, and therefore the coefficient of the qubit state given by Equation (2.89) are $C_e = 1$ and $C_g = 0$. We can see that at time $t = 0$, the probability of the qubit being in the excited state is at value 1, which is consistent with its initial state. The time evolution of the state of the qubit can be seen to collapse until at $t = 3$ seconds, the probability of the qubit state remains constant at value 0.5 for a few seconds. At this period of time, the qubit is experiencing an entanglement with the spin coherent state, where the initial information about the qubit state is now being conveyed into the spin coherent state. Thus, the probability of the qubit state has a value of 0.5 indicating mixed information of being in either excited state or ground state. Later at $t = 18$ seconds, the dynamics of the qubit begins to revive back, as a result of disentanglement between the qubit and the spin coherent state, thus the qubit regains its complete information about its initial state. This revival of the qubit state probability reaches a peak at revival time t_r , where in this case the revival time is roughly at $t = 33$ seconds. The collapse and revival activity of the qubit state probability occurs periodically at later times.

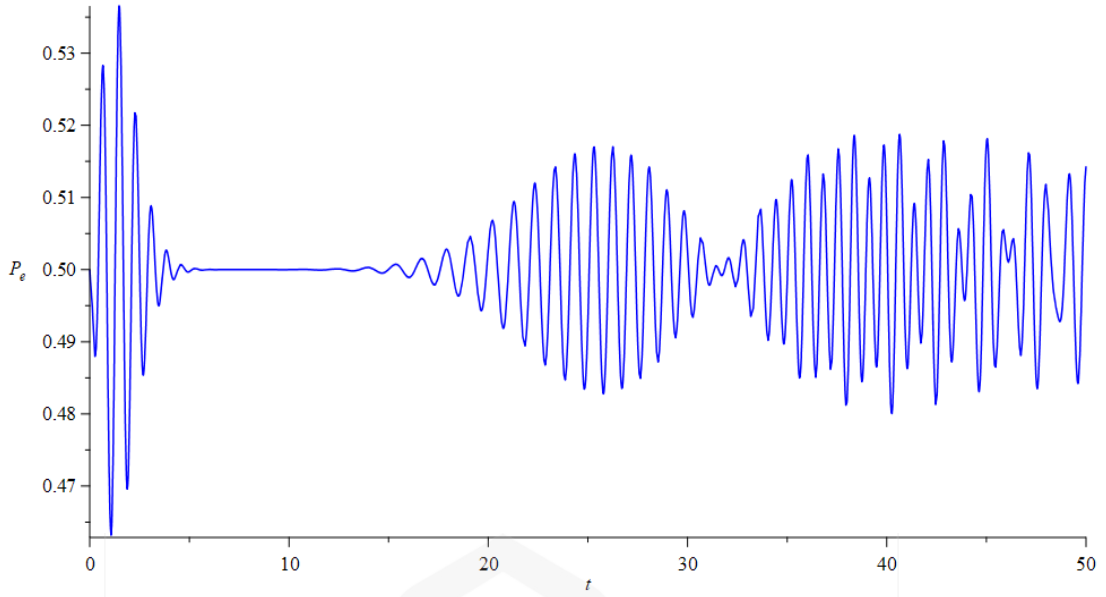
Alternatively, when the initial condition is set for the ground state, $C_e = 0$ and $C_g = 1$, the dynamics of the qubit state probabilities are shown in Figure 4.1 b). At time $t = 0$, we can see the probability of the qubit being in the excited state is at value 0, indicating that it is indeed at the ground state. After that, the dynamics collapse at $t = 3$ seconds before remains constant at value 0.5 as a result of entanglement and the process of information transfer from the qubit to the spin coherent state, then revives back at $t = 17$ seconds and reaches peak at revival time $t = 31$ seconds.



a) $C_e = 1$ and $C_g = 0$



b) $C_e = 0$ and $C_g = 1$



c) $C_e = \frac{1}{\sqrt{2}}$ and $C_g = \frac{1}{\sqrt{2}}$

Figure 4.1: The dynamics of the qubit state probabilities in the one qubit – spin coherent state model at zero detuning from $t = 0$ to $t = 50$ seconds, $\lambda = 1$, $N = 120$ and $|\zeta|^2 = 16$ with three different initial states.

Figure 4.1 c) shows the dynamics of the qubit state probabilities when the initial condition is set to be an equal probability between the excited state and ground state, and therefore $C_e = \frac{1}{\sqrt{2}}$ and $C_g = \frac{1}{\sqrt{2}}$. If the scale of the y-axis is large, we would not see the significant collapse and revival activity of the qubit state probabilities. But when we lower the scale of the y-axis, we can see that at $t = 0$, the point starts at value 0.5 before oscillating. The dynamics of the qubit state probabilities collapses first at about $t = 4$ seconds and remains constant at value 0.5, then revives back at about $t = 15$ seconds before reaching peak revival at $t = 26$ seconds. Although the dynamics seems to have a series of collapse and revival activities, there are actually no significant observations that can be made as the qubit state probabilities fluctuate very minimal around a constant value 0.5. The state of the qubit almost does not change from the beginning although the qubit had an interaction with the spin coherent state. The qubit stays as a mixed excited and ground state as a result of entanglement between the qubit and the spin coherent state.

4.2 MAJORANA SPHERE REPRESENTATION OF THE QUBIT STATE PROBABILITIES AT ZERO DETUNING

4.2.1 Initial State $C_e = 1, C_g = 0$

Figure 4.2 below displays the Majorana Sphere representation when we set the qubit being in the excited state for one complete oscillation. The points inside and on the sphere represents the dynamics of the probability of the qubit state. We set the time from $t = 0$ to $t = 50$ seconds and divided the period into four parts shown in Figure 4.2 a) until Figure 4.2 d) to further analyze the collapse and revival activity of the qubit state probabilities.

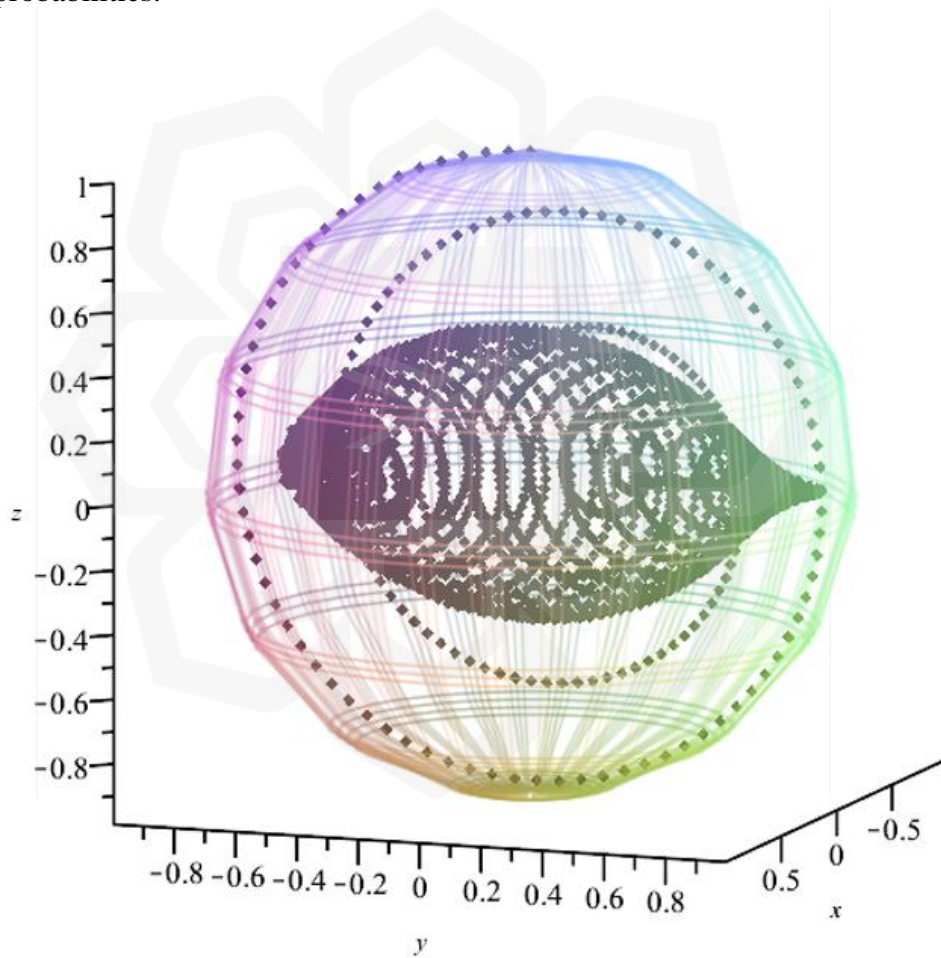


Figure 4.2: Majorana Sphere representation for initial qubit state $C_e = 1, C_g = 0$ with $\lambda = 1, N = 120$ and $|\zeta|^2 = 16$ from time $t = 0$ to $t = 50$ seconds.

In Figure 4.2 a), we can see the point starts at value 1 and it is on the sphere's surface. The rotation vector \mathbf{R} of the starting point has coordinate $\mathbf{R} = (0,0,1)$,

indicating that it is at the sphere's north pole which corresponds to the excited state of the system. Since it is at the surface of the sphere, we know that at time $t = 0$ the qubit is in a pure state, where the qubit contains the complete information about itself being in the excited state. This corresponds to the fact that a spin coherent state system always starts in a pure state. As we can see from Figure 4.1 a), the qubit state is rapidly changing as time evolves, the dynamics of the qubit state probability begins to collapse, and this is shown in Figure 4.2 a) by the swirl which gradually moves towards the center of the sphere, indicating that the qubit is entering the phase of mixed state because there is an occurrence of entanglement between the qubit and the spin coherent state.

From Figure 4.1 a), after the collapse time, the dynamics shows a constant value of 0.5 from time $t = 3$ to $t = 18$ seconds. This brings us to Figure 4.2 b) where we can see the dynamics remains constant for a few seconds and at the end of this particular period, we see the point approaches the surface of the sphere at point $\mathbf{R} = (0,1,0)$, which corresponds to another pure state, known as the attractor state of the qubit. As the point is moving from the center of the sphere, a very mixed state, to the surface of the sphere, a pure state, this means that the qubit and the spin coherent state are almost ready to be disentangled, and the qubit regains its complete information about the state.

The revival activity of the qubit that starts after $t = 18$ seconds in Figure 4.1 a) is represented in the Majorana Sphere representation in Figure 4.2 c). The point on the sphere reverses its movement and again, starts to move spirally from the surface towards the center of the sphere. It is noted that there are more oscillations on this first revival than the initial Rabi oscillation because its structure is more complicated. The state of the qubit is getting more mixed as it moves to the center, because the qubit is experiencing an entanglement with the spin coherent state. A maximally mixed state is represented by the origin of coordinates.

At the time of the second collapse in Figure 4.1 a), the revival oscillations shown in Figure 4.2 c) have again stopped. Figure 4.2 d) shows the oscillations of the second collapse of the qubit state probability. This time the point is gradually moving to the point at $\mathbf{R} = (0, -1, 0)$, which corresponds to the second attractor state. The qubit and the spin coherent state are ready to be disentangled, and the qubit regains its complete information about the state. The oscillations of the collapse and revival activities continue to occur inside the sphere at later times.

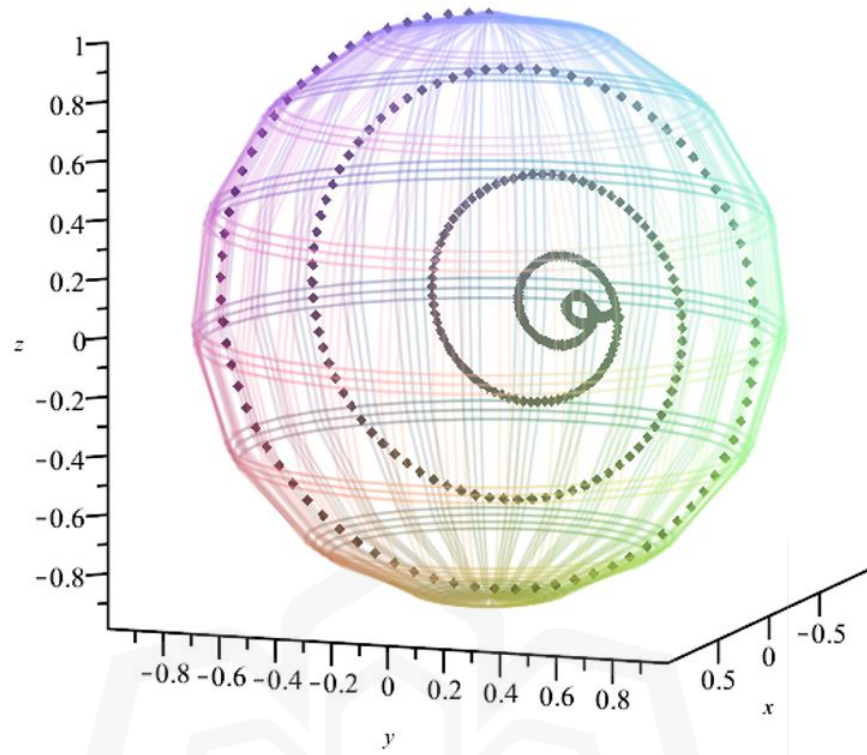


Figure 4.2 a): Period $0 \leq t \leq 5$ seconds.

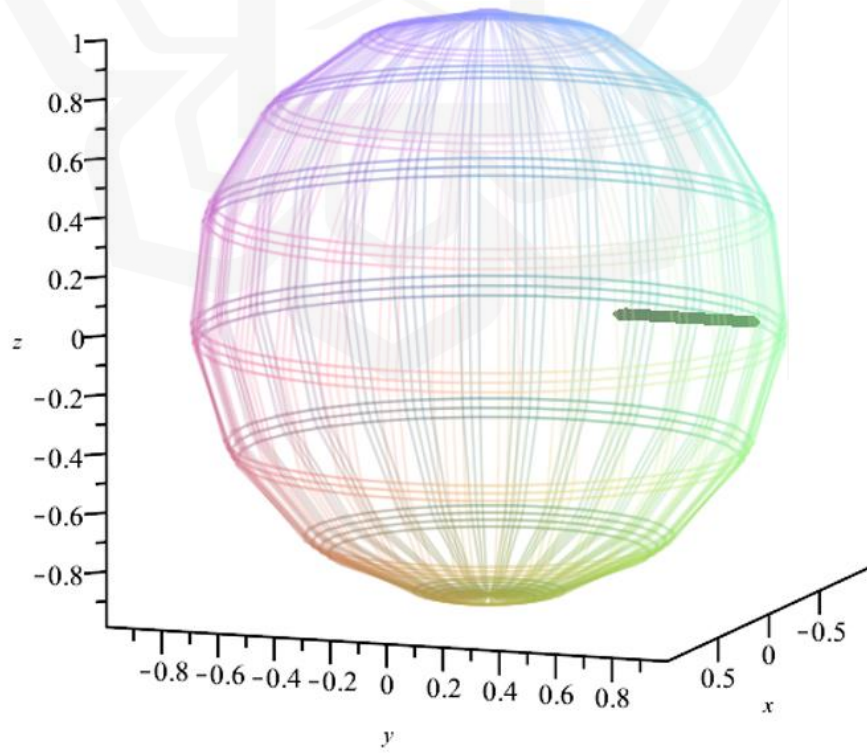


Figure 4.2 b): Period $5 \leq t \leq 15$ seconds.

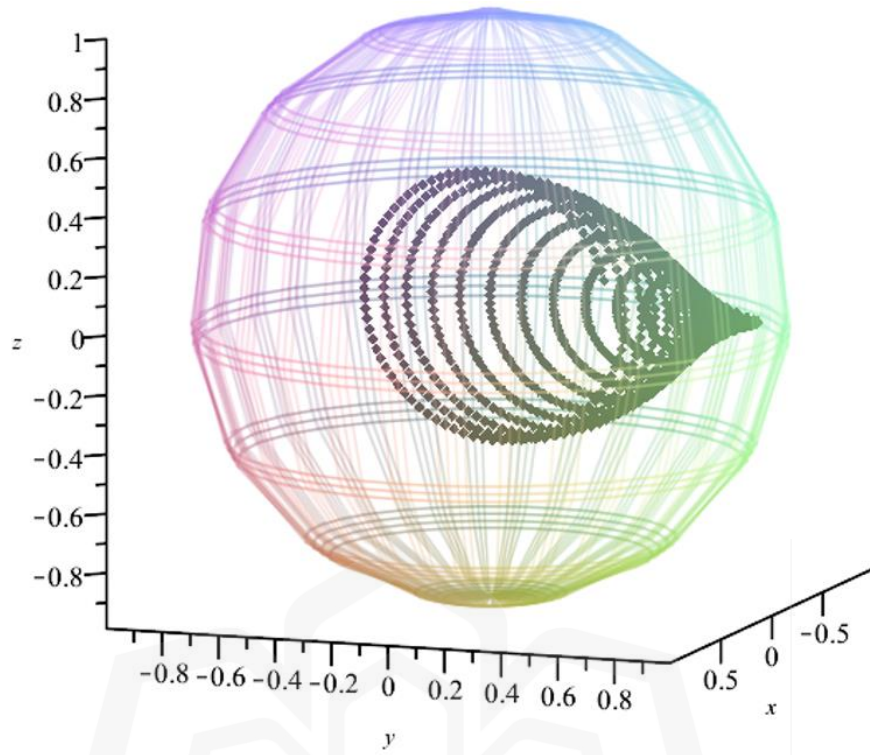


Figure 4.2 c): Period $15 \leq t \leq 33$ seconds.

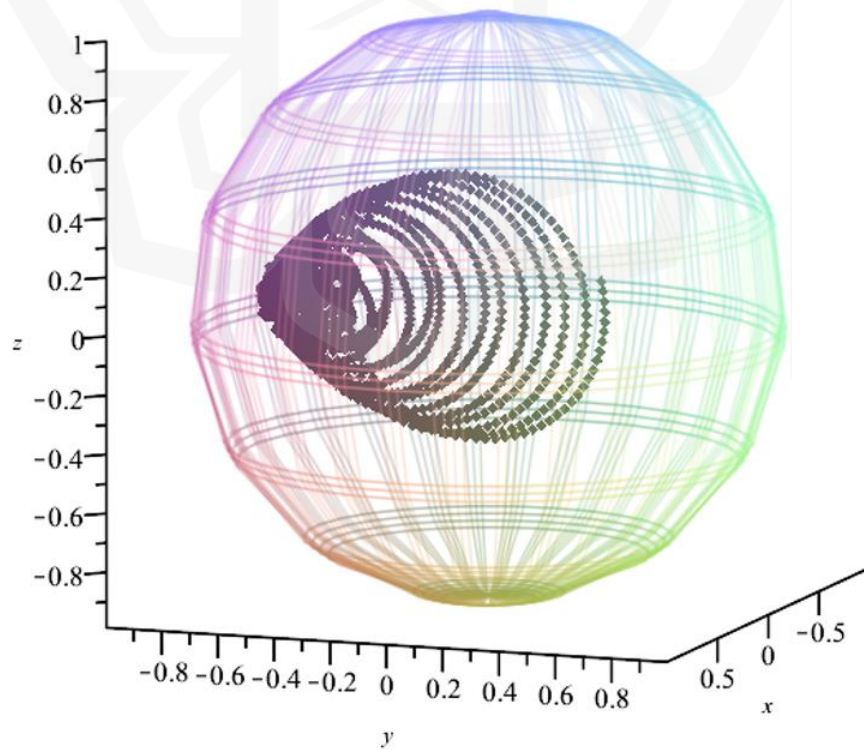


Figure 4.2 d): Period $33 \leq t \leq 50$ seconds.

4.2.2 Initial State $C_e = 0, C_g = 1$

The Majorana Sphere representation when we set the qubit being in the ground state for one complete oscillation is shown in Figure 4.3 below from time $t = 0$ to $t = 50$ seconds. We will compare this figure with Figure 4.1 b) and provide an explanation on the time evolution of the qubit state probability that has been divided to four periods shown in Figure 4.3 a) until Figure 4.3 d).

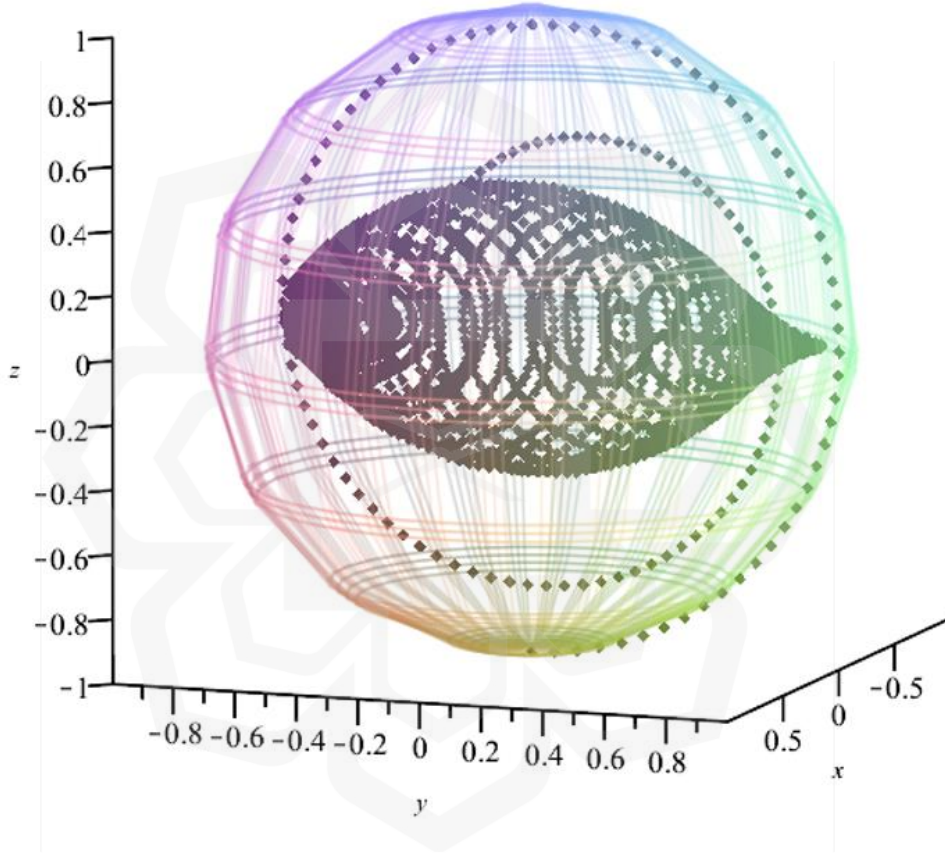


Figure 4.3: Majorana Sphere representation for initial qubit state $C_e = 0, C_g = 1$ with $\lambda = 1, N = 120$ and $|\zeta|^2 = 16$ from time $t = 0$ to $t = 50$ seconds.

Based on Figure 4.1 b), we see the initial period of Rabi oscillations, where the qubit starts at the ground state before oscillating, and then collapses until at about time $t = 3$ seconds. In the Majorana Sphere representation shown in Figure 4.3 a), we can see the point starts at value -1 , and it is at the sphere's surface. The rotation vector \mathbf{R} of the starting point has the coordinate $\mathbf{R} = (0, 0, -1)$, indicating that it is at the sphere's south pole which corresponds to the ground state of the system. We know the qubit is

in pure state at time $t = 0$ since it is at the surface of the sphere; hence it contains complete information about itself being in the ground state. As time evolves, the points gradually swirl towards the center of the sphere, indicating that the dynamics of the qubit state probability collapses and the qubit is entering the phase of mixed state as a result of entanglement between the qubit and the spin coherent state.

After the collapse time, the dynamics in Figure 4.1 b) shows an equal probability of the qubit being in either the excited state or ground state from time $t = 3$ seconds to $t = 17$ seconds. For the same time frame the state of the qubit is represented using Majorana Sphere shown in Figure 4.3 b), where we can see the dynamics remains constant for a few seconds and at the end of this particular period, we see the points approaches the surface of the sphere at point $\mathbf{R} = (0,1,0)$, which corresponds to the attractor state of the system. This indicates that the qubit and spin the coherent state are almost ready to be disentangled as the point moves from the center of the sphere, which is a very mixed state, to the surface of the sphere, which is a pure state.

Figure 4.3 c) shows the consistency of the revival activity in Majorana Sphere representation with the revival oscillations in Figure 4.1 b) that begins after $t = 17$ seconds. The point on the sphere in Figure 4.3 c) reverses direction and once again begins to swirl from the surface to the center of the sphere that portrays a maximally mixed state. The construction of this first revival swirl is more intricate compared to the initial Rabi oscillation, hence there are more oscillations. As the point is approaching the center of the sphere, the state of the qubit is getting more mixed because there is an occurrence of entanglement between the qubit and the spin coherent state. The dynamics of the revival of the qubit state probability reaches the peak at the end of this particular period.

This revival oscillation had halted at the time of the second collapse depicted in Figure 4.1 b). After that, the dynamics collapses again and the oscillations of the second collapse of the qubit state probability is shown in Figure 4.3 d). The point is slowly moving approaching the surface of the sphere to the point at $\mathbf{R} = (0, -1, 0)$, which corresponds to the second attractor state of the system. The qubit and the spin coherent state are now ready to be disentangled, and the qubit regains its complete information about the state. The recurrent collapse and revival activity of the qubit state probabilities can be observed over longer periods of time.

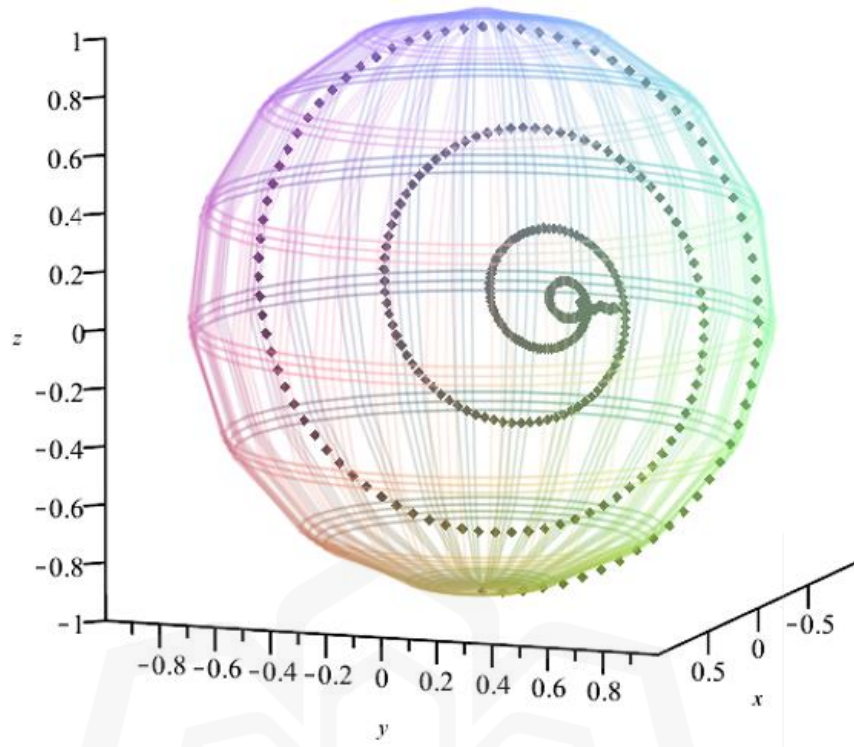


Figure 4.3 a): Period $0 \leq t \leq 5$ seconds.

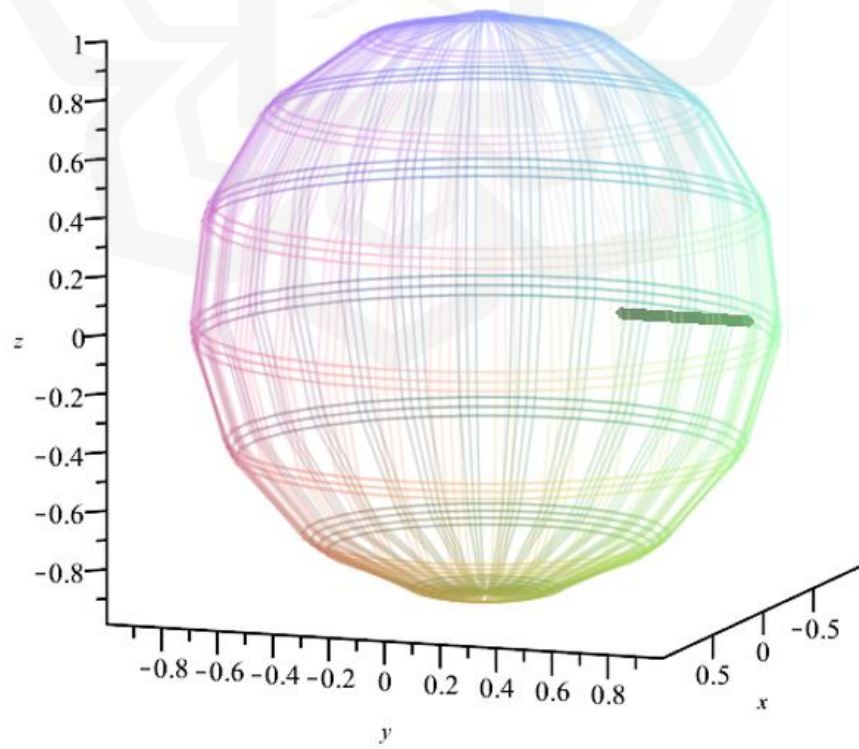


Figure 4.3 b): Period $5 \leq t \leq 15$ seconds.

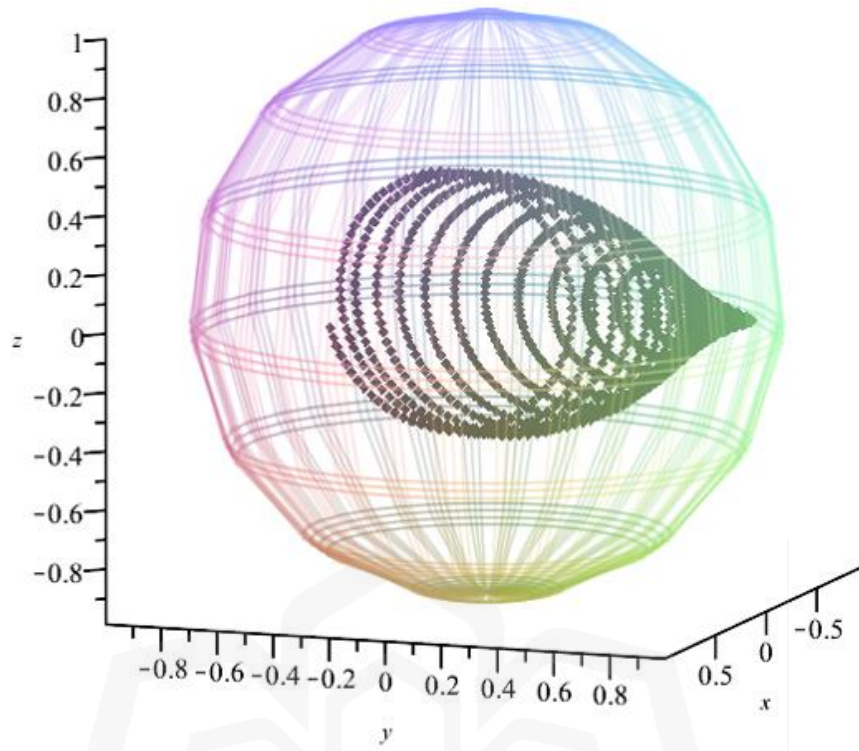


Figure 4.3 c): Period $15 \leq t \leq 31$ seconds.

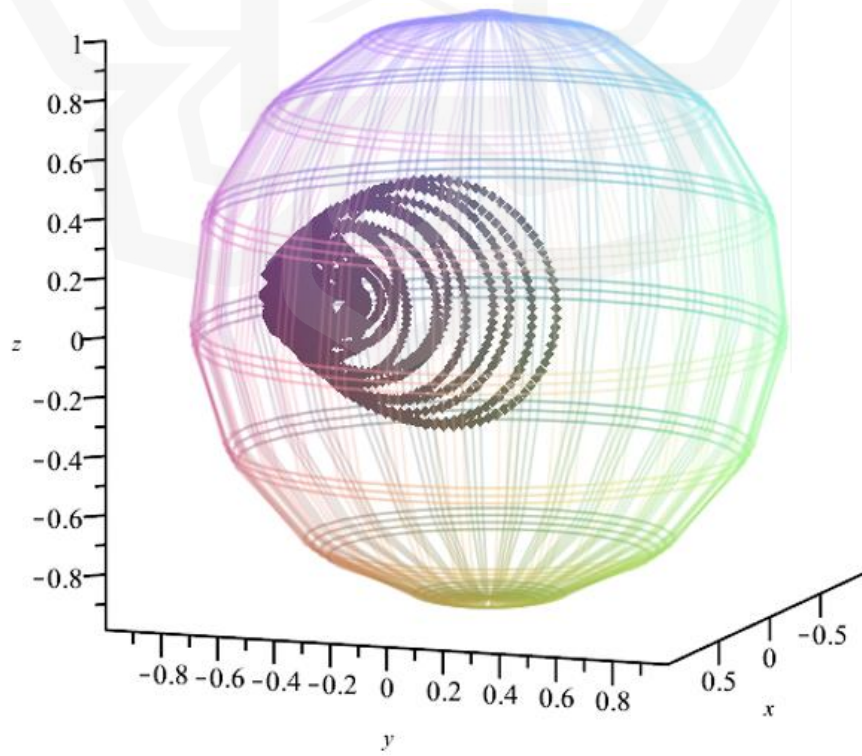


Figure 4.3 d): Period $31 \leq t \leq 50$ seconds.

4.2.3 Initial State $C_e = \frac{1}{\sqrt{2}}, C_g = \frac{1}{\sqrt{2}}$

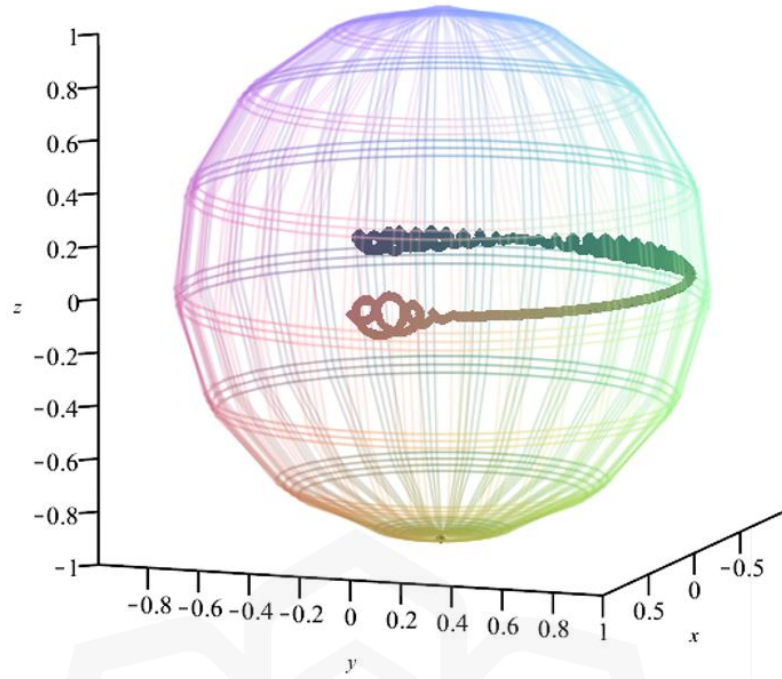
Figure 4.4 illustrates the Majorana Sphere representation when we set the initial condition to be an equal probability between both the excited state and ground state, $C_e = C_g = \frac{1}{\sqrt{2}}$ for two periods of time.

Referring to Figure 4.1 c), it can be observed that the collapse and revival activity of the dynamics of the qubit state probabilities happens at a minimal scale. The probability only remains at constant value 0.5 as if there is no effect from the interaction between the qubit and the spin coherent state.

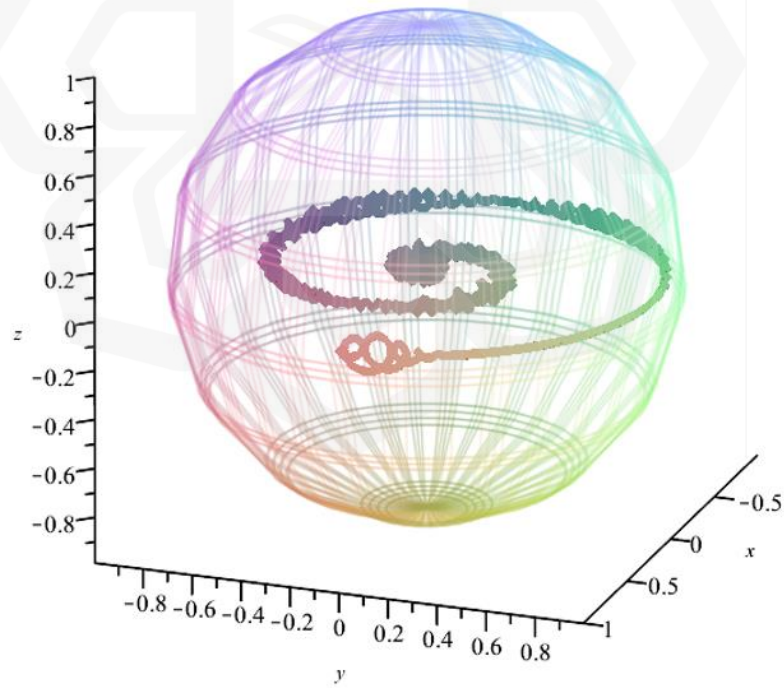
In Figure 4.4 the starting point is at the sphere's surface and has the rotation vector $\mathbf{R} = (1,0,0)$. It is evident that the points did not displays a significant spiral movement that depicts the collapse and revival activity of the qubit state probabilities. The state of the qubit almost does not change although the qubit has an interaction with the spin coherent state.

We can see in Figure 4.4 that the points just move around in a circle in the plane $z = 0$, but at a longer period of time, the point spirals into the center of the sphere as shown in Figure 4.4 b). This explains that the qubit and the spin coherent state are becoming more entangled as the points moves inside the sphere. Eventually after a long period of time, the point stays at the center of the sphere, which means that the entanglement between the qubit and the spin coherent state are maximal.

By comparing the two-dimensional line curve graph with the three-dimensional Majorana Sphere representation, it can be plainly seen that the Majorana Sphere provides a helpful pictorial representation of the qubit state. Both figures are required since they display different things, but together these two figures give a thorough graphical description of the system's evolution over time.



a) Period $0 \leq t \leq 50$ seconds.



b) Period $0 \leq t \leq 200$ seconds.

Figure 4.4: Majorana Sphere representation for initial qubit state $C_e = C_g = \frac{1}{\sqrt{2}}$ with $\lambda = 1$, $N = 120$ and $|\zeta|^2 = 16$ for two different periods.

4.3 MAJORANA SPHERE REPRESENTATION OF THE QUBIT STATE PROBABILITIES WITH DECOHERENCE EFFECTS

In the previous sections, we have considered the Majorana Sphere representation for the one qubit – spin coherent state model where the condition for both frequencies in the Hamiltonian are in resonant. To put it differently, the system is allowed to progress with zero detuning in the frequencies of the qubit and the spin coherent state, so $\delta = \Omega - \omega_N = 0$. In this section, the consequences of having non-zero values of detuning between the frequencies in the system, $\delta \neq 0$ will be investigated. The condition of the qubit being initially in the excited state as will be chosen as reference, hence $C_e = 1, C_g = 0$. The first part of this section will reproduce the work done by Bahari et al. (2018) to explain the influence of finite frequency detunings to the time evolution of the system, and we will observe the non-resonant attributes to the dynamics of the qubit state probabilities in the Majorana Sphere representation. In the second part of this section, we further our research by considering the time evolution of one qubit – spin coherent state model with decoherence effects, where we will do different treatments on the frequency detuning in the system.

4.3.1 Finite Detuning

Finite detuning occurs when the system interacts with the environment. This interaction causes a finite difference between the frequency of the qubit Ω , and the frequency of the spin coherent state ω_N . This difference can be explained by considering two situations in which the qubit is initially in the excited and ground states. When the qubit is initially in excited state, finite detuning occurs when the emitted photon does not release the same energy into the spin coherent state, as compared to the system's lowest possible energy. While when the qubit is initially in ground state, finite detuning happens because the energy of the absorbed photon is not exactly the energy required for the qubit to become excited.

The time evolution of a one qubit – spin coherent state model being initially in the excited state for various values of detuning δ are shown in Figure 4.5. From the figure, it can be seen that the revival peaks and the average for the qubit state probabilities to be in the excited state increase together with the increment in the value

of detuning δ . This behavior displays the high likeliness of the qubit to remain in its starting initial state for the case of high detuning. It is also evident that the revival time for high detuning system such as $\delta = 25$ and $\delta = 50$ take way longer time to be achieved in comparison with the lower detuning case. We can calculate the revival time, t_r for each value of detuning δ by using Equation (2.110), and we tabulate the results in Table 4.1 below.

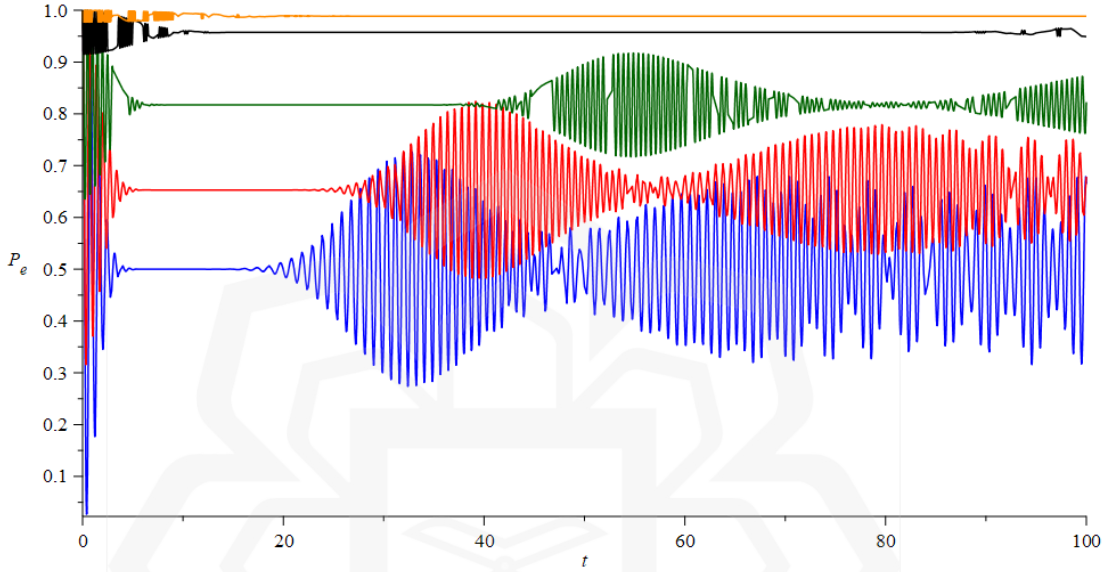


Figure 4.5: The time evolution of one qubit – spin coherent state model being initially in excited state, $\lambda = 1$, $N = 120$, $|\zeta|^2 = 16$ with different values of detuning δ . The blue line shows $\delta = 0$, red $\delta = 5$, green $\delta = 10$, black $\delta = 25$ and orange $\delta = 50$.

Table 4.1: The revival time t_r of the qubit state probabilities for respective value of detuning δ .

Value of detuning, δ	Colour of line curve	Revival time, t_r (s)
0	Blue	32.47
5	Red	38.90
10	Green	53.76
25	Black	111.92
50	Orange	216.65

The Majorana Sphere representation for the time evolution of the qubit state initially at excited state for $\delta = 0$ was shown previously in Figure 4.2 for time $t = 0$ to $t = 50$ seconds, and displayed again here in Figure 4.6 at different viewpoints.

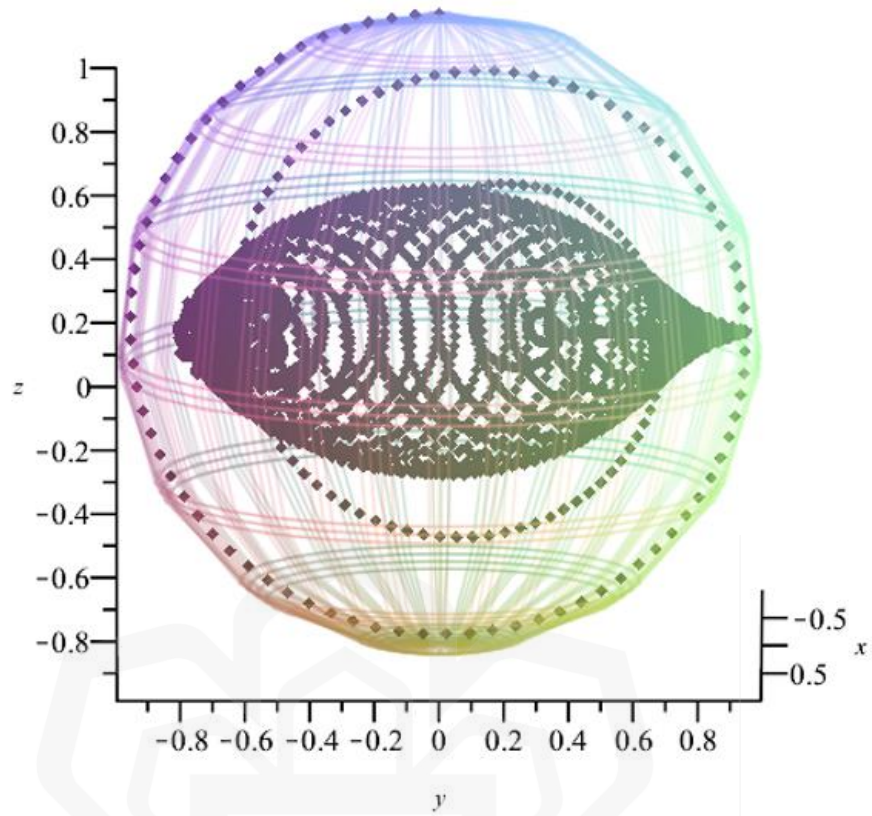


Figure 4.6: Majorana Sphere representation for qubit initially in excited state with $\lambda = 1$, $N = 120$ and $|\zeta|^2 = 16$ from time $t = 0$ to $t = 50$ seconds for $\delta = 0$.

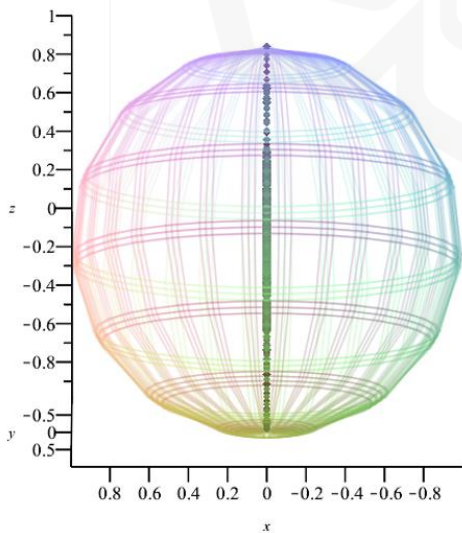


Figure 4.6 a): Rotated horizontally.

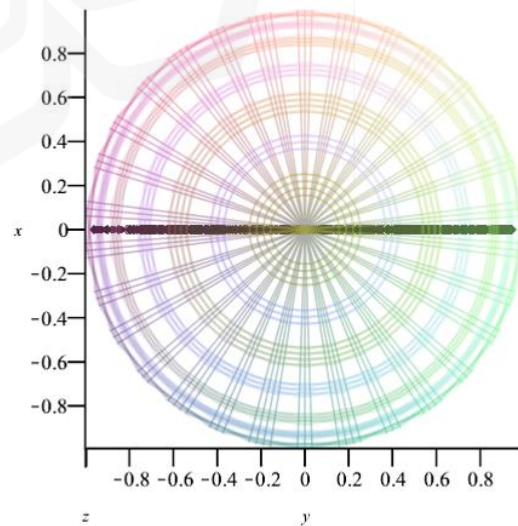


Figure 4.6 b): Rotated vertically.

From the explanation in section 4.2.1, the dynamics of the qubit state probabilities go through the three points which are the point for the initial excited state $(0,0,1)$, the point for the first attractor state $(-\sin \theta, \cos \theta, 0)$, and the point for the second attractor state $(\sin \theta, -\cos \theta, 0)$. From these values, we find that in the zero detuning case, the trajectory will always be in the plane $x \cos \theta + y \sin \theta = 0$ and all the points in Figure 4.6 lie in the plane $x = 0$ for all time as $\theta = 0$.

Figure 4.7 shows the Majorana Sphere representation for the one qubit – spin coherent state model with $\delta = 5$. The qubit is set to be initially in the excited state and the time is set from $t = 0$ to $t = 60$ seconds to let the system evolves for one complete oscillation. The point starts off at the north pole of the sphere at coordinate $(0,0,1)$ which signifies that the qubit is initially in its excited state. Then, the dynamics of the qubit state probabilities collapses and it is indicated in the sphere where the points swirl towards the center of the sphere. The points stop spiralling at $z = 0.3$, where as can be seen in Figure 4.7 a) there is a constant horizontal dynamic which means that the qubit is in a mixed state due to entanglement between the qubit and the spin coherent state. Afterwards, a spiral is developed and this represents the revival activity of the qubit state probabilities. At a later time, the qubit state probabilities collapse once again and this phenomena of ‘collapse and revival’ occur continuously as time evolves.

The shape made by the trajectory in Figure 4.7 nearly look like Figure 4.6, but for this case it is somehow more squeezed towards the sphere’s north pole or the excited level of the qubit, indicating that the qubit is hardly to be found in the sphere’s south pole or the ground state of the qubit. This happens because the qubit that starts in the excited state does not liberate enough energy to the spin coherent state, making it more likely to stay in its excited state over time. Figure 4.7 shows that the points are in a good distance inside the sphere, which indicates that the qubit does not reach the attractor state in comparison with the earlier zero detuning case where the single qubit achieves attractor state twice in the span of 50 seconds. This tells us that for this $\delta = 5$ case, the qubit and the spin coherent state hardly undergo maximal disentanglement and causes the qubit to always stays in a mixed state after $t = 0$. As viewed in Figure 4.7 a) and Figure 4.7 b), the trajectory does not lie flat in the vertical plane as it now spans through the x -axis. The points in the sphere also appears to be a bit scattered after we increase the value of detuning.

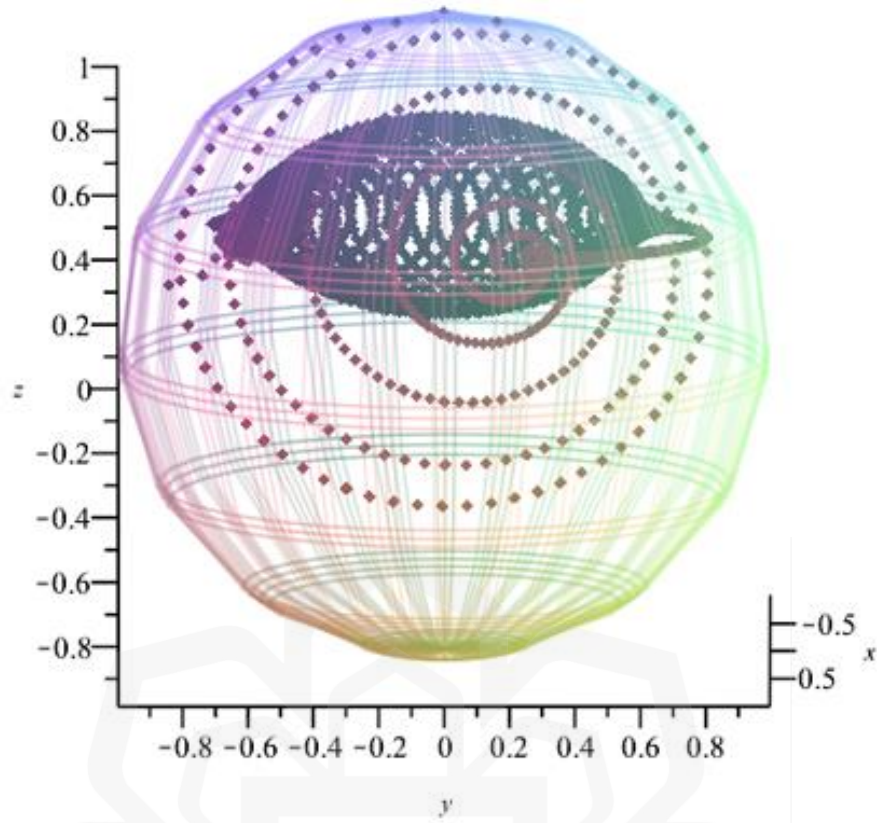


Figure 4.7: Majorana Sphere representation for qubit initially in excited state with $\lambda = 1$, $N = 120$ and $|\zeta|^2 = 16$ from time $t = 0$ to $t = 60$ seconds for $\delta = 5$.

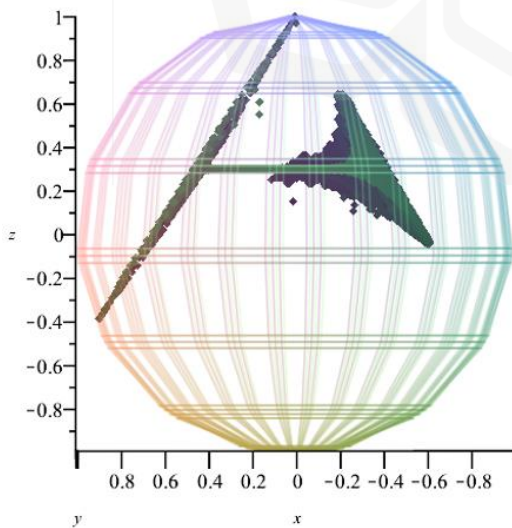


Figure 4.7 a): Rotated horizontally.

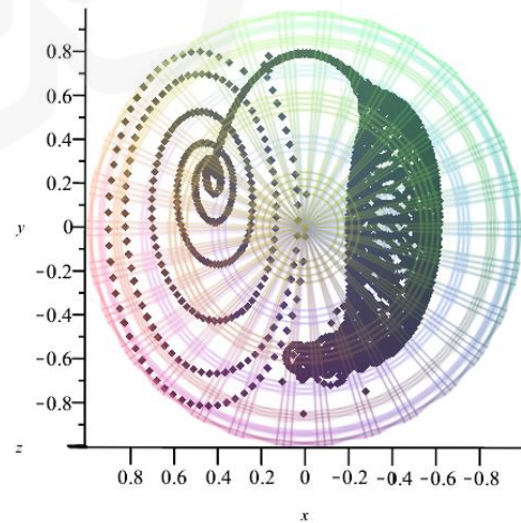


Figure 4.7 b): Rotated vertically.

Figure 4.8 displays the time evolution of one qubit – spin coherent state model that is set to be initially in the excited state for a higher value of detuning $\delta = 25$, from period $t = 0$ until $t = 130$ seconds. As the revival time is now prolonged, the period is also chosen to be longer so that the dynamics of the qubit state probabilities can have one complete oscillation. Figure 4.8 a) and Figure 4.8 b) are also plotted because it is difficult to see the trajectory within the Majorana Sphere. From these figures, we can see that the pattern created by the points is more complex with large number of oscillations.

Figure 4.8 a) shows that the point starts at coordinate $(0,0,1)$, which indicates that the qubit is at the north pole of the sphere hence is initially in excited state. The points then turn into a spiral, gradually fade away and then remain in a horizontal trajectory at about $z = 0.9$. During this time, the phenomenon described by these dynamics is called as the collapse in the qubit state probabilities and the constant horizontal line indicates that the qubit is in a mixed state due to entanglement between the qubit and spin coherent state. After some time, the qubit state probabilities start to revive back and this is illustrated by the development of a new spiral that is located opposite to the initial spiral. A longer period of time is required to display the next activity of collapse and revival, as a result of adding higher detuning which increases the revival time of the qubit state probabilities.

The explanation on the dynamics of the qubit state probabilities in Majorana Sphere for high detuning case is more obvious compared to earlier detuning cases. Transformation in Figure 4.8 shows an even stranger pattern in comparison with the earlier detuning cases. The dynamics of the qubit state probabilities does not reach the surface of the sphere after $t = 0$, which shows that the qubit and the spin coherent state hardly undergo disentanglement, making it very difficult for the qubit to attain attractor state. Thus, the revival time becomes longer because the qubit often remains in mixed state. The dynamics also does not occupy the lower half of the Majorana Sphere, indicating that the qubit never reaches the ground state as time evolves. This unusual behaviour happens because the large value of detuning prevents the energy released due to photon emission into the spin coherent state from bringing the qubit down to its ground state. Hence, it is more likely for the qubit to always stays in its excited state.

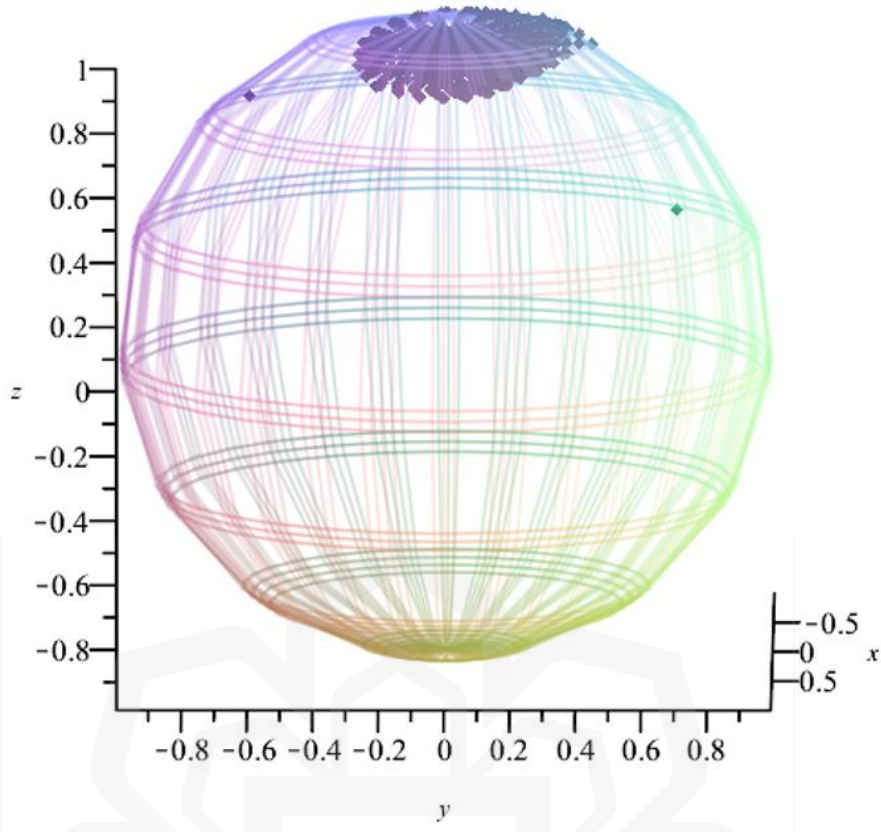


Figure 4.8: Majorana Sphere representation for qubit initially in excited state with $\lambda = 1$, $N = 120$ and $|\zeta|^2 = 16$ from time $t = 0$ to $t = 130$ seconds for $\delta = 25$.

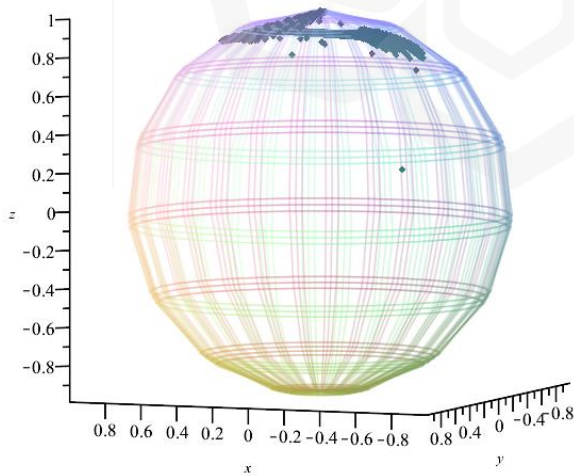


Figure 4.8 a): Rotated horizontally.

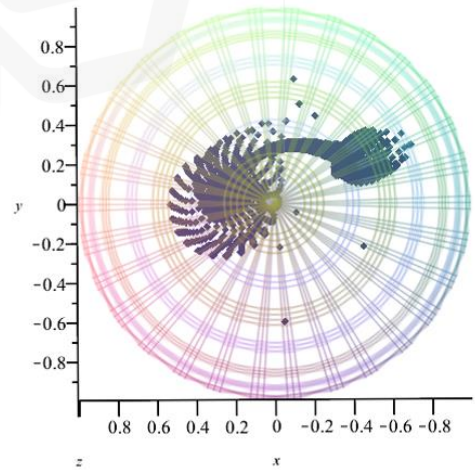


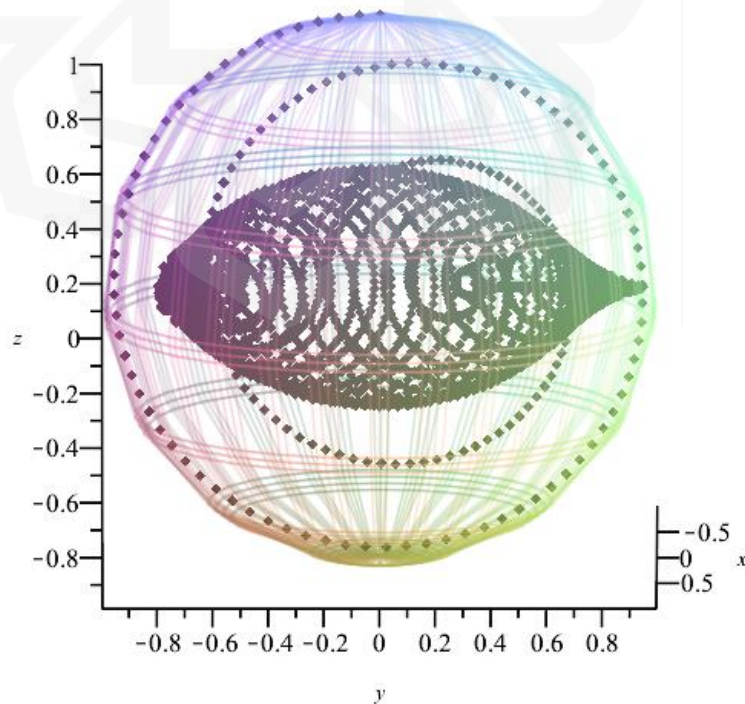
Figure 4.8 b): Rotated vertically.

4.3.2 Distribution of Errors

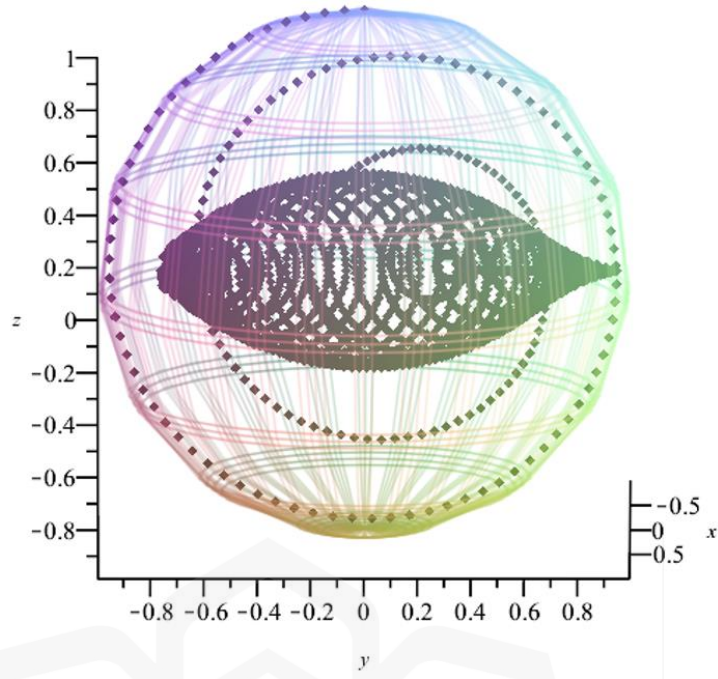
Previous section has shown the effect of having non-zero values of detuning in the one qubit – spin coherent state model. It is crystal clear that the changes in the value of detuning δ affected the revival time of the qubit, the probability of the qubit state, and its dynamics in the Majorana Sphere. In this section, we consider realistic errors that might arise in an empirical system and thus, we chose the ideal condition of $\delta = 0$ but depending on a distribution of errors Δ in the one qubit – spin coherent state model.

Equation (3.35) and the error distribution properties were used to evaluate the reduced density matrix of the qubit over a distribution of δ values. Then the probability of the qubit being in the excited state is evaluated by using Equation (2.107) and transform the dynamics of the qubit state probabilities into the Majorana Sphere representation by using Equation (3.18).

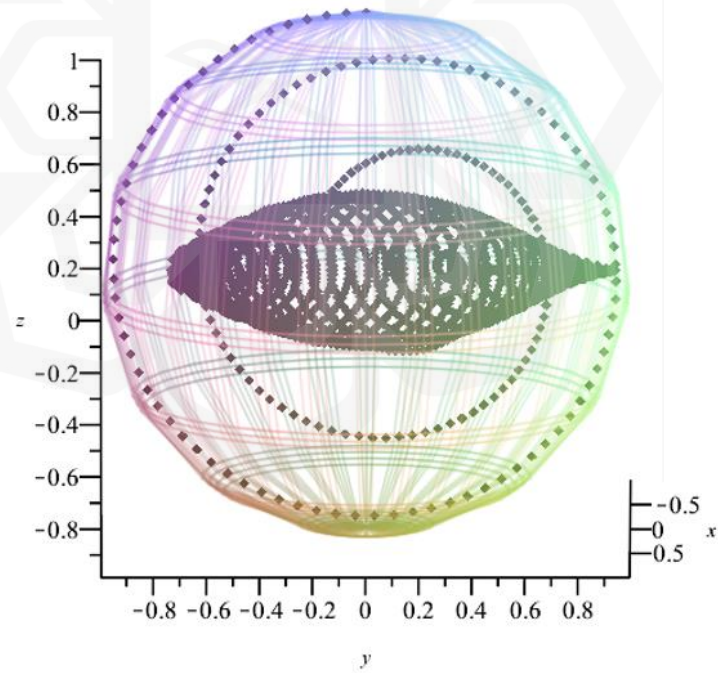
Figure 4.9 below was plotted to display the time evolution of the qubit state in the Majorana Sphere for some values of error distribution widths. We choose $\Delta = 0.3$, $\Delta = 0.5$ and $\Delta = 0.7$ to compare the results with the ideal system of zero detuning as shown in Figure 4.6.



a) $\Delta = 0.3$



b) $\Delta = 0.5$



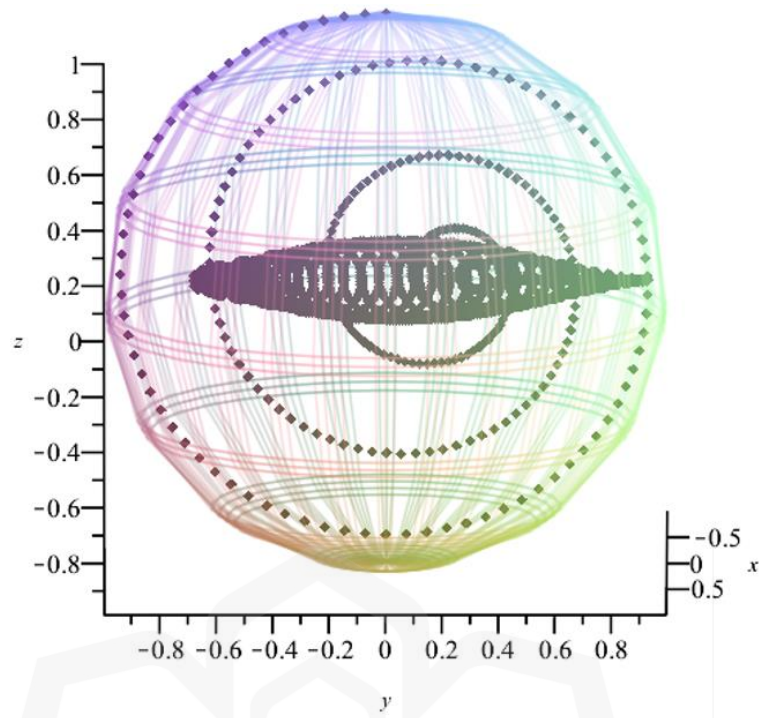
c) $\Delta = 0.7$

Figure 4.9: Majorana Sphere representations of the one qubit – spin coherent state model for an ideal case of zero detuning with decoherence effects from time $t = 0$ to $t = 50$ seconds. The qubit is initially in the excited state with $\lambda = 1$, $N = 120$, $|\zeta|^2 = 16$ and the subfigures show the differences in the system with respective values of $\Delta = 0.3, 0.5$ and 0.7 .

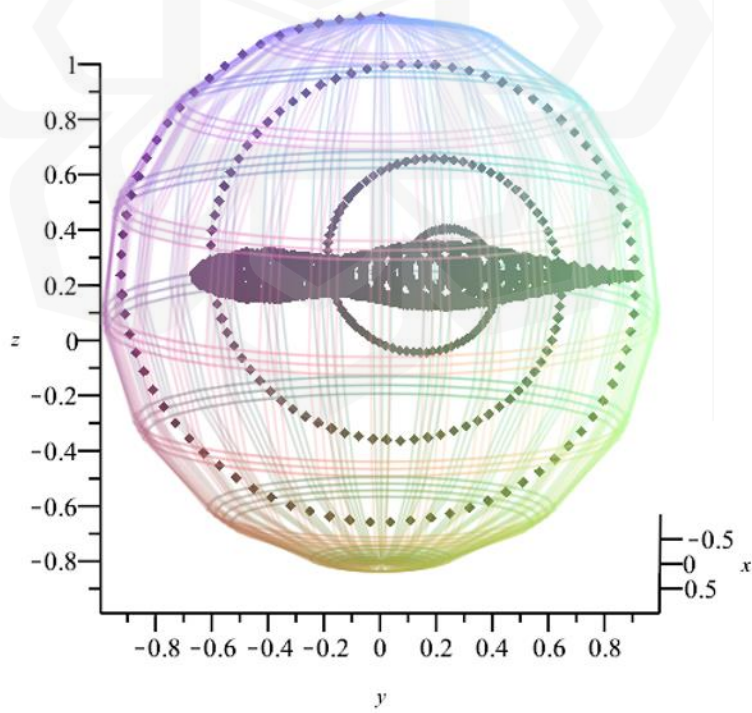
The changes that happen to the trajectory of the qubit state probabilities inside the Majorana Sphere can be seen in the figure, which indicates the decoherence effects on the dynamics of the one qubit – spin coherent state model. Unlike the results obtained from previous section of non-zero detuning case where the trajectory of the qubit state probabilities shifted to the north pole following the increment in the value of detuning δ , the trajectory in this case remains averaged at the center of the sphere even with changes or increment in the error value. The qubit state probabilities still managed to reach the surface of the sphere at point $\mathbf{R} = (0,1,0)$ which suggests that purity of the qubit subsystem is changeless, and the attractor state of the qubit still appears at this certain time. Apparently, a slight difference of this case as compared with the zero detuning case in Figure 4.6 can be noticed at the revival activity or the progressive swirl after the qubit reached attractor state.

We can clearly observe that as the value of error Δ increases, the amplitude of the revival activity of the qubit state probabilities decreases. The revival activity is suppressed due to different revival times caused by different detunings in the ensemble distribution. Alternatively, the addition in the value of error Δ is affecting the purity of the one qubit – spin coherent state model during revival time. The revival amplitude becomes more compressed to the center of the sphere, which suggests that the qubit subsystem has become more of a mixed state due to the additional entropy from the decoherence as a result of entanglement between the qubit with the spin coherent state. This also means that the disentanglement between the qubit and spin coherent state components becomes more rigid as the value of error Δ increases.

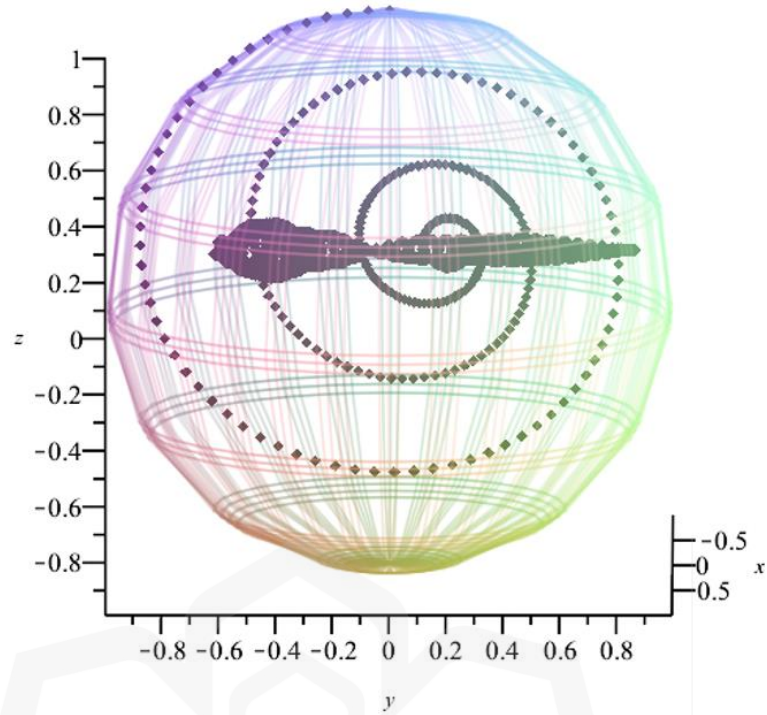
We continue to plot the Majorana Sphere representation of the time evolution of the one qubit – spin coherent state model with larger values of error to determine the highest value of error Δ that the revival swirl can hold. Figure 4.10 shows that as the value of error Δ increases, the dynamics of the qubit state probabilities continue to revive with lower amplitude, until at value $\Delta = 3.5$ shown in subfigure c), the revival almost diminishes. This means that the decoherence effects have also interrupted the constructive interferences and affected the revival activity of the qubit state in the interaction system.



a) $\Delta = 1.5$



b) $\Delta = 2.0$



c) $\Delta = 3.5$

Figure 4.10: Majorana Sphere representations of the one qubit – spin coherent state model for an ideal case of zero detuning with decoherence effects from time $t = 0$ to $t = 50$ seconds. The qubit is initially in the excited state with $\lambda = 1$, $N = 120$, $|\zeta|^2 = 16$ and the subfigures show the differences in the system with respective values of $\Delta = 1.5, 2.0$ and 3.5 .

Increasing the value of error Δ gives us some additional information from the Majorana Sphere representation. The trajectory of the qubit state probabilities inside the Majorana Sphere slowly shifted upwards towards the north pole of the sphere following the increment in the value of error Δ , and it gets more obvious in Figure 4.10 c) where the revival activity of the qubit state probabilities has also slightly shifted to the plane $z = 0.2$. This suggests that the qubit tends to stay in its initial excited state in addition with the revival swirl that almost diminishes when the value of error Δ increases. The trajectory points are also quite a distance from the surface of the sphere after $t = 0$, which means that the qubit does not reach the pure attractor state, and it tends to stay in a mixed state due to harder disentanglement between the qubit and the spin coherent state.

CHAPTER 5

CONCLUSION

In general, the interaction involving atom and field is an important tool to be studied as it gives a massive contribution to the development of quantum information technologies. Among many atom-field interaction models, the Jaynes-Cummings model is considered as one of the fundamental, whereas the spin coherent state model is an extension from the former model. We have studied the interaction system between a single qubit with a spin coherent state and observed many interesting phenomena, where in this research we focused more on the collapse and revival activity of the Rabi oscillation.

We firstly reproduced the calculations related to solving a one qubit – spin coherent state model (Dooley et al., 2013; Bahari, 2018) such as formulating the Hamiltonian of the system, finding the eigenvalues and eigenvectors of the Hamiltonian, and finding the exact solution for the model by solving the time-dependent Schrödinger equation. Next, we plot several graphs which are the collapse and revival curve, attractor state curve, and linear entropy curve to represent the time evolutions of the qubit state probabilities. Then, we proceed by transforming the dynamics of the qubit state probabilities from the one qubit – spin coherent state model into the Majorana Sphere representation, with three different initial states which are for excited state $C_e = 1, C_g = 0$, for ground state $C_e = 0, C_g = 1$, and for when the initial state is an equal probability between the excited and ground state $C_e = \frac{1}{\sqrt{2}}, C_g = \frac{1}{\sqrt{2}}$.

As a result, when the initial state is set for excited state or ground state, we can clearly see the oscillation of the qubit state probabilities in the Majorana Sphere, where the point starts at the north pole or south pole for respective cases. The point starts on the sphere's surface, which is a pure state and gradually moves towards the inside of the sphere, which is a mixed state as a result of qubit – spin coherent state entanglement. The swirl in the dynamics depicts the collapse and revival activity of the Rabi oscillations. After the collapse time, the dynamics remains constant at about time $t = 3$ seconds to $t = 18$ seconds for excited state and $t = 17$ seconds for ground state,

simultaneously the point moves from inside to the surface of the sphere. This indicates that the qubit and the spin coherent state have disentangled and the qubit are in the attractor state. Afterwards, the revival activity of the qubit begins and the point reverses its movement again from the surface towards the center of the sphere. At about $t = 33$ seconds for excited state and $t = 31$ seconds for ground state, the revival oscillations stopped and the second collapse activity begins. This event of collapse and revival continues to occur at later times.

However, this is not the case for when we set the initial state to be an equal probability between the excited state and ground state. We cannot see the spiral movement that represents the collapse and revival activity of the qubit state probabilities in this particular case. Evidently, the points just made a circular trajectory that stays at the center of the sphere at plane $z = 0$ until after a longer period of time, the points spiral into the origin of the sphere and eventually stays there. This means that as time evolves, the qubit and the spin coherent state are becoming more entangled and eventually will achieve maximal entanglement.

We then extend our research by considering a realistic approach to the one qubit – spin coherent state model, where we had divided it into two parts. The first part discussed the consequences of putting a finite frequency detuning on the system, where the frequency of the qubit Ω and the frequency of the spin coherent state ω_N is off-resonant, thus $\delta = \Omega - \omega_N \neq 0$. From the investigation, we found that for the case of qubit initially in the excited state, an increment in the value of detuning δ will increase the probability of the qubit to be in its initial excited state and the revival time will be prolonged. This result was depicted in the Majorana Sphere in which the trajectory of the dynamics of the qubit state probabilities shifted to the north pole of the sphere in contrast to the zero detuning case. As the value of detuning gets higher, the trajectory will only reside on the excited level of the sphere, indicating that the qubit will not reach the ground state. Additionally, the qubit now hardly reaches the attractor state as the trajectory points does not reach the sphere's surface after $t = 0$, and the points just stay in its interior. This means that the qubit tends to stay in the mixed state and decreases the probability of the qubit to become disentangled with the spin coherent state. We can also observe that finite detuning causes the trajectory in the Majorana Sphere to make an additional dimension, as it now spans on the x, y, and z-axes as compared to the flat vertical plane in the case of zero detuning.

For the second part, we consider the time evolution of the one qubit – spin coherent state model with decoherence effect. Gaussian distribution of variable width Δ was used as an example to represent the potential errors that may happen in a real system for the case of an ideal system with zero detuning. Such developed model can be very handy for experimental tasks. Due to the complexity of the calculation, we proceed with a discrete approximation approach to evaluate the density matrix of the qubit by averaging it over the errors. The results show that unlike for the case of finite values of detuning that shifted the qubit state probabilities and prolonged the revival time, the revivals in such quantities are subdued at a particular revival time t_r when errors are seen as a distribution of detuning. As a result of various detunings in the ensemble distribution that have been averaged, it causes the revivals to take place at various times. When the value of error Δ increases, the suppression becomes more significant and it also affected the purity of the qubit subsystem as can be seen from the example of $\Delta = 3.5$, the trajectory does not reach the surface of the sphere after $t = 0$ which means that the qubit does not reach pure attractor state, and it tends to stay in the mixed state due to harder disentanglement between the qubit and the spin coherent state. The qubit is also more likely to stay in its initial excited state as the trajectory is shifted slightly to the sphere's north pole.

In a nutshell, the analyzation of the time evolution of the one qubit – spin coherent state model by using Majorana Sphere representation has shown that the Majorana Sphere has done a very good job in displaying the quantum properties exhibited by the model. As the Majorana Sphere is helpful to represent the qubit system for a multiple qubit case, suggestion for future work is to develop the complex formulation to represent a multiple qubit system, especially the interaction with the spin coherent state, into the Majorana Sphere. Furthermore, since in a multiple qubit case, for example a two-qubit case not only have an entanglement with the field, but also an additional entanglement between the qubits themselves. Hence, it is interesting to know what will happen to the qubit state representation in the Majorana Sphere when the additional variable is introduced. We can also consider the decoherence effects when there are errors in the coupling strength between qubits in a multiple qubit case for future work. Majorana Sphere will essentially help us to understand the properties exhibited by the system.

REFERENCES

- Albino, A. S., Pires, O. M., Nogueira, P., de Souza, R. F., & Nascimento, E. G. S. (2022). Quantum computational intelligence for travelttime seismic inversion. *arXiv preprint arXiv:2208.05794*.
- Arecchi, F. T., Courtens, E., Gilmore, R., & Thomas, H. (1972). Atomic coherent states in quantum optics. *Physical Review A*, 6(6), 2211.
- Bacry, H. (1974). Orbits of the rotation group on spin states. *Journal of Mathematical Physics*, 15(10), 1686-1688.
- Bahari, I. (2018). *Collapse, Revival and Decoherence of Entanglement in Two Qubits Systems* (Doctoral dissertation, University of York).
- Bahari, I., Spiller, T. P., Dooley, S., Hayes, A., & McCrossan, F. (2018). Collapse and revival of entanglement between qubits coupled to a spin coherent state. *International Journal of Quantum Information*, 16(02), 1850017.
- Berman, P. R. (1994). Cavity quantum electrodynamics.
- Bhatta, S., & Dang, J. (2023). Multiclass seismic damage detection of buildings using quantum convolutional neural network. *Computer-Aided Civil and Infrastructure Engineering*.
- Bose, S., & Vedral, V. (2000). Mixedness and teleportation. *Physical Review A*, 61(4), 040101.
- Brattke, S., Varcoe, B. T., & Walther, H. (2001). Preparing Fock states in the micromaser. *Optics Express*, 8(2), 131-144.
- Bužek, V., Moya-Cessa, H., Knight, P. L., & Phoenix, S. J. D. (1992). Schrödinger-cat states in the resonant Jaynes-Cummings model: Collapse and revival of oscillations of the photon-number distribution. *Physical review A*, 45(11), 8190.

- Cirac, J. I., & Zoller, P. (1995). Quantum computations with cold trapped ions. *Physical review letters*, 74(20), 4091.
- Cummings, F. W. (1965). Stimulated emission of radiation in a single mode. *Physical Review*, 140(4A), A1051.
- Devi, A. U., Sudha, & Rajagopal, A. K. (2012). Majorana representation of symmetric multiqubit states. *Quantum Information Processing*, 11(3), 685-710.
- Dirac, P. A. M. (1981). *The principles of quantum mechanics* (No. 27). Oxford university press.
- Dogra, S., Vepsäläinen, A., & Paraoanu, G. S. (2020). Majorana representation of adiabatic and superadiabatic processes in three-level systems. *Physical Review Research*, 2(4), 043079.
- Dooley, S. (2014). *Quantum revivals and generation of non-classical states in an N spin system* (Doctoral dissertation, University of Leeds).
- Dooley, S., & Spiller, T. P. (2014). Fractional revivals, multiple-Schrödinger-cat states, and quantum carpets in the interaction of a qubit with N qubits. *Physical Review A*, 90(1), 012320.
- Dooley, S., McCrossan, F., Harland, D., Everitt, M. J., & Spiller, T. P. (2013). Collapse and revival and cat states with an N-spin system. *Physical review A*, 87(5), 052323.
- Dowling, J. P., & Milburn, G. J. (2003). Quantum technology: the second quantum revolution. *Philosophical Transactions of the Royal Society of London. Series A: Mathematical, Physical and Engineering Sciences*, 361(1809), 1655-1674.
- Eberly, J. H., Narozhny, N. B., & Sanchez-Mondragon, J. J. (1980). Periodic spontaneous collapse and revival in a simple quantum model. *Physical Review Letters*, 44(20), 1323.
- Eckle, H. P., & Johannesson, H. (2017). A generalization of the quantum Rabi model: exact solution and spectral structure. *Journal of Physics A: Mathematical and Theoretical*, 50(29), 294004.

- Elani, Z. (2021). Qubit, Quantum Entanglement and all that: Quantum Computing Made Simple.
- Feng, D. (2019, March). Review of quantum navigation. In *IOP Conference Series: Earth and Environmental Science* (Vol. 237, p. 032027). IOP Publishing.
- Gea-Banacloche, J. (1990). Collapse and revival of the state vector in the Jaynes-Cummings model: An example of state preparation by a quantum apparatus. *Physical review letters*, 65(27), 3385.
- Gea-Banacloche, J. (1991). Atom-and field-state evolution in the Jaynes-Cummings model for large initial fields. *Physical Review A*, 44(9), 5913.
- Gea-Banacloche, J. (1992). A new look at the Jaynes-Cummings model for large fields: Bloch sphere evolution and detuning effects. *Optics communications*, 88(4-6), 531-550.
- Gerry, C., & Knight, P. L. (2005). *Introductory quantum optics*. Cambridge university press.
- Gibney, E. (2019). The quantum gold rush. *Nature*, 574(7776), 22-24.
- Glauber, R. J. (1963). Coherent and incoherent states of the radiation field. *Physical Review*, 131(6), 2766.
- Griffiths, P., & Harris, J. (2014). *Principles of algebraic geometry*. John Wiley & Sons.
- Horowitz, M., & Grumblin, E. (2019). *Quantum computing: progress and prospects*. The National Academies Press.
- Hutton, A., & Bose, S. (2004). Mediated entanglement and correlations in a star network of interacting spins. *Physical Review A*, 69(4), 042312.
- Izsák, R., Riplinger, C., Blunt, N. S., de Souza, B., Holzmann, N., Crawford, O., ... & Schopf, P. (2023). Quantum computing in pharma: A multilayer embedding approach for near future applications. *Journal of Computational Chemistry*, 44(3), 406-421.

- Jarvis, C. E. A. (2009). *Dynamics of Entanglement for Qubits in a Cavity* (Doctoral dissertation, University of Bristol).
- Jarvis, C. E. A., Rodrigues, D. A., Györfy, B. L., Spiller, T. P., Short, A. J., & Annett, J. F. (2009). Dynamics of entanglement and ‘attractor’ states in the Tavis–Cummings model. *New Journal of Physics*, *11*(10), 103047.
- Jarvis, C. E. A., Rodrigues, D. A., Györfy, B. L., Spiller, T. P., Short, A. J., & Annett, J. F. (2010). Collapse and revival of “Schrödinger cat” states. *JOSA B*, *27*(6), A164-A169.
- Jaynes, E. T., & Cummings, F. W. (1963). Comparison of quantum and semiclassical radiation theories with application to the beam maser. *Proceedings of the IEEE*, *51*(1), 89-109.
- Joo, J., Munro, W. J., & Spiller, T. P. (2011). Quantum metrology with entangled coherent states. *Physical review letters*, *107*(8), 083601.
- Knight, P. L., & Shore, B. W. (1993). Schrödinger-cat states of the electromagnetic field and multilevel atoms. *Physical Review A*, *48*(1), 642.
- Lax, P. D. (2007). *Linear algebra and its applications* (Vol. 78). John Wiley & Sons.
- Leboeuf, P. (1991). Phase space approach to quantum dynamics. *Journal of Physics A: Mathematical and General*, *24*(19), 4575.
- Lowdin, P. O. (1964). *Linear algebra and the fundamentals of quantum theory* (No. TN-125).
- Majorana, E. (1932). Atomi orientati in campo magnetico variabile. *Il Nuovo Cimento (1924-1942)*, *9*(2), 43-50.
- Munro, W. J., James, D. F., White, A. G., & Kwiat, P. G. (2001). Maximizing the entanglement of two mixed qubits. *Physical Review A*, *64*(3), 030302.
- Munro, W. J., Nemoto, K., Milburn, G. J., & Braunstein, S. L. (2002). Weak-force detection with superposed coherent states. *Physical Review A*, *66*(2), 023819.

- Nielsen, M. A., & Chuang, I. L. (2010). *Quantum computation and quantum information*. Cambridge university press.
- Qing, Y., Ming, Y., & Zhuo-Liang, C. (2008). Sudden Death of Entanglement between Two Atoms with Initial Tripartite Entangled State in the Tavis–Cummings Model. *Chinese Physics Letters*, 25(3), 825.
- Rabi, I. I. (1937). Space quantization in a gyrating magnetic field. *Physical Review*, 51(8), 652.
- Radcliffe, J. M. (1971). Some properties of coherent spin states. *Journal of Physics A: General Physics*, 4(3), 313.
- Schuster, D. I., Houck, A. A., Schreier, J. A., Wallraff, A., Gambetta, J. M., Blais, A., ... & Schoelkopf, R. J. (2007). Resolving photon number states in a superconducting circuit. *Nature*, 445(7127), 515-518.
- Shor, P. W. (1994, November). Algorithms for quantum computation: discrete logarithms and factoring. In *Proceedings 35th annual symposium on foundations of computer science* (pp. 124-134). Ieee.
- Shore, B. W., & Knight, P. L. (1993). The jaynes-cummings model. *Journal of Modern Optics*, 40(7), 1195-1238.
- Tavis, M., & Cummings, F. W. (1968). Exact solution for an N-molecule—radiation-field Hamiltonian. *Physical Review*, 170(2), 379.
- Vedral, V., Plenio, M. B., Jacobs, K., & Knight, P. L. (1997). Statistical inference, distinguishability of quantum states, and quantum entanglement. *Physical Review A*, 56(6), 4452.
- Wallraff, A., Schuster, D. I., Blais, A., Frunzio, L., Huang, R. S., Majer, J., ... & Schoelkopf, R. J. (2004). Strong coupling of a single photon to a superconducting qubit using circuit quantum electrodynamics. *Nature*, 431(7005), 162-167.
- Wang, C., Gao, Y. Y., Reinhold, P., Heeres, R. W., Ofek, N., Chou, K., ... & Schoelkopf, R. J. (2016). A Schrödinger cat living in two boxes. *Science*, 352(6289), 1087-1091.

- Yarkoni, S., Neukart, F., Tagle, E. M. G., Magiera, N., Mehta, B., Hire, K., ... & Hofmann, M. (2020, November). Quantum shuttle: traffic navigation with quantum computing. In *Proceedings of the 1st ACM SIGSOFT International Workshop on Architectures and Paradigms for Engineering Quantum Software* (pp. 22-30).
- Yu, T., & Eberly, J. H. (2004). Finite-time disentanglement via spontaneous emission. *Physical Review Letters*, 93(14), 140404.
- Yu, T., & Eberly, J. H. (2009). Sudden death of entanglement. *Science*, 323(5914), 598-601.
- Zettili, N. (2009). *Quantum mechanics: concepts and applications*.
- Zimba, J. (2006). Anticoherent spin states via the Majorana representation. *EJTP*, 3(10), 143-156.
- Zinner, M., Dahlhausen, F., Boehme, P., Ehlers, J., Bieske, L., & Fehring, L. (2022). Toward the institutionalization of quantum computing in pharmaceutical research. *Drug Discovery Today*, 27(2), 378-383.

APPENDIX I: CODING SCRIPT

```

> restart;
> with(linalg) :
> with(LinearAlgebra) :
> with(plottools) :
> with(plots) :
>
> a := 0 :
> b := 1 :
> L := 1 :
> N := 120 :
> Di := dI[i] :
>
> d0 := 3.6 :
>
> j := 31 :
>
> dI[1] := -3·d0 :
> dI[j] := 3·d0 :
> STEP :=  $\frac{dI[j] - dI[1]}{j - 1}$  :
> for m from 2 to j - 1 do
>     dI[m] := dI[m - 1] + STEP :
>
> od :
>
> COE :=  $\frac{1}{\text{sqrt}(2 \cdot \text{Pi} \cdot d0^2)}$  :
>
> SEENOL1[0] := 0 : SEENOLT[0] := 0 : SEENOL2[0] := 0 : SEENOL3[0] := 0 :
>     SEENOL4[0] := 0 :
> SEGNIL1[0] := 0 : SEGNILT[0] := 0 : SEGNIL2[0] := 0 : SEGNIL3[0] := 0 :
>     SEGNIL4[0] := 0 :
> SGENIL1[0] := 0 : SGENILT[0] := 0 : SGENIL2[0] := 0 : SGENIL3[0] := 0 :
>     SGENIL4[0] := 0 :
> SGGN2L1[0] := 0 : SGGN2LT[0] := 0 : SGGN2L2[0] := 0 : SGGN2L3[0] := 0 :
>     SGGN2L4[0] := 0 :
>
> SUMCO[0] := 0 :
>

```



> for i from 1 to j by 1 do

$$\begin{aligned}
 EENOL[i] := & Ce \cdot Cn \cdot \cos\left(\frac{L \cdot t}{2} \sqrt{Di^2 + 4 \cdot (n+1) \cdot \left(1 - \frac{n}{N}\right)}\right) + I \cdot \sin\left(\frac{L \cdot t}{2} \sqrt{Di^2 + 4 \cdot (n+1) \cdot \left(1 - \frac{n}{N}\right)}\right) \\
 & \cdot (n+1) \cdot \left(1 - \frac{n}{N}\right) \cdot \left(Ce \cdot Cn \cdot \frac{\left(\frac{1 - \frac{Di}{\sqrt{Di^2 + 4 \cdot (n+1) \cdot \left(1 - \frac{n}{N}\right)}}{2}}{\frac{1 + \frac{Di}{\sqrt{Di^2 + 4 \cdot (n+1) \cdot \left(1 - \frac{n}{N}\right)}}{2}} \right)}{2} - 2 \cdot Cg \cdot Cnp \right. \\
 & \left. \cdot \sqrt{\frac{\left(\frac{1 - \frac{Di}{\sqrt{Di^2 + 4 \cdot (n+1) \cdot \left(1 - \frac{n}{N}\right)}}{2}}{\frac{1 + \frac{Di}{\sqrt{Di^2 + 4 \cdot (n+1) \cdot \left(1 - \frac{n}{N}\right)}}{2}} \right)}{2}} \right) \\
 & \left. \cdot \sqrt{\frac{\left(\frac{1 + \frac{Di}{\sqrt{Di^2 + 4 \cdot (n+1) \cdot \left(1 - \frac{n}{N}\right)}}{2}}{\frac{1 - \frac{Di}{\sqrt{Di^2 + 4 \cdot (n+1) \cdot \left(1 - \frac{n}{N}\right)}}{2}} \right)}{2}} \right) \right) :
 \end{aligned}$$

$$\begin{aligned}
 EENOLT[i] := & Ce \cdot Cn \cdot \cos\left(\frac{L \cdot t}{2} \sqrt{Di^2 + 4 \cdot (n+1) \cdot \left(1 - \frac{n}{N}\right)}\right) - I \cdot \sin\left(\frac{L \cdot t}{2} \sqrt{Di^2 + 4 \cdot (n+1) \cdot \left(1 - \frac{n}{N}\right)}\right) \\
 & + 4 \cdot (n+1) \cdot \left(1 - \frac{n}{N}\right) \cdot \left(Ce \cdot Cn \cdot \frac{\left(\frac{1 - \frac{Di}{\sqrt{Di^2 + 4 \cdot (n+1) \cdot \left(1 - \frac{n}{N}\right)}}{2}}{\frac{1 + \frac{Di}{\sqrt{Di^2 + 4 \cdot (n+1) \cdot \left(1 - \frac{n}{N}\right)}}{2}} \right)}{2} - 2 \cdot Cg \cdot Cnp \right. \\
 & \left. \cdot \sqrt{\frac{\left(\frac{1 - \frac{Di}{\sqrt{Di^2 + 4 \cdot (n+1) \cdot \left(1 - \frac{n}{N}\right)}}{2}}{\frac{1 + \frac{Di}{\sqrt{Di^2 + 4 \cdot (n+1) \cdot \left(1 - \frac{n}{N}\right)}}{2}} \right)}{2}} \right) \\
 & \left. \cdot \sqrt{\frac{\left(\frac{1 + \frac{Di}{\sqrt{Di^2 + 4 \cdot (n+1) \cdot \left(1 - \frac{n}{N}\right)}}{2}}{\frac{1 - \frac{Di}{\sqrt{Di^2 + 4 \cdot (n+1) \cdot \left(1 - \frac{n}{N}\right)}}{2}} \right)}{2}} \right) \right) :
 \end{aligned}$$

$$\begin{aligned}
EGNIL[i] := & Cg \cdot Cn \cdot \cos\left(\frac{L \cdot t}{2} \sqrt{Di^2 + 4 \cdot (n) \cdot \left(1 - \frac{n-1}{N}\right)}\right) + I \cdot \sin\left(\frac{L \cdot t}{2} \sqrt{Di^2}\right. \\
& + 4 \cdot (n) \cdot \left. \left(1 - \frac{n-1}{N}\right)\right) \cdot \left(Cg \cdot Cn \cdot \left(\frac{1 + \frac{Di}{\sqrt{Di^2 + 4 \cdot (n) \cdot \left(1 - \frac{n-1}{N}\right)}}}{2} \right) \right. \\
& - \left. \left. \frac{1 - \frac{Di}{\sqrt{Di^2 + 4 \cdot (n) \cdot \left(1 - \frac{n-1}{N}\right)}}}{2} \right) \right) - 2 \cdot Ce \cdot Cnm \\
& \cdot \sqrt{\left(\frac{1 + \frac{Di}{\sqrt{Di^2 + 4 \cdot (n) \cdot \left(1 - \frac{n-1}{N}\right)}}}{2} \right)} \\
& \cdot \sqrt{\left(\frac{1 - \frac{Di}{\sqrt{Di^2 + 4 \cdot (n) \cdot \left(1 - \frac{n-1}{N}\right)}}}{2} \right)} :
\end{aligned}$$

$$\begin{aligned}
EGNILT[i] := & Cg \cdot Cn \cdot \cos\left(\frac{L \cdot t}{2} \sqrt{Di^2 + 4 \cdot (n) \cdot \left(1 - \frac{n-1}{N}\right)}\right) - I \cdot \sin\left(\frac{L \cdot t}{2} \sqrt{Di^2}\right. \\
& + 4 \cdot (n) \cdot \left. \left(1 - \frac{n-1}{N}\right)\right) \cdot \left(Cg \cdot Cn \cdot \left(\frac{1 + \frac{Di}{\sqrt{Di^2 + 4 \cdot (n) \cdot \left(1 - \frac{n-1}{N}\right)}}}{2} \right) \right. \\
& - \left. \left. \frac{1 - \frac{Di}{\sqrt{Di^2 + 4 \cdot (n) \cdot \left(1 - \frac{n-1}{N}\right)}}}{2} \right) \right) - 2 \cdot Ce \cdot Cnm \\
& \cdot \sqrt{\left(\frac{1 + \frac{Di}{\sqrt{Di^2 + 4 \cdot (n) \cdot \left(1 - \frac{n-1}{N}\right)}}}{2} \right)} \\
& \cdot \sqrt{\left(\frac{1 - \frac{Di}{\sqrt{Di^2 + 4 \cdot (n) \cdot \left(1 - \frac{n-1}{N}\right)}}}{2} \right)} :
\end{aligned}$$

$$SEENOL1[i] := SEENOL1[i-1] + \left(COE \cdot \exp\left(-\frac{dl[i]^2}{2 \cdot d\theta^2}\right) \right) (EENOL[i] \cdot EENOLT[i]) :$$

$$SEENOL2[i] := SEENOL2[i-1] + \left(COE \cdot \exp\left(-\frac{dl[i]^2}{2 \cdot d\theta^2}\right) \right) (EENOL[i] \cdot EGNILT[i]) :$$

$$SEGNIL1[i] := SEGNIL1[i - 1] + \left(COE \cdot \exp\left(\frac{-dI[i]^2}{2 \cdot d\theta^2}\right) \right) (EGNIL[i] \cdot EENOLT[i]) :$$

$$SEGNIL2[i] := SEGNIL2[i - 1] + \left(COE \cdot \exp\left(\frac{-dI[i]^2}{2 \cdot d\theta^2}\right) \right) (EGNIL[i] \cdot EGNILT[i]) :$$

$$CO[i] := evalf\left(COE \cdot \exp\left(\frac{-dI[i]^2}{2 \cdot d\theta^2}\right) \right) :$$

$$SUMCO[i] := SUMCO[i - 1] + CO[i] :$$

od:

> *points* := [seq([i, CO[i]], i=1..j, 1)]:

> plot([*points*]):

>

$$> Cn := \frac{\exp\left(-\frac{nbar}{2}\right) \cdot \text{sqrt}(nbar)^n}{\text{sqrt}(n!)} :$$

$$> Cnp := \frac{\exp\left(-\frac{nbar}{2}\right) \cdot \text{sqrt}(nbar)^{(n+1)}}{\text{sqrt}((n+1)!)} :$$

$$> Cnp2 := \frac{\exp\left(-\frac{nbar}{2}\right) \cdot \text{sqrt}(nbar)^{(n+2)}}{\text{sqrt}((n+2)!)} :$$

$$> C1 := \frac{\exp\left(-\frac{nbar}{2}\right) \cdot \text{sqrt}(nbar)}{\text{sqrt}((1)!)} :$$

$$> C0 := \frac{\exp\left(-\frac{nbar}{2}\right) \cdot \text{sqrt}(nbar)^0}{\text{sqrt}((0)!)} :$$

$$> Cnm := \frac{\exp\left(-\frac{nbar}{2}\right) \cdot \text{sqrt}(nbar)^{n-1}}{\text{sqrt}((n-1)!)} :$$

$$> Cnm2 := \frac{\exp\left(-\frac{nbar}{2}\right) \cdot \text{sqrt}(nbar)^{n-2}}{\text{sqrt}((n-2)!)} :$$

>

>

> *nbar* := 16 :

```

> inf := 100 :
>
> Ce := 1 : Cg := 0 :
>
> P112 :=  $\frac{\text{sum}(\text{SEENOL1}[j], n = 1 .. \text{inf})}{\text{SUMCO}[j]}$  :
>
> plot(P112, t = 0 .. 50, color = blue, numpoints = 600) :
>
> P122 :=  $\left( \frac{\text{sum}(\text{SEENOL2}[j], n = 1 .. \text{inf})}{\text{SUMCO}[j]} \right)$  :
>
> P212 :=  $\frac{\text{sum}(\text{SEGNIL1}[j], n = 1 .. \text{inf})}{\text{SUMCO}[j]}$  :
> P222 :=  $\frac{\text{sum}(\text{SEGNIL2}[j], n = 1 .. \text{inf})}{\text{SUMCO}[j]}$  :
>
> plot(P222, t = 0 .. 50, color = blue, numpoints = 600) :
> #att :=  $\frac{1}{2} \cdot (P112 + I \cdot P122 - I \cdot P212 + P222)$  :
> #plot(att, newtime = 0 .. ran);
>
> PUL := Matrix([[P112, P122], [P212, P222]]) :
> #MIXED STATE
>
> B1 := Sum $\left( \frac{\text{EGNIL}[i]}{\text{EENOL}[i]}, n = 1 .. 100 \right)$  :
>
> B1conj := Sum $\left( \frac{\text{EGNILT}[i]}{\text{EENOLT}[i]}, n = 1 .. 100 \right)$  :
>
>  $\alpha$  := Matrix([[0, 1], [1, 0]]) :
>  $\sigma_y$  := Matrix([[0, -I], [I, 0]]) :
>  $\sigma_z$  := Matrix([[1, 0], [0, -1]]) :
>

```

```

> dens :=  $\frac{P222 - P112}{1 + \text{abs}(B1 \cdot B1\text{conj})}$  · Matrix([[1, B1conj], [B1, abs(B1·B1conj)]]) + Matrix([[0,
P122], [P212, 0]]):
>
> for s from 0 by 0.01 to 50 do
densnew[s] := evalf(subs(t=s, PUL)):

Rxnew[s] := densnew[s] · ox:
TRx[s] := Trace(Rxnew[s]);

Rynew[s] := densnew[s] · oy:
TRY[s] := Trace(Rynew[s]);

Rznew[s] := densnew[s] · oz:
TRz[s] := Trace(Rznew[s]);

end do:
>
> #PURE STATE
>
> denspure :=  $\frac{1}{1 + \text{abs}(B1 \cdot B1\text{conj})}$  · Matrix([[1, B1conj], [B1, abs(B1·B1conj)]]):
> Rx := Trace(denspure · ox):
> Ry := Trace(denspure · oy):
> Rz := Trace(denspure · oz):
>
> #PLOTTING
>
> mixed := [seq([Re(TRx[s]), Re(TRY[s]), Re(TRz[s])], s=0..50, 0.01)]:
> #pure:= [seq([Re(Rx), Re(Ry), Re(Rz)], t=0)]:
>
> #A:=pointplot3d(pure, symbolsize=10):
> B := pointplot3d(mixed, symbolsize=10, labels=[x, y, z]):
> C := plot3d(1, coords=spherical, style=line, scaling=constrained, transparency=0.75):
> display(B, C):
>

```